

Niet-lineair gedrag in een optische versterker
en laser diode gebaseerd terugkoppelingsschema

Non-Linear Behaviour in a Semiconductor Optical Amplifier
and Laser Diode Feedback Scheme

Wouter D'Oosterlinck

Promotor: prof. dr. ir. G. Morthier
Proefschrift ingediend tot het behalen van de graad van
Doctor in de Ingenieurswetenschappen: Elektrotechniek

Vakgroep Informatietechnologie
Voorzitter: prof. dr. ir. P. Lagasse
Faculteit Ingenieurswetenschappen
Academiejaar 2007 - 2008



ISBN 978-90-8578-176-9
NUR 959
Wettelijk depot: D/2007/10.500/50

Promotor:

Prof. dr. ir. G. Morthier

Universiteit Gent, INTEC

Examencommissie:

Prof. dr. ir. R. Verhoeven, voorzitter

Universiteit Gent, Civiele Techniek

Prof. dr. ir. D. Van Thourhout

Universiteit Gent, INTEC

Prof. dr. T. Erneux

Universit Libre de Bruxelles

Prof. dr. ir. M. Smit

TU/e Eindhoven, COBRA

Prof. dr. J. Mørk

Technical University of Denmark, COM

Prof. dr. ir. R. Baets

Universiteit Gent, INTEC

Prof. dr. ir. P. De Visschere

Universiteit Gent, ELIS

Universiteit Gent

Faculteit Ingenieurswetenschappen

Vakgroep Informatietechnologie (INTEC)

Sint-Pietersnieuwstraat 41

9000 Gent

BELGIUM

Tel.: +32-9-264.33.19

Fax: +32-9-264.35.93

Dit werk kwam tot stand in het kader van een specialisatiebeurs van het IWT-Instituut voor de Aanmoediging van Innovatie door Wetenschap en Technologie in Vlaanderen.

This work was carried out in the context of a specialization grant from the Flemish Institute for the Industrial Advancement of Scientific and Technological Research (IWT).

Dankwoord

Starten met het schrijven van je dankwoord betekent dat je even moet terugblikken op wat het nu net is dat je zover gebracht heeft. De vijf jaar die ik in de photonics research group gependend heb, zullen er waarschijnlijk wel “iets” toe bijgedragen hebben dat dit werk uiteindelijk voltooid geraakt is. Maar er zijn ook mensen die, al dan niet bewust, bijgedragen hebben aan het boekje dat nu voor je ligt. Daarom dit dankwoord, bedoeld voor iedereen die zich aangesproken voelt.

Allereerst zou ik graag Roel en Geert bedanken voor de ondersteuning gedurende mijn verblijf in de photonics groep en om me de kans te geven het onderzoek te doen dat tot dit doctoraat geleid heeft. Het jarenlange werk om de structuur te creëren waarin, een nu toch wel al serieus aantal doctoraatsstudenten onderzoek heeft kunnen verrichten, heeft, alvast voor mij, zijn vruchten afgeworpen. Een doctoraat zonder een promotor is natuurlijk onmogelijk. Daarom zou ik Geert nog eens extra willen bedanken voor de vele raad en suggesties die me, doorheen de jaren, toch steeds dat ietsje dichterbij de eindmeet brachten.

Bij vijf jaar doctoreren horen ook een heleboel collega's en anekdotes. De één bleef wat langer hangen dan de ander maar elk verdient toch zijn plaats hier. Mijn tocht in de wereld van de fotonica begon voor mij gedurende mijn thesis onder begeleiding van Jan, die me door zijn begeesting en enthousiasme liet proeven van wat, achteraf gezien, nog zou komen. Met Dries maakte ik het STOLAS verhaal mee wat me deed kennismaken met het gebeuren van de project vergaderingen, milestones en deliverables. Vanaf de eerste bureau die ik bevolkte met Hendrik (hij leerde zijn volk meten waarvoor, naast alle andere dingen, heel veel dank), Wouter, Ilse, Günther, Mingshan en Marko tot mijn huidige werkplek, waarin ik doorheen de jaren het gezelschap mocht genieten van onder andere Stijn, Joost, Kristof, Jos, Dumon, Gino, Joris, Katrien en Joris was het steeds een weliswaar rustige maar toch leuke

boel. Koen, veel succes met het verdere avontuur in het flip-flop universum. Sam, de man samen met wie ik wellicht het meest tijd gesleten heb in de meetkamer, bedankt, niet alleen voor de vele (meet)hulp maar eveneens voor het fijne gezelschap in die anders toch wel eenzame uren, tussen de torens van de WAV-SOA setup.

Koffie drinken is een verslaving. Het is zelfs zo erg dat ik die er normaal gezien geen drink toch steeds maar weer richting de dagelijkse koffiepauze werd gezogen om te luisteren naar de droge mopjes van Peter, de levendige discussies over interessante en frequent toch ook wel totaal oninteressante zaken of om gewoon een chocolaatje mee te pikken. De afwezigen hebben ongelijk en de aanwezigen: bedankt. Tot slot bedankt aan alle collega's, die ik niet allemaal bij naam noem uit gezonde schrik er onderweg iemand bij te vergeten. Het was plezierig werken, ook al waren de geplande en ongeplande uitstapjes na het werk nog net iets plezanter natuurlijk. Verder ook nog een grote merci aan de mensen die ons het leven als doctoraatsstudent op INTEC toch wel een heel stuk gemakkelijker maken: Karien, Ilse, Bernadette, Ilse, Kristien en Luc.

Iwould also like to thank Jakob, Filip and Salvador for their help during my stays at COM and UPV. Thanks to you the experimental part of my work got a huge boost. Special thanks also to Thomas for helping me to better understand the theoretical background of the flip-flop.

Naast werken dient er ook nog tijd te zijn voor vrije tijd. Direct na het werk werd die gevonden in, het ondertussen reeds ter ziele gegane, TDC United. Van een triestig clubke tot een kampioenenploeg en terug, maar vooral een leuk tijdverdrijf. Merci mannen (Tibi, Jos, Gino, Geert, Günther, Dumon, Johan ...). Diederik, bedankt om samen met mij in de Mustang doorheen Californië en omstreken te willen rijden en me in Stanford rond te leiden. Veel succes in Nepal en waar je daarna ook heen trekt. De mannen (en hun (ex)-vrouwen) uit het middelbaar: Koen, Pieter, Gerd, Bjorn en David later aangevuld met Michaël, steeds leuk om nog eens te palaveren over wat was en nog moet komen tijdens de BBQ's. De mensen die al het langst meegaan zijn die uit mijn scoutsjaren in Wondelgem: Mich, Mot, Bram, Maja, Stefaan, Sofie, Jake en Ineke om er maar een paar te noemen. De rest weet ook wel wie ze zijn. Hopelijk blijven onze "sjorringen" altijd even stevig.

En dan zijn er nog die mensen die me steunden in alles wat ik ondernam, mijn ouders. Papa en mama bedankt om me vrij te laten in mijn keuzes maar me toch door jullie raad de goede richting uit

te sturen. Dat ik nog veel mag langskomen om mee te eten of om gewoon eens een bezoekje te brengen. Pieter, bedankt voor de jaren thuis (vooral de laatste dan samen op "onze" zolder), maar natuurlijk ook daarna. Spelletjes spelen of een Leffeke drinken zijn toch wel leuker in gezelschap dan alleen. Verder wens ik jou en Leen veel succes en plezier in mei en daarna. Last but certainly not least, Sabine dank je om met mij samen te leven, me te doen lachen, me te motiveren... Ik zie je graag, nu en nog een hele tijd langer.

De groeten iedereen en tot in den draai.

Wouter D'Oosterlinck
Gent, 15 november 2007

Samenvatting - Summary

Nederlandstalige Samenvatting

Volledig optisch pakket geschakelde netwerken worden vooropgesteld als de toekomstige telecommunicatie netwerken, die kunnen voldoen aan de immense bandbreedte vereisten die een gevolg zijn van de enorme en continue groei van het Internet en de toepassingen erop. Het dataverkeer in zulke netwerken is verdeeld in afzonderlijke data pakketten of combinaties van data pakketten waaraan een hoofding, gewoonlijk met een lagere bit snelheid, is toegevoegd. Aangezien enkel de hoofding wordt behandeld in de tussentijdse knooppunten kunnen deze netwerken transparant zijn met betrekking tot de bit snelheid en de codering van de data zelf. Bovendien kan een hoge transmissie efficiëntie en snelheid bereikt worden. De kleine afmetingen van een volledig optisch knooppunt in vergelijking met een elektro-optisch knooppunt is eveneens het vermelden waard.

Eén van de basis componenten in pakket geschakelde volledig optische netwerken is de (volledig) optische flip-flop. Een optische flip-flop maakt het mogelijk een pakket te schakelen naar een ander (golflengte) kanaal afhankelijk van de hoofding van het pakket. De volledig optische flip-flop schakelt op basis van het resultaat van de verwerking van de hoofding van het pakket in het knooppunt. Het uitgangsvermogen van de flip-flop wordt dan typisch gebruikt als pomp signaal voor een golflengte omzetter. Afhankelijk van de uitgang van de flip-flop wordt het vertraagde data pakket dan overgezet naar een andere golflengte of onveranderd doorgelaten. Op basis van de golflengte van het datasignaal kan dan de verdere schakeling van de data gebeuren met behulp van golflengte selectieve elementen.

Andere componenten vereist in toekomstige volledig optische netwerken zijn onder andere (2R) regeneratoren en golflengte omzeters. Golflengte omzeters kunnen gebruikt worden om signalen over te zetten

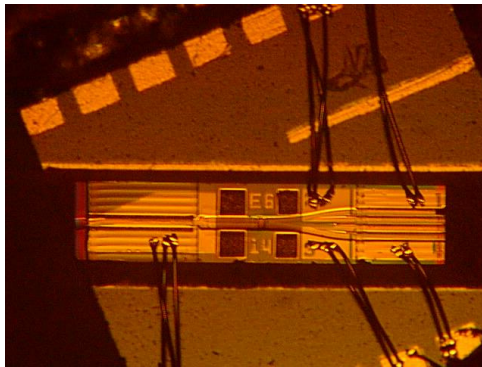
van 1 golflengte kanaal naar een ander met als doel de routing van de signalen door een netwerk te vereenvoudigen evenals opstoppingen in het netwerk te vermijden. 2R regeneratie van optische signalen is vereist omdat signalen in optische netwerken onderhevig zijn aan verschillende degradatie mechanismen zoals de toevoeging van ruis, overspraak en de verzwakking van het signaal.

In dit werk wordt vooral aandacht besteed aan het gebruik van een terugkoppelingsschema, bestaande uit een halfgeleider optische versterker (SOA) en een laser diode, als een volledig optische flip-flop. Daarnaast wordt ook het gebruik van de component als een volledig optische 2R regenerator of golflengte omzetter bestudeerd. Het werkingsprincipe van deze component is gebaseerd op de interactie tussen het laservermogen en een constant ingangssignaal dat geïnjecteerd wordt in de SOA. Deze interactie vindt plaats in zowel de laser diode als de SOA. De optische terugkoppeling tussen de twee signalen leidt, in combinatie met de niet lineaire verandering van de winst in zowel de laser diode als de SOA, veroorzaakt door het laser- en ingangsvermogen, tot bistabiel gedrag van de component in bepaalde gevallen.

In een eerste stadium werd een analytisch model voor een halfgeleider optische versterker ontwikkeld. Dit model werd gebruikt voor zowel de statische als dynamische beschrijving van het gedrag van een SOA. De kwalitatieve resultaten die behaald werden met dit model tonen een goede overeenkomst met resultaten bekomen door een numerieke oplossing van de standaard lopende golf tempo vergelijkingen. Ook bij vergelijking met experimentele resultaten en resultaten uit de literatuur werd een goede kwalitatieve overeenkomst geconstateerd.

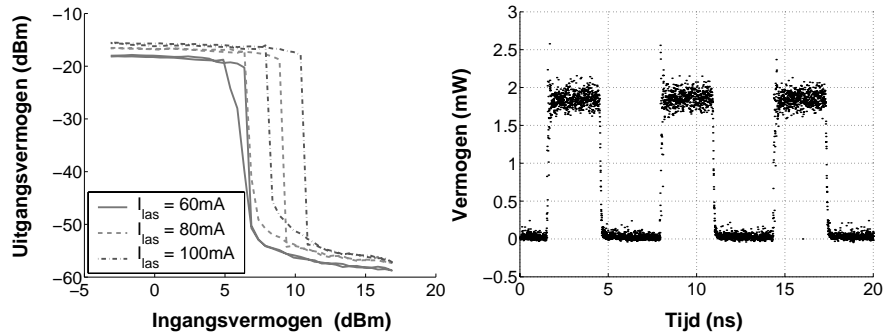
Gebruik makend van de analytische beschrijving van een SOA, in combinatie met een model gebaseerd op tempo vergelijkingen die het gedrag van een halfgeleider laser diode beschrijven, werd de werking van het terugkoppeling schema, bestaande uit een halfgeleider optische versterker en een laser diode onderzocht. Op basis van dit theoretische model werd aangetoond dat de component bistabiel gedrag vertoont voor bepaalde combinaties van aandrijf stromen, koppelingsverhoudingen en ingangsvermogen. De voorwaarde voor het optreden van het bistabiel gedrag als functie van de koppelingsverhoudingen tussen de laser diode en de SOA, het ingangsvermogen en de aandrijfstromen van de laser diode en de SOA werd afgeleid. Er werd aangetoond dat de breedte, hoogte en positie van het bistabiele gebied kan gevarieerd worden als functie van de bedrijfsparameters van

de component. Volledig optische flip-flop werking werd theoretisch gedemonstreerd, gebruik makend van de dynamische set van tempo vergelijkingen corresponderend met de component. De invloed van de puls energie die gebruikt wordt om de component te schakelen werd onderzocht. Op basis daarvan werd vastgesteld dat er een minimale puls energie benodigd is om te schakelen tussen de verschillende stabiele toestanden. Ook werd gevonden dat er een bovenwaarde voor de schakel energie bestaat om snelle en geleidelijke volledig optische flip-flop werking te kunnen garanderen.



Figuur 1: Foto van de component gebruikt in de metingen van de werking van de SOA en DFB laser diode combinatie. Van links naar rechts kunnen de SOA, de MMI-koppelaar en de DFB laser diode onderscheiden worden.

De bistabiliteit die waargenomen werd in de combinatie van een SOA en een DFB laser diode werd verder onderzocht met behulp van een commercieel software pakket en experimenten. Bij de experimenten werd gebruik gemaakt van een component bestaande uit een SOA en een array van 4 laser diodes die door middel van een 1x4 koppelaar met elkaar verbonden zijn. Een foto van de component is te zien in Figuur 1. Bistabiele werking van de component werd gedemonstreerd voor een golflengte bereik van het ingangssignaal van meer dan 25nm. Dit grote golflengte werkingsgebied maakt dat een enkele component bruikbaar is voor verschillende golflengtekanalen. Dit reduceert de complexiteit maar ook de kost van volledig optische netwerken gevoelig. De statische werking van de component als functie van de het ingangsvormogen is te zien in de linkse grafiek in Figuur 2 voor verschillende aandrijfstromen van de laser diode. De aandrijfstroom van de SOA is 120mA.



Figuur 2: Links: statische respons van het laser uitgangsvermogen als functie van het ingangsvermogen voor verschillende aandrijfstromen voor de laser diode en een aandrijfstroom voor de SOA van 120mA. Rechts: Volledig optische flip-flop werking in het laser uitgangsvermogen. De lengte van de pulsen is 100ps en het CW ingangsvermogen is 0.5dBm. De set en reset puls energie is respectievelijk 340fJ and 240fJ.

Dynamische werking van de component werd experimenteel aangetoond voor een golflengtebereik van tenminste 10nm. De evolutie van de minimale energie, vereist om de flip-flop te schakelen, als functie van de lengte van de pulse en het CW ingangsvermogen toont, in combinatie met de afhankelijkheid van de volledig optische flip-flop werking van de puls energie aan, dat de component zeer robuust is ten opzichte van variaties in de pulse lengte of energie en het CW ingangsvermogen. Dit maakt de component zeer geschikt voor gebruik in reële netwerkomgevingen waar deze parameters kunnen variëren in de tijd.

De extinctieverhouding van de flip-flop uitgang is quasi onafhankelijk van veranderingen in de werkingsomstandigheden. De schakeltijden daarentegen zijn zeer afhankelijk van de lengte van de pulsen die gebruikt worden om de flip-flop te schakelen. Schakeltijden (set zowel als reset) van 50ps and set to set (of reset tot reset) werking met een herhalingsfrequentie van 1.25GHz werden gedemonstreerd. Set en reset energieën lager dan 1pJ werden aangetoond. Door 2 DFB laser diodes tegelijk aan te sturen kon gelijktijdige werking van de flip-flop bij verschillende golflengtes bereikt worden met zeer lage set en reset puls energieën van respectievelijk 340fJ en 240fJ voor 100ps lange pulsen. Een voorbeeld van volledig optische flip-flop werking is te zien in de rechtse grafiek in Figuur 2.

De uitvoerige karakterisatie van de volledig optische flip-flop voorgesteld in dit werk toont zowel de robuustheid van de component als de uitstekende werk omstandigheden, vooral wat betreft de minimaal vereiste puls energie, aan.

Het gebruik van de component als volledig optisch beslissingselement en golflengte omzetter werd eveneens onderzocht. Er werd aangetoond dat de component bruikbaar is als 2R regenerator. Een verbetering van de extinctieverhouding met 7dB voor NRZ signalen met een bitsnelheid van 10Gbit/s in zowel transmissie als reflectie mode werd behaald. BER metingen toonden aan dat een verbetering van de gevoeligheid van de ontvanger vooralsnog niet behaald kon worden met deze component. Door de koppeling van en naar de component te verbeteren is het waarschijnlijk toch mogelijk betere resultaten te bekomen.

Volledig optische golflengte omzetting werd gedemonstreerd aan een bitsnelheid van 2.5Gbit/s. Zowel een verbetering van de extinctieverhouding met 11dB als een verbetering van de gevoeligheid van de ontvanger met 3dB voor een BER van 10^{-9} werd aangetoond.

Als besluit kan gesteld worden dat de component, voorgesteld in dit werk, kan gebruikt worden voor verschillende toepassingen. De belangrijkste daarvan is het gebruik als volledig optische flip-flop, waarbij zeer lage schakel energieën, gecombineerd met een grote robuustheid ten opzichte van veranderende werk omstandigheden vastgesteld werden. De component kan gebruikt worden als bouwblok in volledig optische pakket geschakelde knooppunten of in andere netwerk elementen waar de vraag naar korte of lange termijn volledig optische geheugen elementen bestaat.

Summary

All-optical packet or burst switched networks have been proposed as the future telecommunication networks able to cope with the massive bandwidth requirements resulting from the huge and continuous growth of the Internet and its services. The data streams in these networks are divided in individual packets or combinations of packets (burst) on which a header (usually with a lower bitrate) is attached. Because only the header is processed in the intermediate nodes, these networks can be data format and bitrate transparent. Furthermore a high transmission efficiency and high data rate operation can be obtained. Also worth to mention is the low footprint of an all-optical node as compared to an electro-optical node.

One of the key components in packet or burst switched all-optical networks is the all-optical flip-flop, which makes it possible to switch the packet to a different (wavelength) channel depending on the header of the packet. The all-optical flip-flop is switched or not, depending on the result of the processing of the header in the node. The output power from the flip-flop is thereby typically used as the continuous wave input signal for a wavelength converter. The delayed packet information can then be wavelength converted or not depending on the state of the all-optical flip-flop.

Other components needed in future all-optical networks include all-optical (2R) regenerators and wavelength converters. Wavelength converters are used to transfer signals from 1 wavelength channel to another in order to aid in the routing of the signal through the network or to avoid congestion in the network. 2R regeneration is required because signals suffer from several degradation mechanisms when traveling through the network, such as noise addition, crosstalk and attenuation.

This work concentrated on the use of a feedback scheme consisting of a semiconductor optical amplifier (SOA) and a laser diode as an all-

optical flip-flop but also as an all-optical 2R regenerator or wavelength converter. The operation principle of this device is based on the interplay, in both the laser diode and the SOA, between the laser power and a constant input signal injected into the SOA. The optical feedback between the two signals, in combination with the non-linear change in gain in both the laser diode and the SOA, caused by the laser and input signal, leads to bistable operation of the device in certain situations.

As a first step an analytical model of a semiconductor optical amplifier was developed. This model was used for both the static and dynamic description of the behaviour of a SOA. The qualitative results obtained with this model show good agreement with results obtained using a numerical solution of the standard traveling wave rate equations. A comparison with experimental results and results found in literature also showed good qualitative agreement.

Using the analytical description of a SOA in combination with a rate equation model describing the behaviour of a semiconductor laser diode, the operation of the feedback scheme consisting of a semiconductor optical amplifier and a laser diode was studied. It was shown, based on this theoretical model, that the device is bistable for certain combinations of drive currents, coupling ratios and input power. The condition for this bistability was derived as a function of the coupling ratios between the SOA and laser diode, the input power and the drive currents of the laser diode and the SOA. It was demonstrated that the width, height and position of the bistable domain could be varied as a function of the device operating parameters. By solving the dynamic set of equations, corresponding with this device, all-optical flip-flop operation could theoretically be demonstrated. The influence of the pulse energy used to switch the device was investigated. It was shown that a minimal pulse energy was required to switch the device. In addition an upper value for the switch energy, for which fast and smooth all-optical flip-flop operation can be guaranteed, was observed.

The bistability found in a SOA and DFB laser diode pair was investigated using both a commercial software tool and experiments. For the experiments a device consisting of a SOA and an array of 4 laser diodes connected by means of a 1x4 multimode interference (MMI) coupler, as shown in Figure 3 was used. This device can, as theoretically predicted, show bistable operation for certain operating conditions in both the laser and signal output power, when a continuous wave (CW) input signal is injected into the SOA. Bistable operation was experimentally demonstrated over an input signal wavelength range of over 25nm.

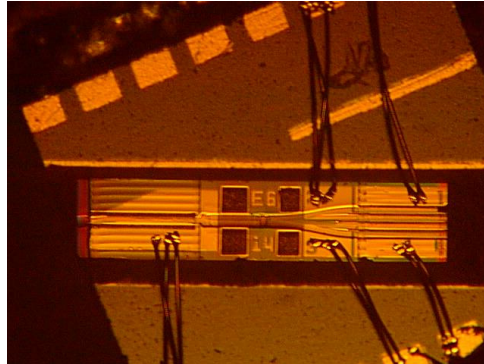


Figure 3: Picture of the device used for the experimental verification of the operation of a SOA and DFB laser diode combination. From left to right the SOA, MMI-coupler and laser diode array can be distinguished.

This makes a single device useable for several different wavelength channels reducing the complexity and cost of all-optical networks. The static operation of the device as a function of the input power is demonstrated in the left graph of Figure 4 for a SOA drive current of 120mA and different laser diode drive currents.

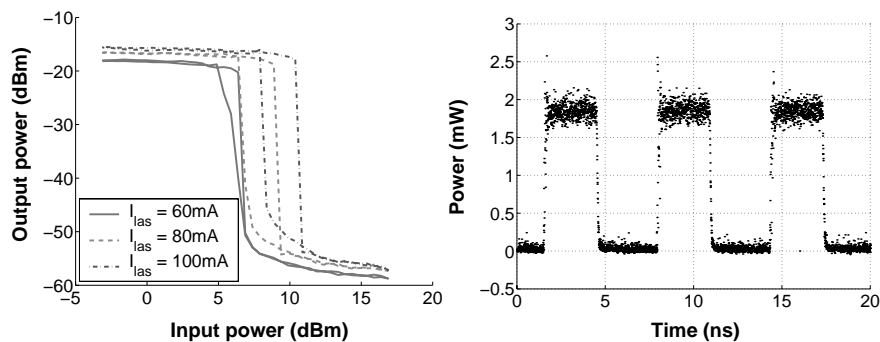


Figure 4: Left: Static response of the laser output power as a function of the input power for different laser drive currents and a SOA drive current of 120mA. Right: All-optical flip-flop operation in the laser output power. The pulse length is 100ps and the CW input power is 0.5dBm. The set and reset pulse energy is 340fJ and 240fJ respectively.

Dynamic operation of the device was experimentally demonstrated over a wavelength range of a least 10nm. The evolution of the minimal required energy, needed to obtain switching as a function of the pulse length and the CW input power showed, together with the de-

pendence of the all-optical flip-flop operation on the pulse energy, that the device is robust with respect to variations of the pulse length, pulse energy and CW input power. This makes it very suitable for use in real network environments. The extinction ratio has been shown to remain relatively constant as a function of changing operating conditions. The switch times on the other hand are highly dependent on the length of the pulses used to perform the switching. Switching times as low as 50ps and set to set (or reset to reset) operation at a repetition rate up to 1.25GHz has been demonstrated. Set and reset pulse energies have been demonstrated below 1pJ. By using two DFB laser diodes at the same time simultaneous multiple wavelength output operation can be obtained with very low set and reset pulse energies of 340fJ and 240fJ respectively for 100ps long pulses. A result of this all-optical flip-flop operation is shown in the right graph of Figure 4. The extensive characterization of the all-optical flip-flop presented in this work shows both the robustness of the device and the excellent operating conditions (primarily the required pulse energy).

The use of the device as an all-optical decision element and wavelength converter was also investigated. The device was shown to operate as a 2R regenerator with clear extinction ratio (ER) improvement up to 7dB for non-return-to-zero (NRZ) signals for a bitrate of 10Gbit/s in both transmission and reflection mode. Bit error rate (BER) measurements showed that an improvement of the receiver sensitivity could not be obtained with this device. By improving the efficiency of the coupling of light into and out of the device progress could be made in that area. All-optical wavelength conversion has also been demonstrated at a bitrate of 2.5Gbit/s showing both an ER improvement of over 11dB and a receiver sensitivity improvement of 3dB for a BER of 10^{-9} .

It can be concluded that the device discussed in this work can be used for various applications, the foremost being the use as an all-optical flip-flop, where very low switching energies in combination with a large robustness to environmental changes has been demonstrated. This device can be used as a building block of all-optical packet switching nodes or other network elements where the need arises for short or long term all-optical memory elements.

English Text

Contents

Dutch Preface	i
Dutch Summary	vii
Summary	xiii
Table of Contents	xix
1 Introduction	1
2 The semiconductor optical amplifier	13
3 Optical feedback between a SOA and a semiconductor laser diode: theoretical analysis	47
4 Bistability in a SOA and DFB laser diode feedback scheme	85
5 Dynamic analysis of an all-optical flip-flop based on a SOA and DFB laser diode	105
6 Optical decision element	149
7 Conclusions	159
List of Figures	165
List of Tables	179
Bibliography	181

Contents

Dutch Preface	i
Dutch Summary	vii
Summary	xiii
Table of Contents	xix
1 Introduction	1
1.1 Modern telecommunication	1
1.2 All-optical network	3
1.2.1 All-optical routing	4
1.2.2 Regeneration	6
1.3 Overview	7
1.4 Publications	8
2 The semiconductor optical amplifier	13
2.1 Introduction	13
2.2 Traveling wave SOA	14
2.3 Static SOA operation	15
2.3.1 SOA with bidirectional injection	17
2.3.2 SOA with unidirectional signal injection	28
2.4 Dynamic SOA operation	32
2.4.1 Theoretical analysis	33
2.4.2 Small signal analysis	37
2.4.3 Optical pulse injection	42
2.5 Conclusions	45
3 Optical feedback between a SOA and a semiconductor laser diode: theoretical analysis	47
3.1 Semiconductor laser diode	47

3.1.1	Rate equation model	48
3.1.2	External power injection	51
3.1.3	Dynamic input power dependence	52
3.2	Optical feedback between a SOA and a semiconductor laser diode	56
3.2.1	Static analysis	57
3.3	Discussion of static results	60
3.3.1	SOA drive current dependency	60
3.3.2	Laser diode drive current dependency	66
3.3.3	Input power dependency	68
3.4	Dynamic analysis	74
3.4.1	Simulation method	74
3.4.2	Steady state operation	76
3.4.3	Dynamic operation	76
3.5	Conclusions	83
4	Bistability in a SOA and DFB laser diode feedback scheme	85
4.1	Introduction	85
4.2	Simulation results	86
4.2.1	Simulation tool and setup	86
4.2.2	Origin of the bistability	88
4.2.3	Changing the coupling ratio	89
4.2.4	Input power dependence	91
4.2.5	Wavelength dependence	93
4.3	Experimental results	94
4.3.1	Device and measurement setup	94
4.3.2	SOA and laser diode drive current dependence	98
4.3.3	Input power dependence	100
4.3.4	Wavelength dependence	102
4.4	Conclusions	104
5	Dynamic analysis of an all-optical flip-flop based on a SOA and DFB laser diode	105
5.1	All-optical flip-flops	105
5.1.1	All-optical flip-flops in literature	107
5.2	Principle of operation	113
5.3	Simulation results	115
5.3.1	Setup	115
5.3.2	Static bistability domain	115
5.3.3	All-optical flip-flop operation	117

5.3.4	Pulse energy dependence	122
5.4	Experimental results	124
5.4.1	Setup	124
5.4.2	All-optical flip-flop operation	126
5.4.3	Wavelength dependence	132
5.4.4	Pulse energy dependence	138
5.4.5	Fast all-optical flip-flop operation	141
5.4.6	Simultaneous multiple wavelength output operation	143
5.5	Conclusions	145
6	Optical decision element	149
6.1	Measurement setup	149
6.2	2R-regeneration	151
6.3	Wavelength conversion	155
6.4	Conclusions	157
7	Conclusions	159
7.1	Overview and conclusions	159
7.2	Future work	162
	List of Figures	165
	List of Tables	179
	Bibliography	181

Chapter 1

Introduction

1.1 Modern telecommunication

Keeping in contact with people around the globe has never been easier than now. Thinking alone of the fact that, a mere 130 years after the invention of the telephone by Graham Bell in 1876, the number of (mobile) phones in use today exceeds 2 billion, makes the world a smaller place to live in. This massive amount of telephones creates the need for a telecommunication network that can support the millions of simultaneously made connections, in terms of connection capacity and bandwidth. Present progress in telecommunication networks is however only marginally driven by the growing telephone traffic. The main driving force behind the ever increasing call for bandwidth is the explosive growth of the internet, and more in particular the increase of high bandwidth applications such as video broadcasting websites like Youtube. The growth of the internet can be observed from Figure 1.1 where the estimated number of hosts in the internet is shown. The total number of users connected to the internet is currently even estimated at over 1 billion [1].

The underlying telecommunication network that delivers the bandwidth currently needed has grown from point to point telegraph connections, over the first transatlantic connection based on copper wire (established in 1866) to a tightly meshed telecommunication network based on electrical (coax) links. The demonstration of the laser in 1960 [3] together with the realization of relatively low loss optical fibers [4] led, especially from the eighties onward, after improvements on both the laser and fiber performance, to a shift towards optical networks. A typical single mode optical fiber nowadays has a bandwidth potential

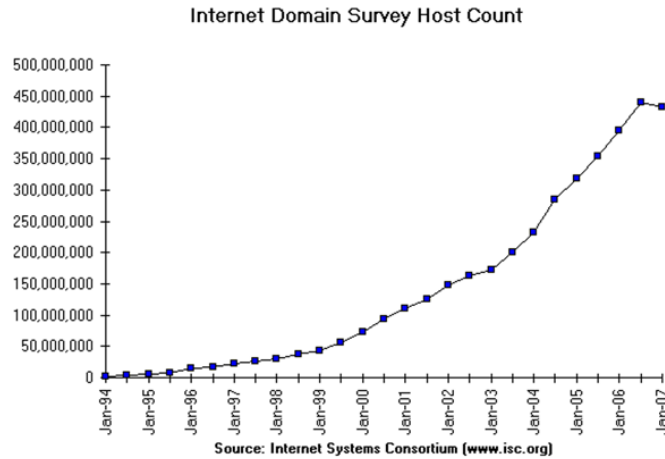


Figure 1.1: Estimated number of hosts in the internet as a function of time [2]

of about 25THz as compared to a typical bandwidth of a coax cable of about 750MHz. When the full bandwidth of an optical fiber could be used this would result in a very high amount of data transmittable through the fiber. The 25THz theoretical bandwidth of an optical fiber corresponds to the 200nm wide wavelength region around the most used telecom wavelengths of $1.3\mu\text{m}$ and $1.55\mu\text{m}$. In the low propagation loss regions found in this wavelength span the loss can be as low as 0.1-0.2dB/km allowing for optical signals to propagate over hundreds of kilometers. The complete available bandwidth of an optical fiber can however not be exploited due to the lack of suitable sources and optical amplifiers in certain wavelength spans in the low propagation loss region of the optical fiber.

By using wavelength division multiplexing (WDM) multiple signals, coming from different sources, can be transported on separate wavelength channels in an optical fiber, thereby increasing the data throughput of that fiber [5, 6, 7, 8]. As the high cost of installing a new optical fiber is mostly caused by the labor costs associated with the cabling itself, adding new wavelength channels on an already existing optical fiber link can greatly reduce the cost of a bandwidth upgrade in a network.

At present the optical links are still primarily limited to the high-capacity point-to-point-transmission connections between network nodes in long-haul backbone networks. In each inner network node the different wavelength channels present in the optical fiber are demultiplexed

(split) and separately converted to the electrical domain before being processed by electronic routers. After processing of the different signals they are again converted to the optical domain and multiplexed before being sent further down the network. One can immediately see that this approach is time consuming and requires a large amount of high-speed electronics to handle the signals, resulting in an electronic bottleneck in the network. A better approach would be to perform all the signal processing in the optical domain without conversions to the electrical domain. Several configurations for these so called all-optical networks have already been investigated [9, 10]. In order to come to a real implementation of an all-optical network all the functionalities, such as routing, buffering and error correction, needed in a network, need to be implemented in the optical domain.

In the following section a simple all-optical packet or burst switched network architecture is demonstrated. Some basic devices and operations needed in such a network are described.

1.2 All-optical network

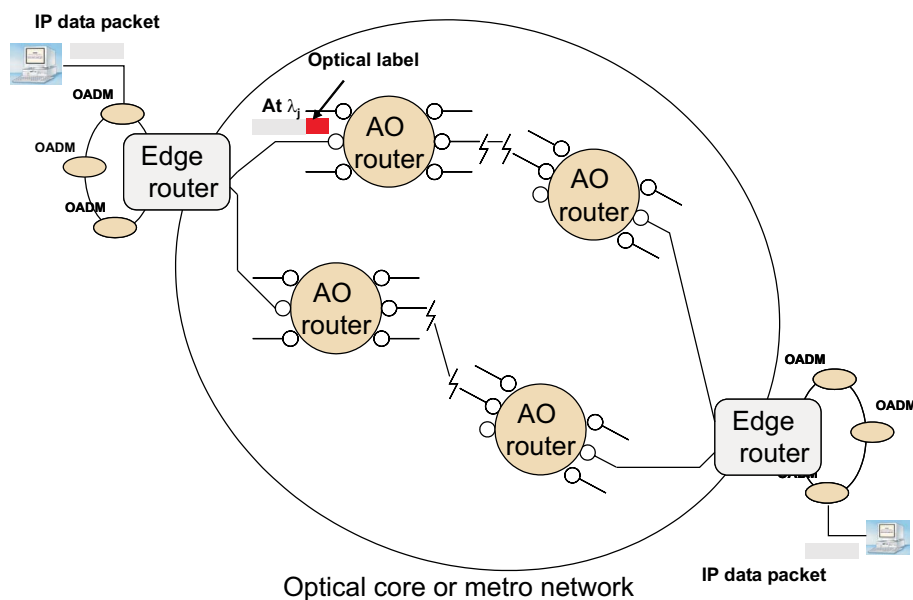


Figure 1.2: Schematic view of a simple all-optical network. IP: internet protocol. OADM: Optical add-drop multiplexer. AO: All-optical.

As mentioned above, all-optical networks are networks where all data operations are performed in the optical domain. An example of a very simple all-optical switched network is shown in Figure 1.2. In a packet or burst (combination of packets) switched network the data is divided in packets or burst of packets which are routed through the network independently. Two packets or packet bursts between the same input and output of the network do not necessarily follow the same path. The path a packet or burst of packets has to follow can depend on the current state of the network and network links, including amongst others the traffic load. When an IP data packet needs to be sent over the network, the electronic data is first transferred to an optical carrier. A header is added to the data packet, which contains the information needed to route the packet through the network. The optical signal is then added to a local area fiber ring by means of an add-drop multiplexer. Each user on the local fiber ring can have a designated wavelength at which to receive and send packets. The local area fiber ring is, through an edge router, connected to the optical metro or core network where the actual routing of the packets takes place, by means of point-to-point connections between all-optical routers, based on the data found in the header of the packets. In the case, where the start and end point of the packet are located on the local fiber ring the packet can get wavelength converted in the edge router immediately and does not have to travel through the core network. When the packet reaches the edge router corresponding to the end point of the connection the packet is transferred, with the appropriate wavelength, to the fiber link. At the add-drop multiplexer corresponding to the end point the optical packet is dropped from the fiber link and converted back to the corresponding electrical packet.

1.2.1 All-optical routing

When a data packet or a burst of packets arrive in an intermediary node the data needs to be routed towards the next node on the path to the output point of the packet. This routing can be done based on the wavelength of the packets by using arrayed waveguide gratings (AWG) [11, 12]. When the routing of a packet is based on the header of the packet the routing can be performed as shown in Figure 1.3.

The incoming packet is split in two parts by means of a splitter. One part is used for header processing and routing, while the other part is buffered using an optical delay line [13, 14] until the routing

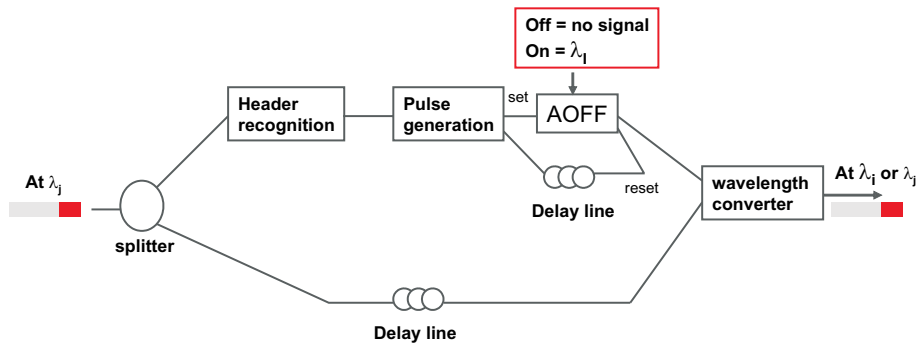


Figure 1.3: Schematic representation of an all-optical packet switch.

of the packet can take place. In the header processing unit the address information in the header of the packet is compared to a predefined list of addresses [15, 16, 17, 18]. Depending on the outcome of the header processing a pulse is generated that can switch the state of an all-optical flip-flop.

An all-optical flip-flop is a device that can operate in one of two (or more) stable optical output states for the same operating conditions. The output state of the device is based on the history of the device and can be changed by injecting optical set or reset pulses into the device. A general overview of different all-optical flip-flops will be given in chapter 5. When a pulse is generated, resulting from a decision in the header processing, it is split along two different paths. The set pulse is used to switch the device from the off state to the on state. In the on state the flip flop emits power at a wavelength different from the wavelength of the packet, which will be used for the routing of the packet. In the off state the device emits no power. After the routing of the packet has taken place the delayed part of the original pulse can then switch the all-optical flip-flop off again.

Using the output of the all-optical flip-flop as the pump power in an all-optical wavelength converter [19, 20] the part of the packet that has been buffered by means of an optical delay line can be transferred to another wavelength channel. When using an AWG switch fabric to route the appropriate wavelength channels inside the optical switch to the correct output ports the routing of the packet in the intermediary node is completed.

Of course the simple network architecture shown in Figure 1.2 is but one of the different approaches that can be used to come to all-optical

networks [21, 22, 23]. In this work a new type of all-optical flip-flop is presented that can be used as part of an all-optical switch as shown in Figure 1.3.

1.2.2 Regeneration

An optical network can suffer from a lot of impairments that can drastically reduce the capacity of the system to transport information. The main system impairments are for instance: attenuation, frequency drift, amplified spontaneous emission, reflections, inter-channel crosstalk, cross phase modulation, self phase modulation, four-wave mixing, polarization mode dispersion and gain variations in optical amplifiers. All these mechanisms lead to a decrease in signal quality for a signal traveling in the network making the detection of the correct signal at the receiver side harder.

Optical signal regeneration has been investigated for over a decade now. Since then, one typically makes a distinction between 2R regeneration (including re-amplification and reshaping) and 3R regeneration (with retiming in addition to the 2R functionality). So far, all-optical regeneration has mainly been investigated for application in high-capacity core networks and the emphasis therefore has been on 3R regeneration (of mainly RZ-coded signals).

Full 3R regeneration is however not always necessary as has been shown recently [24].

Various optical 2R regenerators have been presented over the years and two important groups can be distinguished, the fiber based components and the photonic integrated components. The fiber based components such as the semiconductor laser amplifier loop optical mirror (SLALOM) [25] or the non-linear optical loop mirror (NOLM) [26] are typically very fast but are quite difficult to fabricate due to the long fiber lengths. Integrated devices on the other hand are easier to fabricate, even in large quantities, but are usually not as fast as the fiber based components. Most of these integrated devices are based on interferometric schemes incorporating SOAs although results have also been reported on other devices e.g. devices using saturable absorbers [27]. The integrated interferometric schemes are capable of obtaining steep decision characteristics [28, 29] and high-speed operation up to 40 Gbit/s and beyond [30, 31] but unfortunately rarely at the same time. In addition to that, these devices also suffer from the influence of local environmental changes like temperature and pressure on their

non-linear behaviour and therefore require tight control. Furthermore it is rather hard to make these device polarization independent since both the gain and the refractive index depend on the polarization of the input signal(s).

What is really needed is a robust optical 2R regenerator, which gives a very sharp decision characteristic for a broad range of signal formats, bitrates and wavelengths and is independent of the input polarization. In this work such a decision element based on a DFB laser diode integrated with a semiconductor optical amplifier (SOA) is demonstrated.

1.3 Overview

In this section a short overview of the work presented in this thesis is given.

As could be seen from the introduction above, a lot of functionalities must be implemented in an all-optical form to come to true all-optical networks. Two basic elements used to build the needed all-optical signal processing devices are the semiconductor optical amplifier (SOA) and the semiconductor laser diode. In this thesis the interaction between these 2 devices is theoretically and experimentally investigated. When a SOA and a laser diode are mutually and optically connected to one another strong optical feedback between the laser output power and the signal input power can be observed. This makes the device useable as an all-optical flip-flop and an optical decision element.

Since the SOA is the basic element of this research an analytical approach of the SOA traveling wave rate equations is given in chapter 2. This simple approximative static and dynamic model allows for a qualitative study of the behaviour of a SOA. Both numerical and experimental measurements are done to verify the validity of the model.

Using the SOA model developed in chapter 2 in combination with the standard laser rate equations the behaviour of a SOA and laser diode optical feedback scheme is analyzed. It is theoretically shown that this scheme can exhibit bistable operation and can be used as an (all-optical) flip-flop.

Using different integrated devices together with a commercial simulation tool the static and dynamic behaviour of a SOA and DFB laser diode feedback scheme is extensively investigated in chapter 4 and 5. The behaviour of the device has been studied for different operating conditions and measurement setups. In chapter 5, a short overview of

various all-optical flip-flops and their properties will be given to allow comparison with the results obtained in this work.

In chapter 6 it is experimentally shown that under certain operating conditions the device used as an all-optical flip-flop can also be used as an optical decision circuit and 2R regenerator at bitrates up to 10Gbit/s. Wavelength conversion at bitrates up to 2.5Gbit/s is also demonstrated.

Concluding remarks as well as some thoughts about possible future work in this field are presented in chapter 7.

1.4 Publications

The results obtained within this work have been published in various papers and were presented at various conferences. This paragraph gives an overview of the publications. They can also be found in the publications section of the photonics research group website: <http://photonics.intec.ugent.be>. These publications may be downloaded for personal use only. For any other use, the permission of the copyright owner (usually the publisher of the journal) must be obtained.

The following papers have been published in international peer reviewed journals:

1. K. Huybrechts, W. D'Oosterlinck, G. Morthier, R. Baets, "All-Optical Flip-Flop Operation using a single Distributed Feedback Laser Diode," *IEEE Photonics Technology Letters*, accepted for publication
2. W. D'Oosterlinck, F. Öhman, J. Buron, S. Sales, A. Pérez Pardo, A. Ortigosa-Blanch, G. Puerto, G. Morthier, R. Baets, "All-Optical flip-flop operation using a SOA and DFB laser diode optical feedback combination," *Optics Express*, 15(10), p.6190-6199, May 2007.
3. W. D'Oosterlinck, J. Buron, F. Öhman, G. Morthier, R. Baets, "All-Optical Flip-Flop Based on an SOA/DFB-Laser Diode Optical Feedback Scheme," *IEEE Photonics Technology Letters*, 19(7), p.489-491, April 2007.
4. W. D'Oosterlinck, G. Morthier, R. Baets, T. Erneux, "Optical Bistability in a Traveling-Wave SOA Connected to a DFB Laser Diode: Theory and Experiment," *IEEE Journal of Quantum Electronics*, 42(8), p.739-746, August 2006.

5. W. D'Oosterlinck, G. Morthier, R. Baets, M. Smit, "Very steep optical thresholding characteristic using a DFB laser diode and an SOA in an optical feedback scheme," *IEEE Photonics Technology Letters*, 17(3), p.642-644 February 2005.

The following papers have been presented at international conferences and are published in the conference proceedings:

6. W. D'Oosterlinck, G. Morthier, R. Baets, "Sub-pJ and simultaneous multiple wavelength switching of an all-optical flip-flop based on a DFB-LD with integrated SOA," ECOC 2007.
7. G. Morthier, W. D'Oosterlinck, K. Huybrechts, "All-optical flip-flops based on DFB laser diodes and DFB-arrays," invited paper International Conference on Optical, Optoelectronic and Photonic Materials and Applications (ICOOPMA07), London, 30 July - 3 August, 2007.
8. W. D'Oosterlinck, A. Pérez Pardo, A. Ortigosa-Blanch, G. Puerto, S. Sales, G. Morthier, R. Baets, "1.25GHz repetition rate operation of a SOA-DFB laser diode based all-optical flip-flop," CLEO Europe 2007, Germany, p.CD6-2 June 2007.
9. K. Huybrechts, W. D'Oosterlinck, G. Morthier, R. Baets, "Optical flip-flop operation using an AR-coated distributed feedback laser diode," CLEO 2007, JWA36, United States, May 2007.
10. W. D'Oosterlinck, J. Buron, F. Öhman, G. Morthier, R. Baets, "First experimental demonstration of a SOA/DFB-LD feedback scheme based all-optical flip-flop," CLEO 2007, United States, p.CFM1, May 2007.
11. M. Chacinski, W. D'Oosterlinck, M. Isaksson, G. Morthier, R. Schatz, "Widely Tunable Wavelength Conversion 10 Gb/s Using a Modulated Grating Y-Branch Laser Integrated with an Optical Amplifier," OFC 2007, United States, p.JThA34, 2007.
12. W. D'Oosterlinck, G. Morthier, R. Baets, T. Erneux, "Simulation of the switching of an All-Optical Flip-Flop based on a SOA/DFB-Laser diode Optical Feedback Scheme," 2006 International conference on Photonics in Switching, Greece, p.paper O1.3, 2006.

13. G. Morthier, W. D'Oosterlinck, S. Sales, "Numerical study of ultra-high speed wavelength conversion using a Gain-Clamped SOA in combination with optical filtering," 2006 International conference on Photonics in Switching, Greece, p.paper O3.2, 2006.
14. W. D'Oosterlinck, G. Morthier, R. Baets, T. Erneux, "Optical Bistability in a SOA/DFB-LD Feedback Scheme," Conference on Lasers and Electro-Optics/Quantum Electronics and Laser Science Conference and Photonic Applications Systems, United States, p.CMD5, 2006.
15. G. Morthier, W. D'Oosterlinck, S. Verspurten, "The non-linear behaviour of laser diodes integrated with semiconductor optical amplifiers," ICTON 2005 (invited), 2, Spain, p.102-107, 2005.
16. W. D'Oosterlinck, S. Verspurten, G. Morthier, R. Baets, M. Smit, "Experimental Demonstration at 10Gbit/s of a 2R-Regenerator Based on the Mutual Optical Feedback between a laser diode and an SOA," IPRA 2005, United States, p.IMC 2, 2005.
17. W. D'Oosterlinck, G. Morthier, R. Baets, "A new optical decision circuit based on optical feedback between a laser diode and a semiconductor optical amplifier," Proceedings Symposium IEEE/LEOS Benelux Chapter, Belgium, p.17-20, 2004.
18. G. Morthier, S. Verspurten, W. D'Oosterlinck, "Interferometric photonic circuits for optical signal processing," The 88th OSA Annual Meeting, Frontiers in Optics 2004, Laser Science XX, Collocated with Diffractive Optics and Micro-Optics and Optical Fabrication and Testing Topical Meetings (FiO/LS and DOMO/OF&T 2004), United States, p.FThU3, 2004.
19. W. D'Oosterlinck, G. Morthier, R. Baets, "Demonstration of optical thresholding from a semiconductor optical amplifier coupled to a laser diode," Proceedings of the 30th European Conference on Optical Communication (ECOC 2004), 3, Sweden, p.598-599, 2004.
20. W. D'Oosterlinck, G. Morthier, "Ultra-sharp optical decision characteristic from a laser diode integrated with a semiconductor optical amplifier," Proceedings of the OSA Topical Meetings (Optical Amplifiers and Their Applications Integrated Photonics Research), United States, p.JWB9 (1-3), 2004.

The following papers have been presented at local symposia:

21. W. D'Oosterlinck, "All-optical flip-flop employing a DFB-SOA optical feedback scheme," 7th UGent-FirW Doctoraatssymposium, interactive poster session, Belgium, p.paper nr. 17, 2006.
22. W. D'Oosterlinck, "A new all optical decision circuit based on feedback between a laser diode and a semiconductor optical amplifier," 6th UGent-FirW Doctoraatssymposium, Belgium, p.37 (paper nr. 25), 2005.

Chapter 2

The semiconductor optical amplifier

In this chapter the semiconductor optical amplifier (SOA) will be theoretically described. Starting from the standard traveling wave SOA rate equations (section 2.2) an analytical expression is derived describing the SOA output power(s) as a function of the input power(s). This is done for both the static (section 2.3) and the dynamic case (section 2.4). A comparison will then be made with the numerical solutions, obtained from the standard rate equations, as well as with experimental results, obtained with a commercially available device.

2.1 Introduction

The semiconductor optical amplifier has emerged as a key component in various aspects of all-optical telecommunication networks. Due to the large gain for modest injection currents and the highly non-linear response, a semiconductor optical amplifier is very suitable as a part of various all-optical signal processing devices such as all-optical regenerators [32, 33], all-optical wavelength converters [34, 35], all-optical switches [36, 37], ... In contrast to fiber amplifiers they can also be used for on-chip amplification when used on a photonic integrated circuit, thus leading to smaller (and cheaper) devices.

Because of the importance of the SOA, as a building block for a multitude of signal processing devices, the need for proper simulation tools or methods, to describe the operation of a SOA, has led to a large num-

ber of modeling tools to simulate the static and/or dynamic behaviour of a semiconductor optical amplifier [38, 39, 40, 41, 42, 43, 44, 45].

Since the SOA is a key element in this research a simple to use static and dynamic model has been developed based on the traveling wave equations. This model can be used as a first step in the theoretical study of future SOA based devices.

2.2 Traveling wave SOA

A traveling wave semiconductor optical amplifier is a Fabry Perot laser diode type of device with anti-reflection coated facets that reduce the power reflectivity at these facets to below 10^{-4} . This extremely low reflectivity allows one to neglect the influence of reflections in the theoretical analysis of this type of SOA's. Due to the low facet reflectivity the normal lasing condition for Fabry Perot (FP) type laser diodes ($g_{th} = \alpha - \frac{1}{2L} \ln(R_l R_r)$, with R_l and R_r being the power reflectivity of the left and right hand side facet of the SOA respectively) is much harder to fulfill. This allows for a much higher current injection as compared to FP laser diodes and therefore also a much higher obtainable optical gain in the SOA. Because of the higher gain for a signal injected into the SOA the power inside the SOA can grow rapidly while traveling from the input to the output, leading to a big asymmetry in the power distribution inside the SOA. In its turn this asymmetry in the power distribution leads to a big difference in carrier depletion at both sides of the SOA, resulting in a strong spatial hole burning effect in the SOA. The normal laser rate equations need to be expanded with a term accounting for this longitudinal dependence of the carrier density inside the SOA. This leads to the so called traveling wave SOA equations, which are given by [46]

$$\frac{\partial P^+}{\partial z} + \frac{1}{v_g} \frac{\partial P^+}{\partial t} = (g(N) - \alpha_i) P^+ \quad (2.1)$$

$$-\frac{\partial P^-}{\partial z} + \frac{1}{v_g} \frac{\partial P^-}{\partial t} = (g(N) - \alpha_i) P^- \quad (2.2)$$

$$\pm \frac{\partial \phi^\pm}{\partial z} + \frac{1}{v_g} \frac{\partial \phi^\pm}{\partial t} = -\frac{\alpha}{2} g(N) \quad (2.3)$$

Due to the higher (possible) injected current into a SOA the average carrier density can be significantly higher than in FP semiconductor laser diodes. Since the generated spontaneous emission in a semi-

conductor optical waveguide can be described as being proportional to the square of the carrier density ($\sim BN^2$, with B the bimolecular recombination constant [47]) and because the amplification in a SOA is relatively high, the total amplified spontaneous emission (ASE) power level can be rather high. In the following analysis it is assumed that the input signal is sufficiently large as to dominate the ASE generated inside the SOA. For that reason (and for simplicity) the influence of ASE is neglected which might lead to a slight overestimation of the gain in the SOA. In the following analysis ultrafast gain nonlinearities such as carrier heating and spectral hole burning are neglected, which is a good approximation as long as the modulation frequency at which the SOA is used remains relatively low (below something like 20GHz). The carrier rate equation used is given by [47]

$$\frac{\partial N}{\partial t} = \frac{I}{qV} - \frac{N}{\tau_c} - \frac{g(N)}{\hbar\omega_0 wd} (P^+ + P^-) \quad (2.4)$$

The modal gain g is defined by

$$g(N) = \Gamma a(N - N_0) \quad (2.5)$$

The forward and backward traveling powers are given by P^+ and P^- respectively while ϕ is the phase of the forward and backward propagating signal. The carrier density is given by N . The other parameters used are given in Table 2.1 along with some typical values.

By numerically solving equations 2.1 to 2.5 the response of a SOA to different input signals can be obtained. To account for the longitudinal dependence of the carrier density (and gain) equations 2.1 and 2.2 are usually solved in a concatenation of small sections of the SOA. In these small sections the carrier density is assumed to be constant. Seeing that this approach takes the solution of a set of 3 partial differential equations in each section, which may be time consuming, the following paragraphs provide an analytical approximation of these equations. Both the static and dynamic response of the SOA will be treated.

2.3 Static SOA operation

A traveling wave SOA can be fully described by the equations 2.1 to 2.5 and the input and output power at both the left hand side and the right hand side facet. Figure 2.1 shows the convention made here for these input and output powers.

Parameter	Typical value	Description
v_g	$8.33 \times 10^7 \text{ m s}^{-1}$	Group velocity
α_i	$2000 - 4000 \text{ m}^{-1}$	Effective loss coefficient
α	3-5	Linewidth enhancement factor
I	0.05-0.3A	Injection current
q	$1.6 \times 10^{-19} \text{ C}$	Elementary charge
V	$w \times d \times L$	Volume of the active layer
w	$1 - 2.5 \times 10^{-6} \text{ m}$	Active layer width
d	$0.1 - 0.3 \times 10^{-6} \text{ m}$	Active layer thickness
L	$300 - 1500 \times 10^{-6} \text{ m}$	Device length
τ_c	$100 - 300 \times 10^{-12} \text{ s}$	Spontaneous carrier lifetime
$\hbar\omega_0$	$1.28 \times 10^{-19} \text{ J}$	Photon energy
Γ	0.3-0.45	Confinement factor
a	$2.7 \times 10^{-20} \text{ m}^2$	Differential gain coefficient
N_0	$1 \times 10^{24} \text{ m}^{-3}$	Transparency carrier density

Table 2.1: Explanation of the parameters in the equations used to describe the traveling wave SOA.

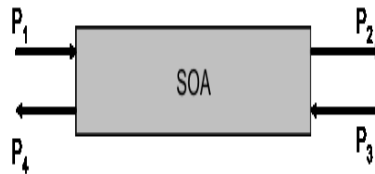


Figure 2.1: Schematic view of the SOA and the various input and output signals.

P_1 is the power injected into the SOA from the left hand side ($P^+(0)$), P_3 is the power injected into the SOA from the right hand side ($P^-(L)$). P_2 is the right hand side output power ($P^+(L)$) and P_4 is the left hand side output power ($P^-(0)$).

The steady state SOA equations for the forward and backward intensities P_{\pm} and the carrier density N are given by:

$$\frac{\partial P_+}{\partial z} = (g(N) - \alpha_i) P_+ \quad (2.6)$$

$$\frac{\partial P_-}{\partial z} = -(g(N) - \alpha_i) P_- \quad (2.7)$$

$$0 = \frac{I}{qV} - \frac{N}{\tau_c} - \frac{g(N)}{\hbar\omega_0 wd} (P_+ + P_-) \quad (2.8)$$

From the equations above one can distinguish two separate cases with respect to the input signals, a state where both the input signal at the left hand side facet and the input signal at the right hand side facet are different from zero (bidirectional SOA) and a state where one of the two input powers is zero (unidirectional SOA). These two cases will be discussed separately below.

2.3.1 SOA with bidirectional injection

Theoretical analysis

When light is injected into a SOA from both the left hand side and the right hand side the SOA can be described by Equations 2.6-2.8. From dividing Equation 2.6 and Equation 2.7 it can be directly noted that $\frac{\partial P_+}{\partial z} / \frac{\partial P_-}{\partial z} = -P_+ / P_-$, implying that in the static analysis

$$P_+(z) P_-(z) = C \quad (2.9)$$

C is an arbitrary constant yet to be determined. Using (2.9) we may eliminate P_+ from (2.8). The carrier density rate equations can then be rewritten as a function of the backward propagating power.

$$0 = (g_0 - g) - \frac{g}{P_{sat}} \left(P_- + \frac{C}{P_-} \right) \quad (2.10)$$

The new parameters g_0 , I_0 and P_{sat} , which respectively correspond to the unsaturated gain of the SOA, the injection current needed to

reach transparency and the input saturation power of the SOA, are given by

$$g_0 = \Gamma a N_0 \left(\frac{I}{I_0} - 1 \right) \quad (2.11)$$

$$I_0 = \frac{q V N_0}{\tau_c} \quad (2.12)$$

$$P_{sat} = \frac{\hbar \omega_0 w d}{\Gamma a \tau_c} \quad (2.13)$$

From (2.10) the modal gain g can be determined as

$$g = \frac{g_0}{1 + \frac{\left(P_- + \frac{C}{P_-} \right)}{P_{sat}}} \quad (2.14)$$

Substituting (2.14) into (2.7) we obtain

$$\frac{\partial P_-}{\partial z} = - \left(\frac{g_0 P_- - \alpha_i \left(P_- + \frac{(P_-^2 + C)}{P_{sat}} \right)}{P_- + \frac{(P_-^2 + C)}{P_{sat}}} \right) P_- \quad (2.15)$$

This equation is separable and can be integrated as

$$\int_{P_3}^{P_-} \frac{P + \frac{P^2 + C}{P_{sat}}}{P \left(g_0 P - \alpha_i \left(P + \frac{P^2 + C}{P_{sat}} \right) \right)} dP = - \int_L^z dz \quad (2.16)$$

The integral in the left hand side is solvable using the partial fraction method. To this end, the integral is rewritten as

$$\frac{P_{sat}}{\alpha_i} \int_{P_3}^{P_-} \frac{P + \frac{P^2 + C}{P_{sat}}}{P \left(P^2 - P P_{sat} \left(\frac{1}{\theta} - 1 \right) + C \right)} dP = \int_L^z dz \quad (2.17)$$

where $\theta \equiv \frac{\alpha_i}{g_0}$. The denominator of the fraction in equation 2.17 consists of a term P and a quadratic function of P . It is assumed that the quadratic function admits two real roots. This is the case if θ is sufficiently small (which is true when the unsaturated gain g_0 is large as compared to the internal losses α_i). This condition is generally met in a SOA under normal operating conditions. The two roots of the quadratic function are denoted by $P = P_a$ and $P = P_b > P_a$. The

solutions of the quadratic function in the denominator of Equation 2.17 can be found as

$$P_{a,b} = \frac{P_{sat} \left(\frac{1}{\theta} - 1 \right) \pm \sqrt{P_{sat}^2 \left(\frac{1}{\theta} - 1 \right)^2 - 4C}}{2} \quad (2.18)$$

For small θ these roots can be approximated as

$$P_a = \frac{C\theta}{P_{sat}} \quad \text{and} \quad P_b = \frac{P_{sat}}{\theta} \quad (2.19)$$

Rewriting the integrand in Equation 2.17 using the solutions of the quadratic function yields

$$\frac{P + \frac{P^2+C}{P_{sat}}}{P[P^2 - PP_{sat}(\frac{1}{\theta} - 1) + C]} = \frac{A}{P} + \frac{B}{P - P_a} + \frac{D}{P - P_b} \quad (2.20)$$

The numerators in the right hand side of Equation 2.20 can be found as

$$\begin{aligned} A &= \frac{1}{P_{sat}} \\ B &= \frac{P_a + \frac{P_a^2+C}{P_{sat}}}{P_a(P_a - P_b)} = \frac{\frac{1}{\theta}}{P_a - P_b} = -\frac{1}{\sqrt{P_{sat}^2(1-\theta)^2 - 4C\theta^2}} \\ D &= \frac{P_b + \frac{P_b^2+C}{P_{sat}}}{P_b(P_b - P_a)} = \frac{\frac{1}{\theta}}{P_b - P_a} = -B \end{aligned} \quad (2.21)$$

Assuming $P_a < P_- < P_b$ (actually stating that the denominator of the integrand is different from zero), the integral from Equation 2.17 becomes

$$\begin{aligned} \int^{P_-} \frac{P + \frac{P^2+C}{P_{sat}}}{P(P^2 - PP_{sat}(\frac{1}{\theta} - 1) + C)} dP &= \int^{P_-} \frac{A}{P} + \frac{B}{P - P_a} - \frac{B}{P - P_b} dP \\ &= A \ln(P_-) + B \ln(P_- - P_a) \\ &\quad - B \ln(P_- - P_b) \end{aligned} \quad (2.22)$$

Solving this equation leads to

$$\frac{P_{sat}}{\alpha_i} \left[A \ln\left(\frac{P_-}{P_3}\right) + B \ln\left(\frac{P_- - P_a}{P_3 - P_a}\right) - B \ln\left(\frac{P_b - P_-}{P_b - P_3}\right) \right] = (z - L) \quad (2.23)$$

Using the condition $P_+P_- = C$ at the left and right hand side of the SOA a solution of the respective SOA output powers can be found as a function of the input powers. At $z=0$ we obtain

$$P_1P_4 = C \quad (2.24)$$

while at $z=L$,

$$P_2P_3 = C \quad (2.25)$$

In order to determine an equation for P_4 alone, Equation 2.23 is evaluated at $z = 0$ where $P_- = P_4$ resulting in

$$\frac{P_{sat}}{\alpha_i} \left[\begin{array}{l} A \ln \left(\frac{P_4}{P_3} \right) + B \ln \left(\frac{P_4 - P_a}{P_3 - P_a} \right) \\ - B \ln \left(\frac{P_b - P_4}{P_b - P_3} \right) \end{array} \right] = -L \quad (2.26)$$

By using (2.21) this can be rewritten as

$$\frac{P_{sat}}{\alpha_i} \left[\begin{array}{l} \frac{1}{P_{sat}} \ln \left(\frac{P_4}{P_3} \right) + \frac{g_0}{\alpha_i(P_a - P_b)} \ln \left(\frac{P_4 - P_a}{P_3 - P_a} \right) \\ + \frac{g_0}{\alpha_i(P_b - P_a)} \ln \left(\frac{P_b - P_4}{P_b - P_3} \right) \end{array} \right] = -L \quad (2.27)$$

Using (2.18) the left hand side output power can be completely written as a function of the device parameters and an equation for P_4 as a function of the input powers P_1 and P_3 can be obtained.

$$\frac{P_{sat}}{\alpha_i} \left[\begin{array}{l} \frac{1}{P_{sat}} \ln \left(\frac{P_4}{P_3} \right) \\ g_0 \ln \left(\frac{P_4 - \frac{P_{sat} \left(\frac{g_0}{\alpha_i} - 1 \right) - \sqrt{P_{sat}^2 \left(\frac{g_0}{\alpha_i} - 1 \right)^2 - 4P_1P_4}}{2}}{P_3 - \frac{P_{sat} \left(\frac{g_0}{\alpha_i} - 1 \right) - \sqrt{P_{sat}^2 \left(\frac{g_0}{\alpha_i} - 1 \right)^2 - 4P_1P_4}}{2}} \right) \\ - \frac{\alpha_i \sqrt{P_{sat}^2 \left(\frac{g_0}{\alpha_i} - 1 \right)^2 - 4P_1P_4}}{2} \\ g_0 \ln \left(\frac{\frac{P_{sat} \left(\frac{g_0}{\alpha_i} - 1 \right) + \sqrt{P_{sat}^2 \left(\frac{g_0}{\alpha_i} - 1 \right)^2 - 4P_1P_4}}{2} - P_4}{\frac{P_{sat} \left(\frac{g_0}{\alpha_i} - 1 \right) + \sqrt{P_{sat}^2 \left(\frac{g_0}{\alpha_i} - 1 \right)^2 - 4P_1P_4}}{2} - P_3} \right) \\ + \frac{\alpha_i \sqrt{P_{sat}^2 \left(\frac{g_0}{\alpha_i} - 1 \right)^2 - 4P_1P_4}}{2} \end{array} \right] = -L \quad (2.28)$$

An analog analysis can be done for the right hand side output power P_2 resulting in

$$\frac{P_{sat}}{\alpha_i} \left[\begin{array}{l} \frac{1}{P_{sat}} \ln \left(\frac{P_2}{P_1} \right) \\ g_0 \ln \left(\frac{\frac{P_2 P_3}{P_1} - \frac{P_{sat} \left(\frac{g_0}{\alpha_i} - 1 \right) - \sqrt{P_{sat}^2 \left(\frac{g_0}{\alpha_i} - 1 \right)^2 - 4P_2 P_3}}{2}}{P_3 - \frac{P_{sat} \left(\frac{g_0}{\alpha_i} - 1 \right) - \sqrt{P_{sat}^2 \left(\frac{g_0}{\alpha_i} - 1 \right)^2 - 4P_2 P_3}}{2}} \right) \\ - \frac{\alpha_i \sqrt{P_{sat}^2 \left(\frac{g_0}{\alpha_i} - 1 \right)^2 - 4P_2 P_3}}{P_{sat} \left(\frac{g_0}{\alpha_i} - 1 \right) + \sqrt{P_{sat}^2 \left(\frac{g_0}{\alpha_i} - 1 \right)^2 - 4P_2 P_3} - \frac{P_2 P_3}{P_1}} \\ g_0 \ln \left(\frac{\frac{P_{sat} \left(\frac{g_0}{\alpha_i} - 1 \right) + \sqrt{P_{sat}^2 \left(\frac{g_0}{\alpha_i} - 1 \right)^2 - 4P_2 P_3}}{2} - \frac{P_2 P_3}{P_1}}{P_{sat} \left(\frac{g_0}{\alpha_i} - 1 \right) + \sqrt{P_{sat}^2 \left(\frac{g_0}{\alpha_i} - 1 \right)^2 - 4P_2 P_3} - P_3} \right) \\ + \frac{\alpha_i \sqrt{P_{sat}^2 \left(\frac{g_0}{\alpha_i} - 1 \right)^2 - 4P_2 P_3}}{P_{sat} \left(\frac{g_0}{\alpha_i} - 1 \right) + \sqrt{P_{sat}^2 \left(\frac{g_0}{\alpha_i} - 1 \right)^2 - 4P_2 P_3}} \end{array} \right] = -L \quad (2.29)$$

Equations 2.28 and 2.29 give a static analytical solution for the output power at the left hand side facet and at the right hand side facet of the SOA for externally injected signals at both the right and left hand side of the device respectively. They are however still quite difficult to interpret. In the special case where the modal gain is much bigger than the internal losses the losses can, as an approximation, be neglected in the above analysis, yielding

$$\ln \left(\frac{P_4}{P_3} \right) + \frac{1}{P_{sat}} \left((P_4 - P_3) - P_1 P_4 \left(\frac{1}{P_4} - \frac{1}{P_3} \right) \right) = g_0 L \quad (2.30)$$

$$\ln \left(\frac{P_2}{P_1} \right) + \frac{1}{P_{sat}} \left((P_2 - P_1) - P_2 P_3 \left(\frac{1}{P_2} - \frac{1}{P_1} \right) \right) = g_0 L \quad (2.31)$$

Results

Equations 2.30 and 2.31 are a lot simpler than equations 2.28 and 2.29 and can easily be solved numerically. In Fig. 2.2 the output power and gain for the forward and backward propagating signals is shown for various values of the internal loss coefficient α_i as a function of the right hand side injected power (P_3). The left hand side injected power (P_1) is kept constant at 0dBm in this case.

It can be noted that with decreasing internal loss the gain curve shifts to higher gain levels but the overall shape of the gain graph (as well as that of the output versus input power graph) remains the same. Using equations 2.30-2.31 instead of equations 2.28-2.29 for the static simulation of a SOA leads to an overestimation of the SOA signal gain but still gives a qualitative solution of the SOA rate equations. Due to

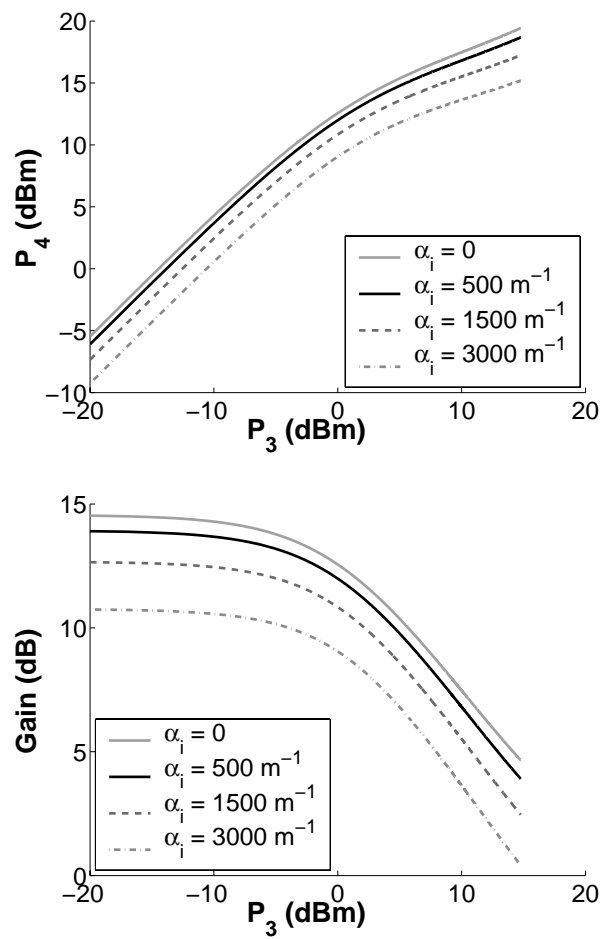


Figure 2.2: Output power (P_4) and gain for the backward propagating signal as a function of the right hand side input power (P_3) with $P_1 = 0\text{dBm}$ and $I_{SOA} = 200\text{mA}$ for different values of α_i .

their relative simplicity the lossless equations tend to lead to faster solutions and easier handling while still giving a fairly accurate description of the response of a SOA. From Figure 2.2 the normal non-linear output versus input power relation of a SOA can be observed. A linear gain region where the signal single pass gain remains constant, and a saturation region where the output power of the SOA saturates due to longitudinal spatial hole burning, resulting in a decrease of the single pass gain, can be seen.

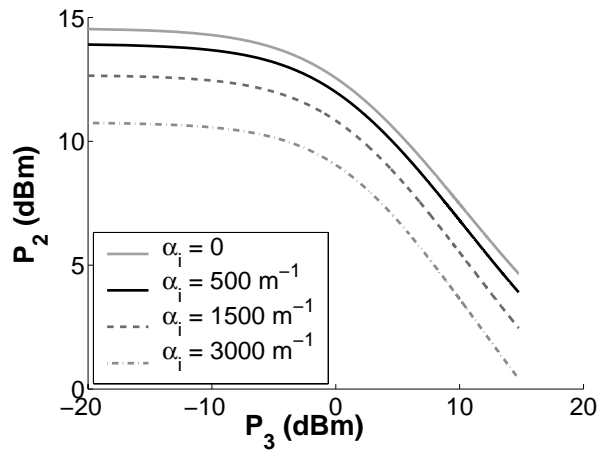


Figure 2.3: Output power (P_2) and gain for the forward propagating signal as a function of the right hand side input power (P_3) with $P_1 = 0\text{dBm}$ and $I_{SOA} = 200\text{mA}$ for different values of α_i .

When keeping the left hand side input power (P_1) constant at 0dBm , while changing the right hand side input power (P_3), the dependence of the right hand side output power (P_2) and gain can be found as shown in Figure 2.3. It can be noted that since this is the symmetrical case as in Figure 2.2 the single pass gain of the SOA is identical.

When the SOA drive current is increased from 200mA to 400mA it is obvious that the influence of the internal loss coefficient will be reduced (as can be seen in Fig. 2.4). This can be directly observed from equations 2.1-2.4. As the carrier density in the SOA is proportional to the number of injected carriers (or the drive current) and the gain is a linear function of the carrier density one can note that the relative importance of the losses is reduced.

The response of the SOA to different backward injected powers is shown in Figure 2.5. The modal gain decreases, as expected with increasing backward injected power. At the same time the (left hand

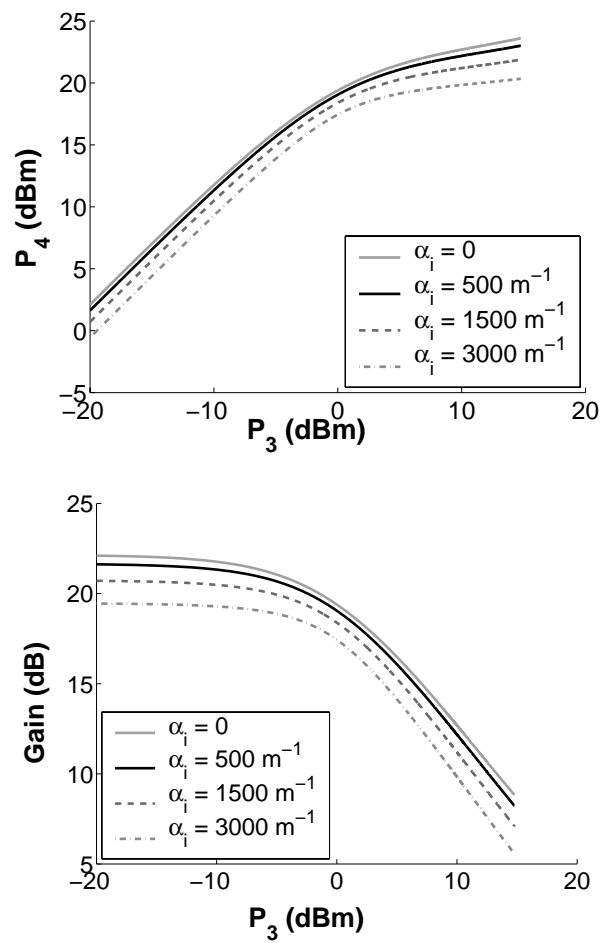


Figure 2.4: Output power (P_4) and gain for the backward propagating signal as a function of the right hand side input power (P_3) with $P_1 = 0\text{dBm}$ and $I_{SOA} = 400\text{mA}$ for different values of α_i .

side) input saturation power increases with increasing right hand side injected power. This can be explained by the fact that the longitudinal spatial hole burning, due to the right hand injected signal, causes an overall reduction of the gain in the SOA, with the highest gain reduction towards the left hand side of the SOA. The gain of the SOA is a function of the carrier density, as can be seen in Equation 2.5 and the carrier density decreases with increasing powers present in the SOA (Equation 2.8). The reduction of gain along the SOA results in less amplification of the forward propagating signal. The same forward propagating signal can still receive a linear (although reduced) gain for an increased right hand side input power, due to the fact that the signal receives less amplification at the front side (left hand side) of the device, leading to lower power levels at the right hand side of the device, which in its turn leads to less saturation near the right hand side of the device.

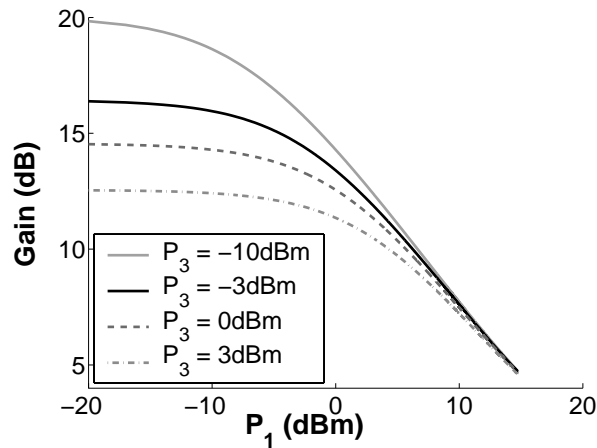


Figure 2.5: Static single pass gain of the SOA as a function of the left hand side input power (P_1) for different values of the right hand side input power (P_3).

Comparison with a numerical model

Solving the traveling wave rate equations given in 2.1-2.4 numerically allows for a comparison with the results obtained from equations 2.28 and 2.29. In Figure 2.6 the right hand side output power of the SOA (P_2) is given in both cases as a function of the right hand side input power (P_3) for different values of the internal loss α_i . The left hand side input power $P_1 = 0$ dBm and the SOA drive current $I_{SOA} = 200$ mA.

The numerical solution of the traveling wave equations was performed by dividing the SOA in 25 equal parts, in which the traveling wave equations are solved. In these sections the carrier density is assumed to be constant. This approximation is valid if the length of the sections is sufficiently short. By dividing the SOA into sections the longitudinal spatial hole burning in the device can be taken into account.

The two models lead to almost identical results, which validates the analytical solution as given above. Both the lossless and the lossy case are shown to be almost identical between the two solution methods. By increasing the number of sections used in the solution of the traveling wave equations the agreement between the different approaches can even be increased.

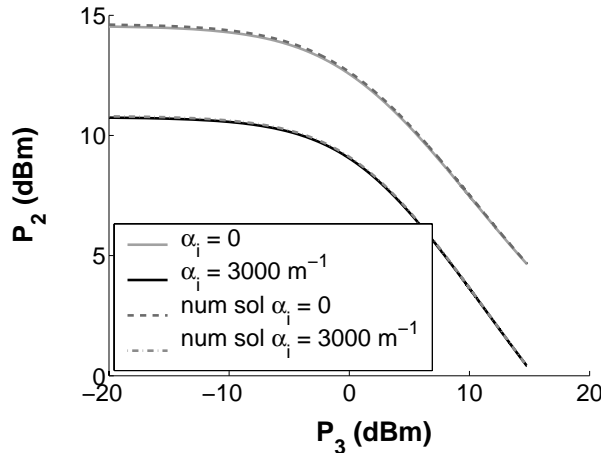


Figure 2.6: Comparison of the output power (P_2) for the forward propagating signal as a function of the right hand side input power (P_3) with $P_1 = 0\text{dBm}$ and $I_{SOA} = 200\text{mA}$ for different values of α_i . Both the solution obtained by solving equation 2.29 as the numerical solution of the traveling rate equations is shown.

In the special case where only one section is considered in the numerical solution of the lossless traveling wave equations the carrier density along the SOA is considered to be constant. The gain of the SOA can then be written as

$$g = \frac{g_0}{1 + \frac{P_{avg,+} + P_{avg,-}}{P_{sat}}} \quad (2.32)$$

The unsaturated gain g_0 and the SOA saturation power are again given by equations 2.11 and 2.13. Equations 2.1 and 2.2 can then be rewritten as

$$P_2 = P_1 e^{\left(\frac{g_0 L}{1 + \frac{P_{avg,+} + P_{avg,-}}{P_{sat}}} \right)} \quad (2.33)$$

$$P_4 = P_3 e^{\left(\frac{g_0 L}{1 + \frac{P_{avg,+} + P_{avg,-}}{P_{sat}}} \right)} \quad (2.34)$$

The average forward and backward traveling power can be found by using equations 2.1 and 2.2 as

$$P_{avg,+} = \frac{1}{L} \int_0^L P^+ dz = \frac{1}{gL} (P_2 - P_1) \approx \frac{1}{g_0 L} (P_2 - P_1) \quad (2.35)$$

$$P_{avg,-} = \frac{1}{L} \int_L^0 P^- dz = \frac{1}{gL} (P_4 - P_3) \approx \frac{1}{g_0 L} (P_4 - P_3) \quad (2.36)$$

The approximation $g \approx g_0$ can be used in situations where the gain saturation in the SOA is limited, as is the case for low (total) input powers to the SOA. Combining equations 2.33-2.34 and the approximations obtained in equations 2.35-2.36 yields

$$P_{2,4} = P_{1,3} e^{\left(\frac{g_0 L}{1 + \frac{(P_2 - P_1) + (P_4 - P_3)}{g_0 L P_{sat}}} \right)} \quad (2.37)$$

This equation can be further simplified by considering that

$$\frac{(P_2 - P_1) + (P_4 - P_3)}{g_0 L P_{sat}} < 1 \quad (2.38)$$

In that case a first order Taylor series expansion can be used, which results in

$$P_{2,4} = P_{1,3} e^{\left(g_0 L \left(1 - \frac{(P_2 - P_1) + (P_4 - P_3)}{g_0 L P_{sat}} \right) \right)} \quad (2.39)$$

This solution is exactly the same as obtained in equations 2.30 and 2.31, which follow from an analytical derivation of these equations from the traveling wave rate equations. This shows that by using the approximations above and starting from a situation with a constant carrier density the same and correct analytical solution can be obtained, although only for very low input powers for which the approximation $g \approx g_0$ holds.

Experimental results

To further validate the use of our analytical approach measurements were performed on a commercially available SOA. The measurement setup used for these static measurements is given in Figure 2.7 with the input and output powers corresponding to the above analysis. The output power of a tunable laser source is amplified by an EDFA and then passes through a variable optical attenuator used to control the input power into the SOA. Circulators at the left and right hand side of the SOA are used to split the forward and backward propagating powers.

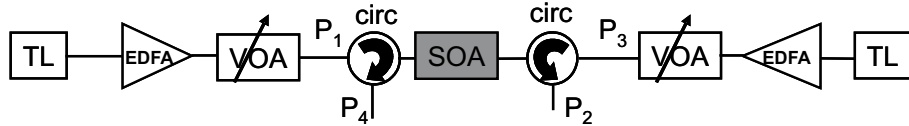


Figure 2.7: Measurement setup for the static characterization of a SOA. C TL: Tunable laser source, EDFA: Erbium Doped Fiber Amplifier, VAO: variable optical attenuator and circ: optical circulator.

In Figure 2.8 the gain of the SOA is given as a function of the left hand side input power for different current settings of the SOA. The right hand side injected input power was -1.8dBm in this case. In correspondence with Figure 2.2 and Figure 2.4 the saturation behaviour of the SOA can be observed. An increase of the modal gain with increasing SOA drive current can be seen.

When increasing the right hand side injected power a decrease of the gain accompanied with an increase of the input saturation power can be observed in Figure 2.9. This experimentally obtained results shows good agreement with the theoretically obtained results shown in Figure 2.5.

2.3.2 SOA with unidirectional signal injection

Theoretical analysis

The simplest implementation of a semiconductor optical amplifier is the one in which the SOA is used as a unidirectional single pass optical amplifier. In that case $P_1 > 0$ and $P_3 = 0$ and Equations 2.6-2.8 can be reduced to

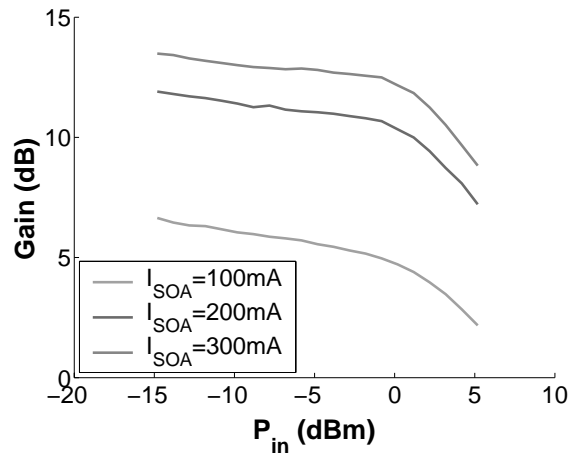


Figure 2.8: Output power (P_2) and gain for the forward propagating signal as a function of the left hand side input power (P_1) with the backward injected power (P_3) set to -1.8dBm for different values of the SOA drive current (I_{SOA}).

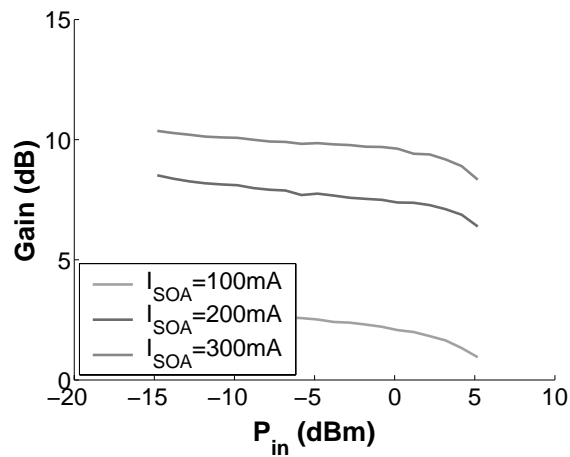


Figure 2.9: Gain of the SOA as a function of the left hand side input power (P_1) with the backward injected power (P_3) set to 1.46dBm for different values of the SOA drive current (I_{SOA}).

$$\frac{\partial P_+}{\partial z} = (g - \alpha_i) P_+ \quad (2.40)$$

$$P_+(0) = P_1 \quad (2.41)$$

$$0 = \frac{g_0 - g}{\tau_c} - \frac{g}{E_{sat}} P_+ \quad (2.42)$$

Using an analog approach as in section 2.3.1 a solution for the output power P_2 as a function of the device parameters and P_1 can be obtained.

$$\frac{1}{g_0 - \alpha_i} \ln \left(\frac{P_2}{P_1} \right) - \frac{g_0}{(g_0 - \alpha_i) \alpha_i} \ln \left(\frac{\left(\frac{g_0 - \alpha_i}{\alpha_i} \right) P_{sat} - P_2}{\left(\frac{g_0 - \alpha_i}{\alpha_i} \right) P_{sat} - P_1} \right) = L \quad (2.43)$$

Again this equation can be reduced by setting the internal losses in the SOA to zero.

$$\ln \left(\frac{P_2}{P_1} \right) + \frac{1}{P_{sat}} (P_2 - P_1) = g_0 L \quad (2.44)$$

The lossless equation can also easily be derived from Equation 2.31 by setting the right hand side injected power (P_3) to zero. Equation 2.43 on the other hand can be obtained from Equation 2.29 by taking the limit of this equation towards $P_3 = 0$.

Results

As in section 2.3.1 a comparison of the gain of the SOA as a function of the input power for different values of the internal loss factor was made. From Fig. 2.10 the same behaviour as in the bidirectional case can be observed. The signal gain of the SOA increases with decreasing internal loss but again the overall response of the SOA remains the same.

Comparison with a numerical model

Again a comparison with a numerical solution of the traveling wave rate equations is made. The result is shown in Figure 2.11. The drive current of the SOA is 200mA. Good agreement between the two solution methods can be observed. The same approximative approach, with a constant carrier density, leads to the same result as obtained in 2.44.

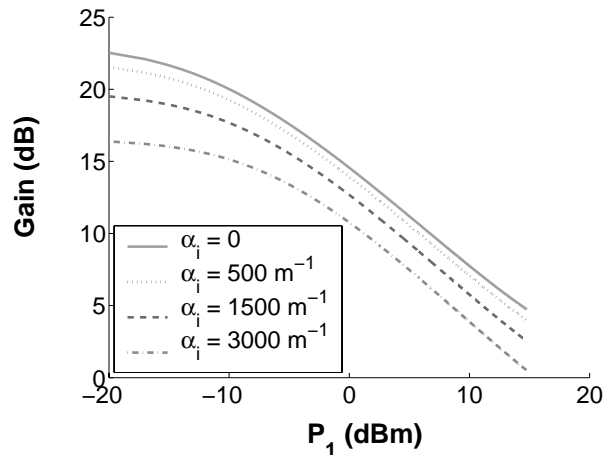


Figure 2.10: Gain of the SOA as a function of the left hand side input power (P_1) with $I_{SOA} = 200\text{mA}$ for different values of α_i .

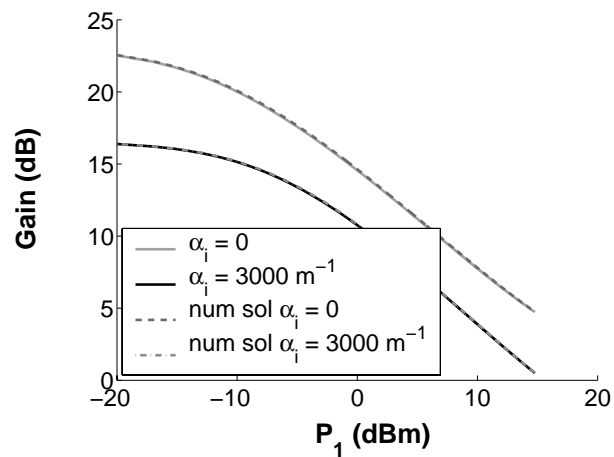


Figure 2.11: Comparison of the gain of the SOA as a function of the left hand side input power (P_1) with $I_{SOA} = 200\text{mA}$ for different values of α_i . Both the solution obtained by solving equation 2.44 as the numerical solution of the traveling rate equations is shown.

Experimental result

An experimentally obtained result, using the setup shown in Figure 2.7, is given in Figure 2.12. An increase in gain with increasing drive current can be seen as expected from the numerical results. For very high SOA drive currents gain saturation as a function of the drive current can be observed in the linear gain regime. The input saturation power however still increases with increasing drive current.

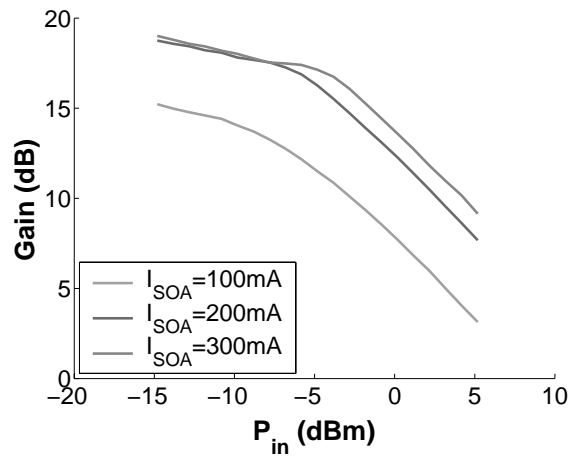


Figure 2.12: Experimentally obtained gain of the SOA as a function of left hand side input power (P_1) for different values of the SOA drive current (I_{SOA}).

From the static analysis it can be concluded that by neglecting the internal losses in a SOA the above analysis still gives a fairly good approximation of the device operation. When one is dealing with a concatenation of several devices that are all interconnected the lossless equations can, due to their limited complexity, provide a more intuitive understanding of the scheme's operation.

2.4 Dynamic SOA operation

The previous section provided an analytical solution for the static SOA rate equations, both with and without internal losses present. To fully characterize a SOA a dynamic analysis of its behaviour is also required. In this section the standard (lossless) SOA rate equations are reduced (with some approximations) to a single differential equation. As in the

treatment of the static solution of the SOA, 2 cases can again be distinguished, a bidirectional case where power is injected into both the left hand side and right hand side facets and a unidirectional case where power is only injected from one side.

2.4.1 Theoretical analysis

Bidirectional injection

Again the most general description of a semiconductor optical amplifier deals with the presence of both forward and backward propagating signals in the SOA. To simplify the dynamic analysis of the SOA the internal losses are considered to be zero. This was shown in the previous section to lead to a slight overestimation of the SOA gain, while the general behaviour of the SOA remained the same. The lossless traveling wave SOA rate equations are given by

$$\frac{\partial P^+}{\partial z} + \frac{1}{v_g} \frac{\partial P^+}{\partial t} = gP^+ \quad (2.45)$$

$$-\frac{\partial P^-}{\partial z} + \frac{1}{v_g} \frac{\partial P^-}{\partial t} = gP^- \quad (2.46)$$

$$\frac{\partial N}{\partial t} = \frac{I}{qV} - \frac{N}{\tau_c} - \frac{g}{\hbar\omega_0 wd} (P^+ + P^-) \quad (2.47)$$

with the modal gain g again defined by

$$g = \Gamma a(N - N_0) \quad (2.48)$$

Combining Equation 2.47 and Equation 2.48 results in

$$\frac{\partial g}{\partial t} = \frac{1}{\tau_c} \left(\frac{\tau_c I \Gamma a}{qV} - N_0 \Gamma a - g - \frac{g \tau_c \Gamma a}{\hbar\omega_0 wd} (P^+ + P^-) \right) \quad (2.49)$$

$$\frac{\partial g}{\partial t} = \frac{1}{\tau_c} \left(g_0 - g - \frac{g}{P_{sat}} (P^+ + P^-) \right) \quad (2.50)$$

with the unsaturated gain g_0 , the current needed to obtain transparency I_0 and the input saturation power P_{sat} defined by equations 2.10. Changing the coordinates from (z, t) to (Z, t) with $Z = \frac{z}{L}$ and L being the total length of the device yields

$$\frac{\partial P^+}{\partial Z} + \frac{L}{v_g} \frac{\partial P^+}{\partial t} = gLP^+ = GP^+ \quad (2.51)$$

$$-\frac{\partial P^-}{\partial Z} + \frac{L}{v_g} \frac{\partial P^-}{\partial t} = gLP^- = GP^- \quad (2.52)$$

$$\frac{\partial G}{\partial t} = \frac{1}{\tau_c} \left(g_0L - G - \frac{G}{P_{sat}} (P^+ + P^-) \right) \quad (2.53)$$

where $G = gL$.

In a quasi steady state approximation these equations can be reduced to

$$\frac{\partial P^+}{\partial Z} = GP^+ \quad (2.54)$$

$$-\frac{\partial P^-}{\partial Z} = GP^- \quad (2.55)$$

$$\frac{\partial G}{\partial t} = \frac{1}{\tau_c} \left(g_0L - G - \frac{G}{P_{sat}} (P^+ + P^-) \right) \quad (2.56)$$

In this approximation both the forward and backward propagating signals are considered to be varying slowly with respect to the traveling time through the SOA ($\frac{L}{v_g} \sim 5.5ps$). The time dependent character of the SOA response is then governed by the time dependence of the SOA gain (Equation 2.56). The approximation could also be used for relatively small variations of the signals, when only the influence of changing input signals on the order of a couple of transit times through the SOA are considered.

The input powers at both sides of the device are given by

$$P^+(0) = P_{(1,CW)} + P_{(1,AC)} \quad (2.57)$$

$$P^-(1) = P_{(3,CW)} + P_{(3,AC)} \quad (2.58)$$

The input powers are each split into a linear combination of their DC and AC components. The powers along the length of the device are given by solving (2.54) and (2.55)

$$P^+(Z) = P^+(0) e^{\int_0^Z G(t,Z') dZ'} \quad (2.59)$$

$$P^-(Z) = P^-(1) e^{-\int_1^Z G(t,Z') dZ'} \quad (2.60)$$

With

$$H = \int_0^1 G(t, Z') dZ' \quad (2.61)$$

(2.56) becomes after integration from 0 to 1 along the Z-coordinate

$$\begin{aligned} \frac{\partial H}{\partial t} &= \frac{1}{\tau_c} \left(g_0 L - H - \frac{1}{P_{sat}} (P^+(1) - P^+(0) - P^-(1) + P^-(0)) \right) \\ \frac{\partial H}{\partial t} &= \frac{1}{\tau_c} \left(g_0 L - H - \frac{P^+(0)}{P_{sat}} (e^H - 1) + \frac{P^-(1)}{P_{sat}} (1 - e^H) \right) \end{aligned} \quad (2.62)$$

If we define $P_{(2,CW)}$ as

$$P_{(2,CW)} = P_{(1,CW)} e^H \quad (2.63)$$

$$H = \ln \left(\frac{P_{(2,CW)}}{P_{(1,CW)}} \right) \quad (2.64)$$

Combining (2.62) and (2.63) leads to

$$\begin{aligned} \frac{\partial P_{(2,CW)}}{\partial t} &= \frac{1}{\tau_c} P_{(2,CW)} \left(g_0 L - \ln \left(\frac{P_{(2,CW)}}{P_{(1,CW)}} \right) - \frac{1}{P_{sat}} (P_{(2,CW)} - P_{(1,CW)}) \right) \\ &+ \frac{1}{\tau_c} P_{(2,CW)} \left(-\frac{P_{(1,AC)} + P_{(3,AC)}}{P_{sat}} \left(\frac{P_{(2,CW)}}{P_{(1,CW)}} - 1 \right) \right) \\ &+ \frac{1}{\tau_c} P_{(2,CW)} \left(\frac{P_{(3,CW)}}{P_{sat}} \left(1 - \frac{P_{(2,CW)}}{P_{(1,CW)}} \right) \right) \end{aligned} \quad (2.65)$$

This equation shows the dependence of the right hand side SOA output power as a function of the powers incident on the SOA. The evolution of the other output powers ($P_{(2,AC)}$, $P_{(4,CW)}$ and $P_{(4,AC)}$) can be obtained in a similar way by solving equation 2.65 for another output vs input combination. An alternative way is of course to use equation 2.63 to calculate the gain of the SOA. Using the obtained gain the respective output powers can be obtained by solving equation 2.63 for the appropriate input signal.

Unidirectional injection

When power is injected from one side only the analysis of [46] can be followed. Starting from equations 2.45 and 2.47 and by using the coordinate transformation (z, t) to (z, τ) with $\tau = t - \frac{z}{v_g}$ we obtain

$$\frac{\partial P^+}{\partial z} = gP^+ \quad (2.66)$$

$$\frac{\partial g}{\partial \tau} = \frac{1}{\tau_c} \left(g_0 - g - \frac{gP^+}{P_{sat}} \right) \quad (2.67)$$

Integrating equations 2.66 and 2.67 over the amplifier length provides

$$\frac{\partial H}{\partial \tau} = \frac{1}{\tau_c} \left(g_0 L - H - \frac{P_+(0)}{P_{sat}} (e^H - 1) \right) \quad (2.68)$$

with

$$H(\tau) = \int_0^L G(z, \tau) dz \quad (2.69)$$

Using

$$\begin{aligned} P_{2,CW}(\tau) &= P_{1,CW} e^{H(\tau)} \\ P_{2,AC}(\tau) &= P_{1,AC}(\tau) e^{H(\tau)} \end{aligned} \quad (2.70)$$

we obtain in analogy with the bidirectional case

$$\begin{aligned} \frac{\partial P_{(2,CW)}}{\partial \tau} &= \frac{P_{(2,CW)}}{\tau_c} \left(g_0 L - \ln \left(\frac{P_{(2,CW)}}{P_{(1,CW)}} \right) \right) \\ &- \frac{P_{(2,CW)}}{\tau_c} \left(\frac{1}{P_{sat}} (P_{(2,CW)} - P_{(1,CW)}) \right) \\ &- \frac{P_{(2,CW)}}{\tau_c} \left(\frac{P_{(2,CW)}}{P_{sat}} (P_{(1,CW)}) \left(\frac{P_{(2,CW)}}{P_{(1,CW)}} - 1 \right) \right) \end{aligned} \quad (2.71)$$

Since no additional assumptions regarding the time constant of the input signals was made here equation 2.71 is valid for any type of injected pulse. It can also be noted that equation 2.65 can be reduced to equation 2.71 by assuming the backward propagating signals to be equal to zero.

2.4.2 Small signal analysis

Numerical results

Using equations 2.65 and 2.71 an analysis of the dynamic behaviour of a SOA can be done, such as a small signal analysis. Figure 2.13 shows the small signal gain obtained in the counter-propagating scheme for different CW input powers. In the counter-propagating scheme a CW pump power is injected at the left hand side of the device while at the right hand side of the device a RF probe signal with an amplitude and mean value of 10% of the CW signal is injected.

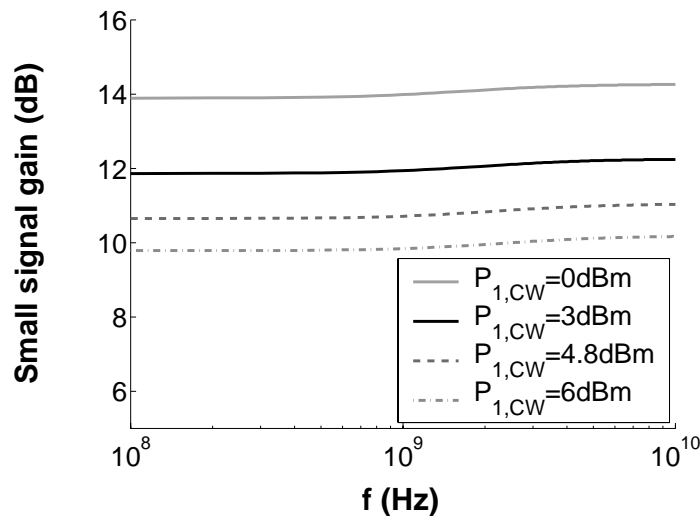


Figure 2.13: Simulated small signal gain in the counter-propagating scheme for different CW input powers and a SOA drive current of 200mA.

From Figure 2.13 it can be seen that the small signal gain in the counter-propagating scheme remains nearly constant which corresponds with results obtained elsewhere [48]. This effect might be explained by considering the fact that the small signal modulated right hand side input power first passes through the region with the highest longitudinal spatial hole burning effect. The CW signal injected into the SOA from the left hand side facet causes an asymmetric carrier distribution along the length of the SOA leading to higher gain saturation levels at the right hand side of the device. In the saturated region of the SOA the local gain is highly dependent on the input power variations. Since in the counter propagation region the amplitude of the backward propagating small signal is still relatively small at the right hand side of the

device, the influence of this modulation enhancement due to the local saturation of the SOA is limited. The small signal gain is found to be almost equal to the CW gain without the presence of the modulated small signal across the whole frequency range considered.

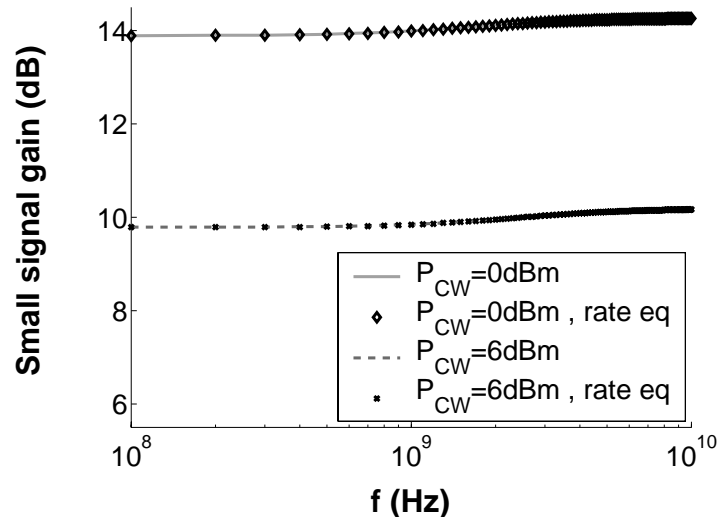


Figure 2.14: Comparison between the analytical solution of the dynamic response of a SOA and the standard traveling wave rate equation approach for the counter-propagating scheme for different CW input powers and a SOA drive current of 200mA.

In order to verify the accuracy of the analytical solution of the traveling wave SOA equations, given above, a comparison between the solution obtained with Equation 2.65, and a numerical and stepwise solution of the traveling wave SOA equations is shown in Fig. 2.14. From the figure it can be seen that the two methods to describe the small signal behaviour of the SOA provide nearly identical results. This implies that the approximations used to come to Equation 2.65 are valid.

Figure 2.15 shows the small signal response of the SOA in the co-propagation regime obtained from Equation 2.71. To come to these results the left hand side input power is modulated with a 10% modulation depth. The small signal gain is then obtained as the ratio of the output modulation amplitude to the modulation amplitude of the input signal. From Figure 2.15 the well-known high-pass characteristic of a SOA in the co-propagation regime can be observed [49, 50, 51]. The high frequency limit of the small signal gain is again the large signal CW gain without the presence of the modulation component. The

reduction in small signal gain for the lower modulation frequency can be explained by considering that in contrast to the counter-propagation regime the modulated signal is now first injected into the less saturated front side of the SOA. This initially leads to less influence of power fluctuations on the gain. As the signal progresses towards the right hand side of the SOA however both the actual power of the modulated signal and the saturation of the SOA is increased. This leads to a higher influence of the small signal variations on the local gain of the SOA, leading to a reduction of the small signal gain. For the higher modulation frequencies it again holds that the variations on the input power are averaged out with respect to the SOA gain as a result of the limited carrier lifetime (and gain recovery time) in the SOA.

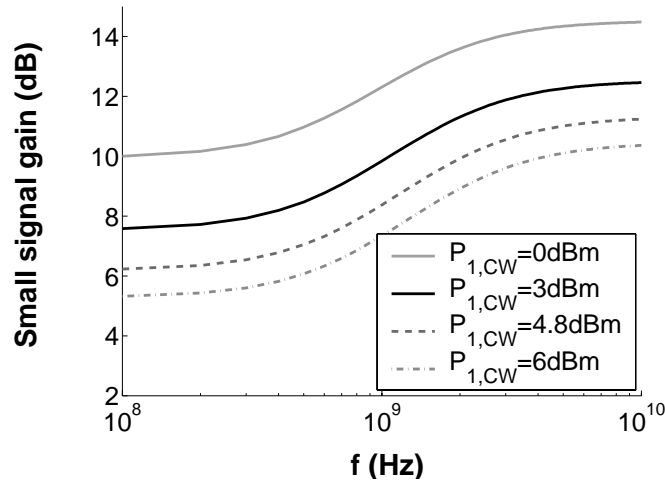


Figure 2.15: Simulated small signal gain in the co-propagating scheme for different CW input powers and a SOA drive current of 200mA.

Experimental results

As a further step to validate the use of the analytical model small signal experiments were carried out. The experimental setup used to obtain the small signal gain of a SOA in the counter-propagation regime is shown in Figure 2.16. Light from a (tunable) laser source is boosted by an EDFA and afterwards attenuated using a variable optical attenuator. This amplification and subsequent attenuation allows for tight control of the actual input power injected into the SOA as well as a broad range of SOA input powers. Using a splitter the signal is split into two, with

the larger part fed to the left hand side facet of the SOA by means of an optical circulator (used to split the forward and backward propagating signal at the left hand side facet of the SOA). The other part is modulated with a sine wave generated by a RF signal generator, with a modulation depth of 100%. The frequency of the modulation is swept to obtain the frequency dependence of the small signal gain. The mean power level of the modulated signal is adjusted using an EDFA and variable optical attenuator, to 10% of the CW (left hand side) input power. The modulated signal is then fed to the right hand side facet of the SOA. At the left hand side facet the amplified backward propagating signal can again be obtained by means of a circulator. The small signal gain in the counter propagating regime is defined here as the ratio between the amplitude of the modulation before and after passage through the SOA.

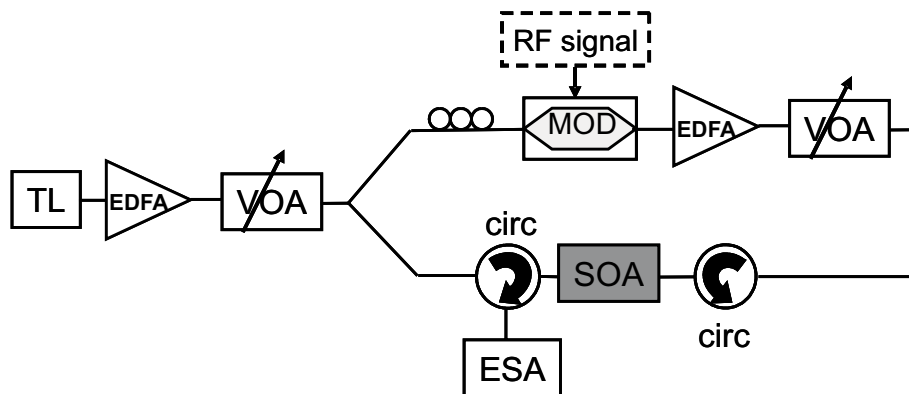


Figure 2.16: Measurement setup for the static characterization of a SOA. Used abbreviations are TL: Tunable laser source, EDFA: Erbium Doped Fiber Amplifier, VAO: variable optical attenuator and circ: optical circulator.

The experimental results shown in Figure 2.17 indicate clearly that the theoretical results obtained for the small-signal gain of a SOA in the counter propagating regime are at least qualitatively accurate. Again a nearly constant small signal gain as a function of the modulation frequency can be observed.

An experimental verification of the results obtained from Equation 2.65 is done as well. The measurement setup used for the small signal analysis in the co-propagation regime is shown in Figure 2.18. The power of the signal emitted from a (tunable) laser source is again controlled by using an EDFA and variable optical attenuator. The signal is

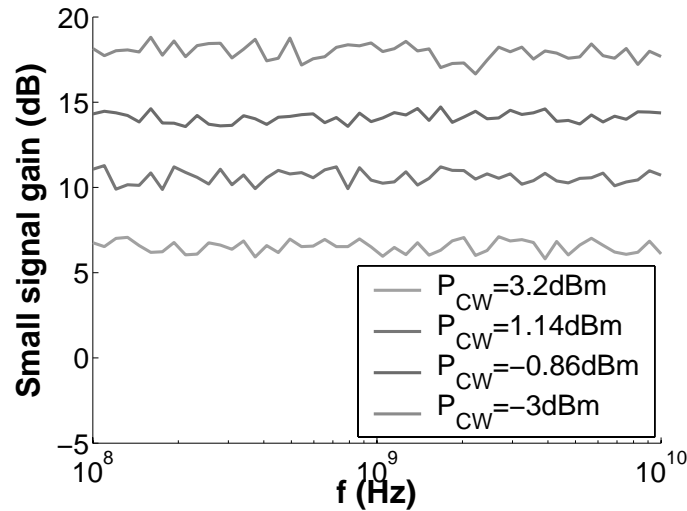


Figure 2.17: Experimentally obtained small signal gain in the counter-propagating region for different CW input powers and a SOA drive current of 300mA.

then externally modulated with a modulation depth of about 10% and fed to the left hand side facet of the laser diode. The frequency of the modulation is swept to obtain the frequency dependence of the small signal gain. After passing through the laser diode the amplitude of the modulated component is measured using an electrical spectrum analyzer and compared to the amplitude of the modulated signal at the input to obtain the small signal gain.

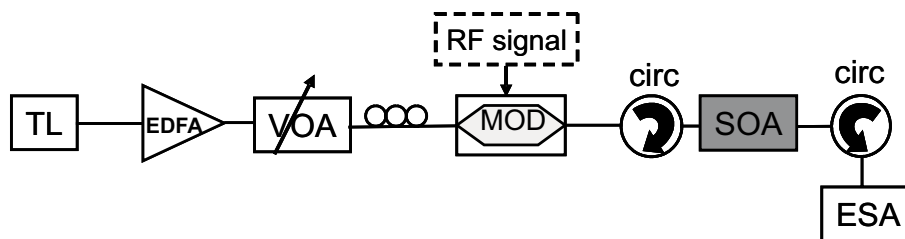


Figure 2.18: Measurement setup for the static characterization of a SOA. Used abbreviations are TL: Tunable laser source, EDFA: Erbium Doped Fiber Amplifier, VOA: variable optical attenuator and circ: optical circulator.

Some experimentally obtained small signal gain responses are shown in Figure 2.19. The same high-pass behaviour as obtained from the

theoretical analysis can be observed. This shows that at least for the small signal analysis of a semiconductor optical amplifier the analytical model, which results in Equations 2.65 and 2.71 can be used to describe the response of a SOA.

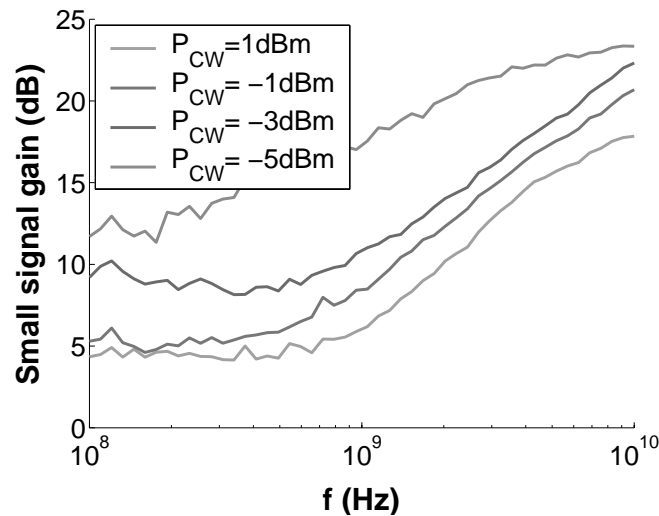


Figure 2.19: Experimentally obtained small signal gain in the co-propagating region for different CW input powers and a SOA drive current of 300mA.

2.4.3 Optical pulse injection

A special case to consider in the analysis of a SOA is when the SOA is injected with a single, short and strong optical pulse. Again, as in the small signal analysis the pulses can be injected from both sides of the SOA. When a rectangular optical pulse is injected at the same side of the CW input signal a response as in Figure 2.20 can be observed which can also be seen in [52, 53, 54]. The power of the CW input signal is 0dBm and the optical pulse is injected at $t = 1.2ns$. It can clearly be seen that initially the pulse is amplified with the CW gain present just before the pulse injection causing a step in the total output power of the SOA. Almost immediately after injection the optical pulse causes a depletion of carriers in the SOA leading to saturation and reduction of the SOA gain. As can be seen from the response to the longer (400ps) pulse the carrier depletion relaxes down to a quasi steady state value after a certain period of time (of the order of 150-200ps). When the injected pulse has passed through the SOA, the output power of the SOA drops

suddenly to a value below the steady state situation before the pulse arrival. After that the carrier density (and therefore also the gain and SOA output power) recover gradually back to their initial state. It can be noted that, when increasing the pulse power, the gain recovery time increases as well due to the higher level of carrier depletion that needs to be canceled out.

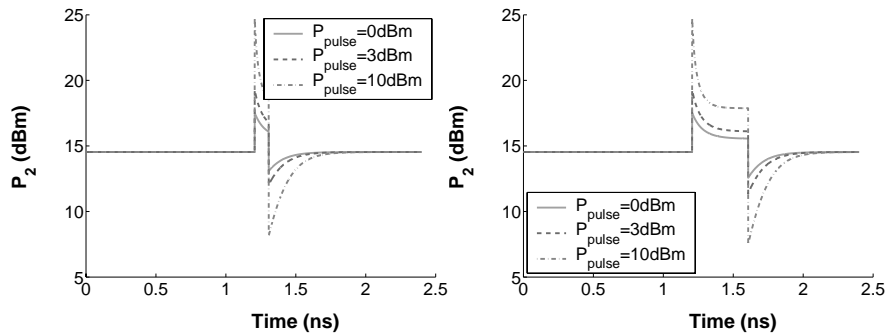


Figure 2.20: Right hand side output power (P_2) of the SOA as a function of time. The CW input power is 0dBm. A 100ps (left) and 400ps (right) long optical pulse is injected into the r.h.s. facet at $t=1.2$ ns. The SOA current is 120mA.

In the case of a short and strong optical pulse injected into the right hand side of the device the output response of the left hand side injected CW signal can be seen from Figure 2.21 in agreement with [52]. Again the power of the CW input signal is 0dBm and the rectangular optical pulse is injected into the SOA at $t = 1.2$ ns. The right hand side output power of the device immediately decreases in this case due to the carrier depletion by the injected optical pulse. Again a quasi steady state is reached after a certain time for longer pulse durations as can be seen from the case of 400ps long pulses. After the injected pulse has passed the SOA the carriers and hence the gain can recover back to the original state of before the injection of the pulse. As in the previous case, with the injection of the optical pulse in the left hand side of the SOA, the recovery time increases when the pulse power increases due to a larger hole in the carrier reservoir of the SOA.

Figure 2.22 gives a comparison between the model from Equations 2.65 and 2.71 and the numerical solution of the traveling wave SOA rate equations. Optical pulses injected from both the right and left side of the SOA are considered. A good comparison between the two models can be observed.

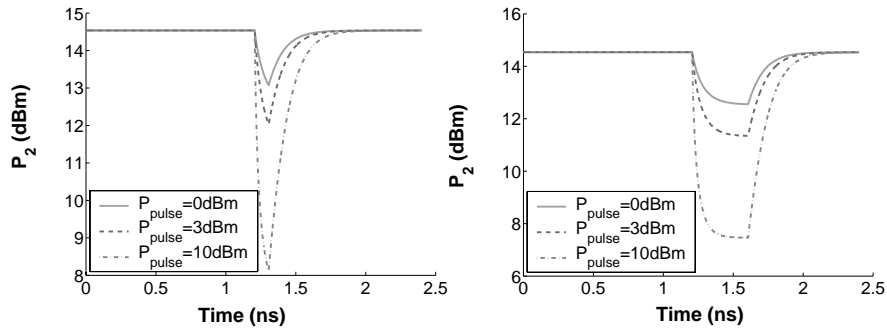


Figure 2.21: Right hand side output power (P_2) of the SOA as a function of time. The CW input power is 0dBm. A 100ps (left) and 400ps (right) long optical pulse is injected into the l.h.s. facet at $t=1.2\text{ns}$. The SOA current is 120mA.

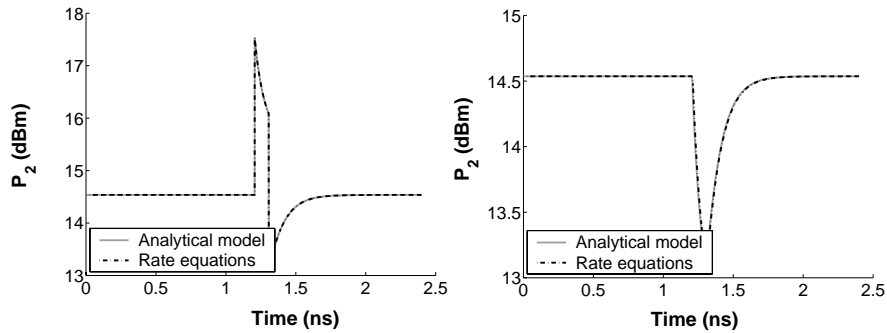


Figure 2.22: Right hand side output power (P_2) of the SOA as a function of time. The CW input power is 0dBm. A 100ps long optical pulse is injected into the l.h.s. (left) or r.h.s. (right) facet at $t=1.2\text{ns}$. The SOA current is 120mA.

Thus far the assumption has been made, in the dynamical analysis of the SOA, that the internal waveguide losses can be neglected. Figure 2.23 shows that this approximation is valid for a qualitative description of the SOA by comparing the results obtained with Equations 2.65 and 2.71, which assume a lossless SOA, and the traveling wave rate equations with an internal loss coefficient of $\frac{30}{cm}$. The same behaviour of the output power (and hence also the carrier density and gain) of the SOA can be observed when an optical pulse is injected from either side of the SOA. Again, as in the static analysis, we note that the lossless approximation of a SOA leads to an overestimation of the gain and therefore also the output power, while the temporal response remains fairly equal. This justifies the use of the lossless approximation of the SOA for a qualitative study of the static and dynamic behaviour of an SOA.

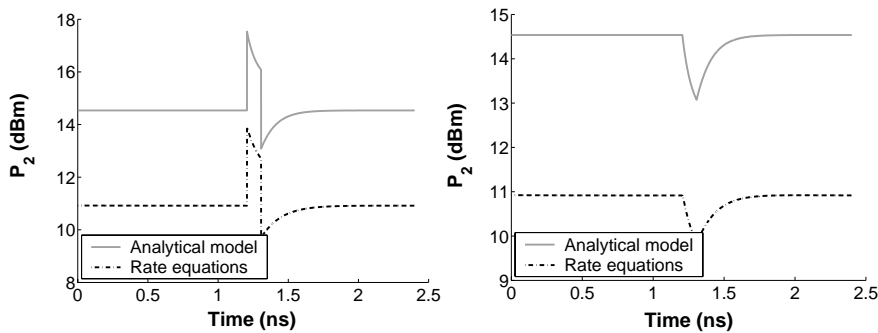


Figure 2.23: Right hand side output power (P_2) of the SOA as a function of time calculated using the lossless solution of Equation 2.65 and the traveling wave rate equations with $\alpha_i = \frac{30}{cm}$. The CW input power is 0dBm. A 100ps long optical pulse is injected into the r.h.s. (right) and l.h.s. (left) facet at $t=1.2$ ns. The SOA current is 120mA.

2.5 Conclusions

A simple to use and intuitive analytical model to describe the static and dynamic behaviour of a semiconductor optical amplifier has been developed. In order to come to this model some approximations are made, such as neglecting the amplified spontaneous emission generated in the SOA. For both the static and dynamic analysis a distinction

has been made between a SOA under bidirectional and a SOA under unidirectional injection.

In the static case an expression was found, describing the dependence of the output power as a function of the input power(s). By neglecting the internal loss of the SOA a more simplified expression could then be found. By neglecting the internal loss of the SOA the gain of the SOA is overestimated. While this leads to obvious changes in the quantitative description of the SOA, the qualitative conclusions found with this approach remain valid. This is demonstrated by means of numerical and experimental results.

For the dynamic description of a SOA the internal loss factor was neglected leading to an overestimation of the SOA gain. An analytical expression was found describing the behaviour of the output power as a function of the different input powers. Both a small signal and large signal analysis based on the developed analytical model have been made.

The model describing the static and dynamic behaviour of a SOA presented in this chapter can be used in the investigation of more complex SOA based devices, as will be shown in the following chapter.

Chapter 3

Optical feedback between a SOA and a semiconductor laser diode: theoretical analysis

From the previous chapter an analytical approximation of the standard traveling wave equations for a semiconductor optical amplifier has been obtained. In this chapter the standard rate equation model of a DFB type laser diode is approximated in the static case and combined with the obtained SOA model to yield a new analytical model to describe the static behaviour of an optical feedback scheme consisting of a semiconductor optical amplifier and a laser diode. For the dynamic study of this new concept the dynamic equation obtained for the SOA output power as a function of the different input powers can be combined with the rate equations describing a laser diode under external power injection regime.

3.1 Semiconductor laser diode

Just like semiconductor optical amplifiers are one of the key building blocks used for signal processing applications in all-optical networks, so are (tunable) semiconductor laser diodes essential for (amongst others) the transmission of data in these networks. Since the invention of the first homojunction semiconductor laser diode by Hall in 1962 [55] the development of semiconductor laser diodes has seriously taken

off, resulting in a wide range of different laser diode schemes, such as the distributed feedback laser diode (DFB) [56], the distributed Bragg reflector laser diode (DBR) [57, 58] and more complex schemes such as the sampled superstructure grating widely tunable twin guide laser diode (SSG-TTG) [59]. Over time, several models have been developed in order to simulate the behaviour of several types of laser diodes, ranging from very simple rate equation models to far more complex solutions, using for example coupled mode theory. Here the simple rate equation model will be used to describe the behaviour of a semiconductor laser diode [60, 61]. Again this solution leads to a more qualitative instead of a quantitative solution.

3.1.1 Rate equation model

In its simplest form a semiconductor optical laser diode can be formed by placing a gain medium inside an optical cavity, as shown in Figure 3.1. R_1 and R_2 represent the left hand side and right hand side facet power reflectivity, which can be wavelength dependent. A cavity can however also be formed by using a grating structure as is the case in DFB and DBR laser diodes. $P_{las,1}$ and $P_{las,2}$ are the left hand side and right hand side output power of the laser diode respectively.



Figure 3.1: Schematic view of a semiconductor laser diode.

Inside the cavity of a laser diode the dynamics of the average carrier density N in the active layer of the gain medium, and the number of photons S_{las} corresponding to the laser field in the cavity, can be described by the following rate equations

$$\frac{\partial N}{\partial t} = \frac{I}{qV} - \frac{N}{\tau_e} - \frac{v_g \Gamma g S_{las}}{V} \quad (3.1)$$

$$\frac{\partial S_{las}}{\partial t} = v_g \Gamma g S_{las} - \frac{S_{las}}{\tau_p} + \beta \frac{N}{\tau_e} V \quad (3.2)$$

In the equations above I represents the injection current, q the elementary charge constant, V the volume of the active region ($V=wdL$,

with w , d and L the width, thickness and length of the active region respectively), τ_e the carrier lifetime in the active region and v_g the group velocity in the gain medium. The gain g is given by $g = a(N - N_0)$ with a the differential gain coefficient and N_0 the transparency carrier density. The spontaneous emission coupling factor β accounts for the amount of spontaneous emission that is coupled into the laser mode. The photon lifetime τ_p is given by

$$\frac{1}{\tau_p} = v_g (\alpha_i + \alpha_{mirror}) \quad (3.3)$$

The first term in Equation 3.3 accounts for the loss of photons due to absorption mechanisms while the second term accounts for the mirror losses. This corresponds to the photons escaping the cavity through the right hand side and left hand side facets. The amount of photons actually leaving the facets during each round trip time of the laser field in the cavity and the corresponding laser output power are given by

$$P_{out,i} = c_i S_{las} \frac{\hbar\omega_0 v_g}{L} \quad (3.4)$$

Here $\hbar\omega_0$ represents the energy of one photon in the laser field. The emission efficiency c_i gives the fraction of the average internal power of the laser diode that exits the left or right hand side facet. The value of c_i depends on various device parameters. In the further analysis it is chosen as 0.7. The values of the device parameters used for the simulation of a simple semiconductor laser diode are given in Table 3.1.

In Figure 3.2 the output power of the laser diode as a function of the input current is shown. The device parameters used are the same as in Table 2.1. Up until the threshold current the laser output power is very low, while for currents above the threshold condition the laser output power rapidly increases. Above the threshold current the influence of the spontaneous emission coupled into the laser mode is negligible. Below the threshold current the graphs for β higher than or equal to zero deviate only a small bit.

From Figure 3.2 it can be concluded that a linear approximation of the laser output power as a function of the input current can be used. This approximation, which uses the assumption $\beta = 0$ leads to a value for S_{las} of zero below the threshold current. The threshold condition is determined by the fact that at the threshold the gain just compensates the internal and mirror losses, leading to a total round trip gain in the laser diode equal to 1.

Parameter	Typical value	Description
v_g	$8.33 \times 10^7 \text{ m.s}^{-1}$	Group velocity
α_i	3000 m^{-1}	Effective loss coefficient
α_{mirror}	5000 m^{-1}	Effective loss coefficient
I	0-0.2 A	Injection current
q	$1.6 \times 10^{-19} \text{ C}$	Elementary charge
V	$w \times d \times L$	Volume of the active layer
w	$2 \times 10^{-6} \text{ m}$	Active layer width
d	$0.2 \times 10^{-6} \text{ m}$	Active layer thickness
L	$300 \times 10^{-6} \text{ m}$	Device length
τ_c	$300 \times 10^{-12} \text{ s}$	Spontaneous carrier lifetime
$\hbar\omega_0$	$1.28 \times 10^{-19} \text{ J}$	Photon energy
Γ	0.2	Confinement factor
a	$2.7 \times 10^{-20} \text{ m}^2$	Differential gain coefficient
N_0	$1 \times 10^{24} \text{ m}^{-3}$	Transparency carrier density
β	$0.5 \text{--} 1 \times 10^{-4}$	Spontaneous emission coupling factor

Table 3.1: Explanation of the parameters in the equations used to describe a semiconductor laser diode.

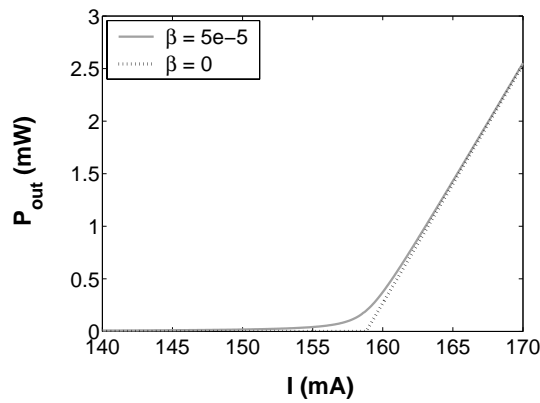


Figure 3.2: Laser output power as a function of the input current.

$$g_{th} = \frac{1}{\tau_p \Gamma v_g} \quad (3.5)$$

$$I_{th} = \frac{qV}{\tau_e} \left(\frac{1}{a\tau_p \Gamma v_g} + N_0 \right) \quad (3.6)$$

For input currents above the threshold current a linear dependence between the input current and laser output power can be found taking into account that the modal gain g remains equal to the threshold gain g_{th} .

$$P_{out,i}(I) = c_i \frac{v_g}{L} \hbar \omega_0 \left(\frac{\tau_p (I - I_{th})}{q} \right) \quad (3.7)$$

3.1.2 External power injection

Equation 3.1 can be extended to account for external injected power into the cavity yielding [62]

$$\frac{\partial N}{\partial t} = \frac{I}{qV} - \frac{N}{\tau_e} - v_g \Gamma g \frac{S_{las}}{V} - v_g \Gamma g \zeta \frac{S_{ext}}{V} \quad (3.8)$$

$$\zeta = \frac{e^{(\Gamma g - \alpha_i)L} - 1}{L(\Gamma g - \alpha_i)} \quad (3.9)$$

$$S_{ext} = \frac{L P_{ext}}{v_g \hbar \omega_1} \quad (3.10)$$

With ζ being a correction factor for the gain felt by the injected signal and S_{ext} the photon density externally injected into the laser diode each laser cavity round trip time.

Figure 3.3 shows the response of the laser output power as a function of externally injected power. Again a threshold characteristic can be observed. As long as the externally injected power remains below a certain threshold value the gain of the laser diode is locked at the threshold gain (Equation 3.5). When the input power increases beyond this threshold input power the gain in the laser diode drops below the threshold gain, needed to obtain lasing, and the laser diode switches off. The input threshold power of the laser diode is given by

$$P_{in,th} = \frac{v_g \hbar \omega_1}{L} V \frac{\frac{1}{\tau_e} \left(\frac{1}{v_g \Gamma a} + N_0 \tau_p \right) - \frac{\tau_p I}{qV}}{\zeta_{th}} \quad (3.11)$$

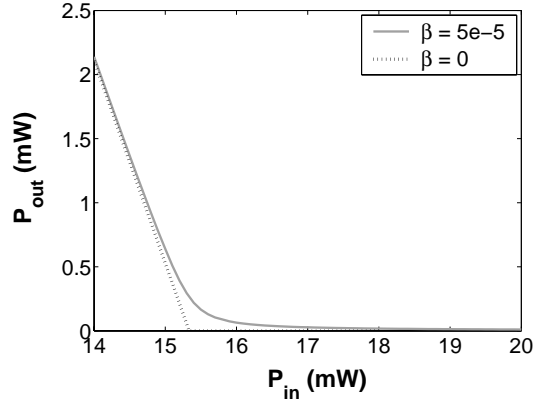


Figure 3.3: Laser output power as a function of injected power for a laser current of 200mA.

From Figure 3.3, it again follows that an analysis of the response of the output power of a laser diode, with respect to externally injected input powers can, as a good approximation, be carried out without taking the spontaneous emission coupled into the laser mode into account. In that case the output power of the laser diode for input powers below the threshold input power can be written as a function of the device and input parameters:

$$P_{out,i}(P_{ext}) = c_i V \frac{v_g}{L} \hbar \omega_0 \left(\frac{\tau_p I}{qV} - \frac{1}{\tau_e} \left(\frac{1}{v_g \Gamma_a} + N_0 \tau_p \right) \right) - c_i \frac{v_g}{L} \hbar \omega_0 \left(-\zeta_{th} \frac{L}{v_g} \frac{P_{ext}}{\hbar \omega_1} \right) \quad (3.12)$$

The laser output power for injected powers higher than the threshold input powers is considered to be zero. Equation 3.12 results in a piecewise linear function for the output power of the laser diode, as a function of the externally injected power for a constant drive current. From this equation a general approximation of the static output versus input power of a laser diode for a constant input current can be found as

$$P_{out,i}(P_{in}) = P_{las}(P_{in}) = P_{las}(0) - y' P_{in} \quad (3.13)$$

3.1.3 Dynamic input power dependence

When the input power to a semiconductor laser diode is changed in time, Equations 3.2 en 3.8 need to be solved to obtain the time depen-

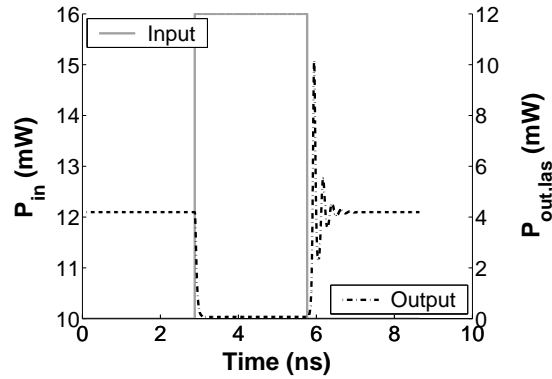


Figure 3.4: Dynamic response of the laser output power as a function of the externally injected power for for a laser current of 200mA.

dent laser output power and the average carrier density in the SOA. Figure 3.4 shows the dynamic response of the laser diode as a function of the externally injected input power into the laser diode. The same device settings as used to obtain Figure 3.3 are used. The injected input power is changed between 10 and 16mW. These power levels correspond to a laser diode in the on and the off state respectively in the static case. When the externally injected input power is increased from 10mW to 16mW the laser diode switches off almost immediately. On the other hand when the input power is decreased again a turn-on delay and relaxation oscillating behaviour can be observed. This behaviour of course corresponds to the normal switch-on behaviour of the laser output power as a function of the applied drive current [56].

The delay between the decrease in the input power and the turn-on action of the laser diode, as well as the laser relaxation oscillations can be better seen from Figure 3.5, which gives a more detailed look at these phenomena. The ringing effect stems from the interplay between the carrier lifetime (τ_e) and the photon lifetime (τ_p) and can be explained by considering that, when the input power is suddenly decreased (or alternatively the drive current is increased) the carrier density will start to increase and after some time even exceed the threshold carrier density N_{th} , at which time the photon density in the laser diode will rapidly increase. As the photon density increases the carrier density decreases again due to the amplified stimulated emission, and as a result the photon density decreases as well. This again results in an increase of the carrier density and so on, until the steady state of both

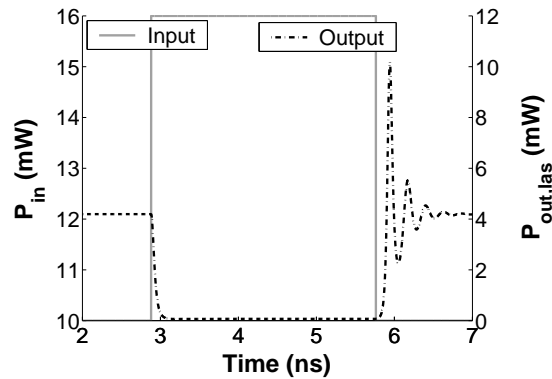


Figure 3.5: Dynamic response of the laser output power as a function of the externally injected power for for a laser current of 200mA. Zoom in around the switch on and off of the laser diode.

the carrier density and the photon density is reached. This effect can be observed from Figure 3.6.

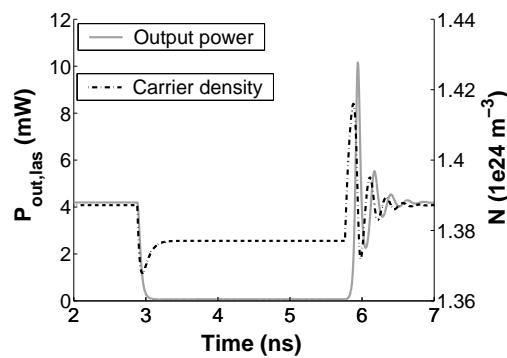


Figure 3.6: Dynamic response of the laser output power and carrier density as a function of the time with external power injected as in Figure 3.5 for a laser current of 200mA. Zoom in around the switch on and off of the laser diode.

It can clearly be seen that when the input power is decreased that the carrier density starts to recover at once. But is not until the carrier density passes the steady state carrier density of the laser diode in the on state (corresponding to the threshold carrier density) that the laser output power starts to increase significantly. This essentially is the cause of the turn-on delay visible in semiconductor laser diodes.

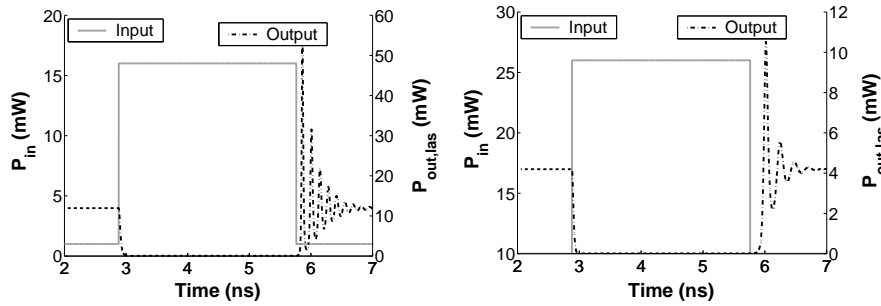


Figure 3.7: Dynamic response of the laser output power as a function of the input power for a laser current of 200mA.

The turn-on delay in a semiconductor laser diode is usually dependent on the difference in carrier density between the on and the off state, which is related to the difference between the 2 input powers (or alternatively the currents). This can be seen in Figure 3.7 where the switch off and switch on of the laser diode is shown for various combinations of externally injected powers.

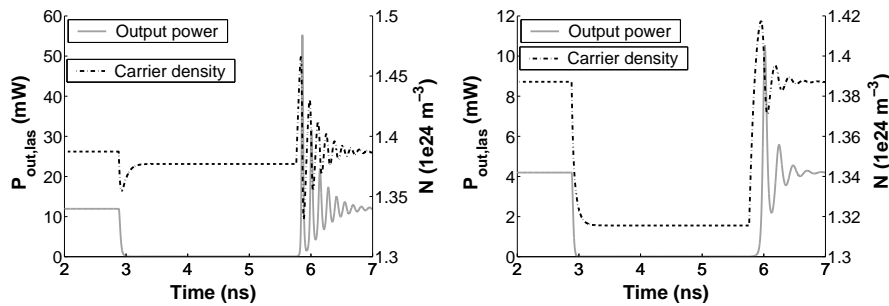


Figure 3.8: Dynamic response of the laser output power as a function of time for varying input powers as in Figure 3.7 for a laser current of 200mA.

As the externally injected power used to quench the laser diode is increased, the turn on delay also increases. This can also be observed from Figure 3.8 where it should be noted that the turn on delay is tightly related to the hole in the carrier density caused by the input power. The higher the externally injected power, the deeper the hole in the carrier density is. This of course leads to a longer recovery time for the threshold carrier density once the input power is sufficiently decreased.

3.2 Optical feedback between a SOA and a semiconductor laser diode

In an attempt to increase the output power of a laser diode, SOA's are sometimes integrated with the laser diode. This is specifically done in the case of tunable lasers composed of an array of wavelength shifted laser diodes to compensate for the coupling loss introduced in the combiner section of the device [63]. Several models have already been developed to compare the properties of the laser output power, such as the relative intensity noise (RIN) and the side mode suppression ratio, with and without the use of a SOA [64, 65, 66, 67]

Here the behaviour of a mutually and optically coupled SOA and semiconductor laser diode with light injection will be investigated using the previous obtained equations in Chapter 2 and Section 3.1. Both a static and dynamic analysis of the behaviour of the device as a function of the input signals will be made. A schematic representation of the device is shown in Figure 3.9.

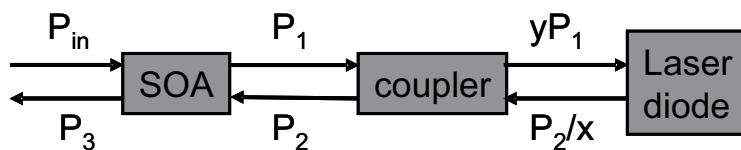


Figure 3.9: Schematic view of a semiconductor laser diode mutually and optically coupled to a SOA.

The SOA and the (DFB) semiconductor laser diode are connected through a coupler resulting in a fraction x of the SOA output power and an identical fraction of the laser output power to be coupled to either the SOA or the laser diode. The input power to the device is injected from the left hand side facet of the SOA. The scheme presented can be implemented as a hybrid version (with a separate SOA and laser diode interconnected by means of fibers), or as an integrated device where both devices are fabricated on the same photonic chip. The coupling between the two devices can be done by butt-coupling the devices (resulting in a coupling ratio of (almost) 1) or by means of other fixed or flexible coupling schemes, such as a Multimode interferometer (MMI) [68] or a Mach-Zehnder interferometric (MZI) switch [69].

In the following analysis it is assumed that the injected signal (P_{in}) is not reflected back to the SOA at or in the laser diode. This assumption holds if the facets of the laser diode are anti-reflection coated and if the

wavelength of the injected signal is sufficiently different from the Bragg wavelength of the laser diode. Furthermore only the lossless approach will be considered for simplicity reasons, although some comparison will be done with the lossy case. The analytical model shown in this section was first published in [70].

3.2.1 Static analysis

From Equation 3.13 we can conclude that, as long as the input power to the laser diode, being the amplified input signal, is low enough the laser diode operates above threshold and emits power. This laser output power is then partly injected into the SOA, as shown in Figure 3.9. The coupling ratio from laser diode to SOA and from SOA to laser diode is denoted as x . The injection efficiency of power into the laser diode is denoted as y' (Equation 3.13). When the input power to the laser diode rises above a certain value the gain of the laser diode is quenched and the laser diode is switched off, hence no laser power is injected into the SOA. Two different situations can therefore be distinguished, one where the laser diode is in the on-state and where power is injected into the SOA from both sides, and a state where the laser diode is in the off state and where power is injected into the SOA from one side only.

These 2 situations are shown below and are obtained from Equations 2.31 , 2.44 and 3.13.

$$g_0L = \ln\left(\frac{P_1}{P_{in}}\right) + \frac{1}{P_{sat}} \left((P_1 - P_{in}) - P_1P_2 \left(\frac{1}{P_1} - \frac{1}{P_{in}} \right) \right) \quad (3.14)$$

$$\frac{P_2}{x} = P_{las} - yP_1 \quad (3.15)$$

P_{las} represents the output power of the laser diode without external injection ($P_{in} = 0$). Equation 3.15 can be derived from Equation 3.13 by stating that $y = xy'$. The second situation is described by

$$g_0L = \ln\left(\frac{P_1}{P_{in}}\right) + \frac{1}{P_{sat}} ((P_1 - P_{in})) \quad (3.16)$$

$$P_2 = 0 \quad (3.17)$$

Rewriting Equation 3.14 as a function of P_{in} versus P_2 , using Equation 3.15 gives

$$g_0L = \ln \left(\frac{xP_{las} - P_2}{xyP_{in}} \right) + \frac{1}{P_{sat}} \left[P_2 \left(\frac{xP_{las} - P_2}{xyP_{in}} - 1 \right) - P_{in} + \frac{P_{las}}{y} - \frac{P_2}{xy} \right] \quad (3.18)$$

Using the equations above an analysis of the optical feedback between the externally injected power into the SOA and the output power of the laser diode can be made. Figure 3.10 shows the response of the laser output power with respect to the input power injected into the SOA. All powers have been scaled with respect to the saturation power P_{sat} of the SOA in the further analysis, i.e. $p_{in} = \frac{P_{in}}{P_{sat}}$, $p_2 = \frac{P_2}{P_{sat}}$, ...

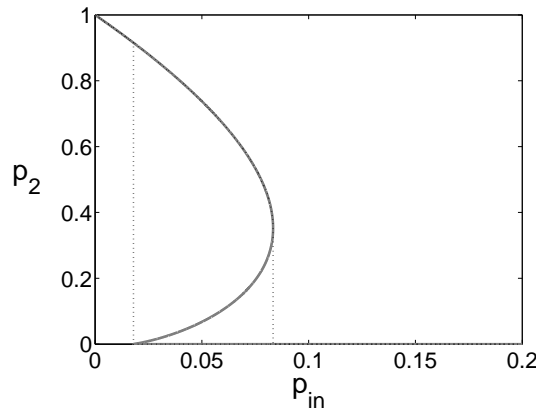


Figure 3.10: Static response of the laser output power p_2 as a function of the input power p_{in} for $p_{las} = 1$, $g_0L = 5$ and $x = y = 1$.

From Figure 3.10 it can be noted that the laser output power versus SOA input power shows bistable operation over a certain range of input powers. The dashed line shows the switching points between the lower and upper stable branches of this optical feedback scheme. An analog bistable operation can also be found when looking at the SOA output power as a function of the SOA input power, as shown in Figure 3.11.

For increasing input powers the laser output power decreases according to Equation 3.18 up until the right boundary of the bistable domain. At the right hand side boundary the laser output power switches from the upper branch to the lower branch of the bistable domain. When the input power is increased further the laser output power remains switched off. From Figure 3.11 the inverse behaviour can be observed. For increasing input powers an increase in the SOA output

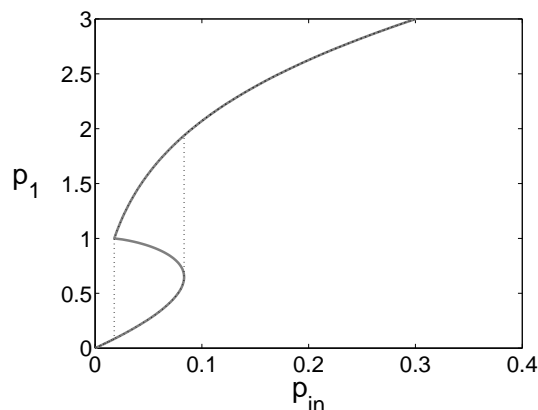


Figure 3.11: Static response of the SOA output power p_1 as a function of the input power p_{in} for $p_{las} = 1$, $g_0L = 5$ and $x = y = 1$.

power can be observed. For input powers higher than the right boundary value the SOA output power follows Equation 3.16. The output power of the SOA keeps following this equation when decreasing the input power again up to the point, where the SOA output power becomes low enough for the laser diode to switch on again. This point defines the left hand boundary of the bistable domain in both Figure 3.10 and Figure 3.11.

The bistability observed in Figure 3.10 and Figure 3.11 can be explained by the feedback between the signal and laser power. When the input signal power is increased from zero, the laser diode operates above threshold meaning that the laser injects power into the SOA. This laser power saturates the gain of the SOA, causing an increase of required input power to obtain the SOA output power needed to quench the laser diode. When the laser does switch off for a certain signal input power, the gain of the SOA suddenly increases due to the drop in total injected power into the SOA and the SOA output power rises, which keeps the laser diode quenched. When the input signal is then decreased again a higher SOA gain can be obtained for equal input signal powers. This is a result of the absence of the laser output power along the lower branch of the bistable domain. This keeps the laser diode quenched below the input power needed to first quench the laser diode at increasing input powers. Once the input signal power is low enough to get a SOA output power below the laser threshold input power the laser switches on again and suppresses the gain of the SOA,

causing a decrease in the signal output power and an increase in the laser output power.

3.3 Discussion of static results

From the previous section we learned that an optical feedback scheme between a SOA and a semiconductor laser diode can exhibit bistability. This section will take a closer look at the conditions to obtain this bistability and the dependence of its width and height on some device parameters, such as g_0L (corresponding to the SOA drive current as can be seen from Equation 2.11) and p_{las} (corresponding to the laser diode drive current as can be seen from Equation 3.7). The behaviour of the device will also be investigated with respect to the coupling ratios x and y between the laser diode and the SOA.

3.3.1 SOA drive current dependency

Changing the drive current of the laser diode or the SOA results in a change of the stand alone laser output power (without injection of optical power into the laser diode) and the gain of the SOA respectively. A higher gain of the SOA results in a higher output power of the SOA for identical input powers, which can lead to the laser diode switching off at lower input powers. An increase in the stand alone laser output power on the other hand results in a shift towards higher required injected input powers into the laser diode in order to obtain a switch off. The behaviour of the device as a function of the SOA drive current (related to the unsaturated gain of the SOA (g_0L) by Equation 2.11) can be seen in Figures 3.12 and 3.13, which also show that the output power of the laser diode and the output power of the SOA exhibit bistable operation, as a function of the drive current of the SOA. Note that here $p_2 < p_{las}$ because of the fact that in the lossless case $p_1 = p_{in}$ when $g_0L = 0$.

Condition for bistable operation

A condition to obtain bistability when only changing the SOA drive current can be obtained from Equation 3.18 and Equation 3.17. The width of this bistability can also be determined by finding the left and right boundary values of the bistable domain with respect to the unsaturated gain of the SOA. For the following analysis p_{in}, p_{las}, x and y are

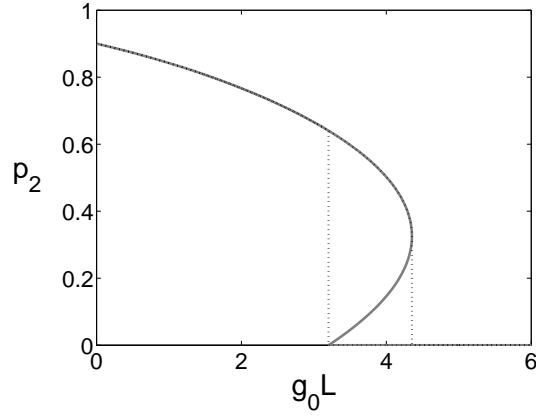


Figure 3.12: p_2 as a function of g_0L for $p_{las} = 1$, $p_{in} = 0.1$ and $x = y = 1$.

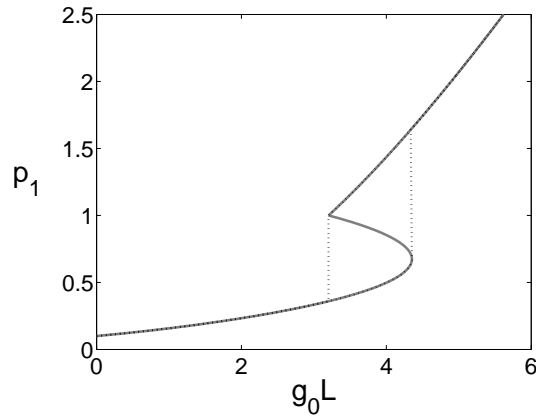


Figure 3.13: p_1 as a function of g_0L for $p_{las} = 1$, $p_{in} = 0.1$ and $x = y = 1$.

considered to be constant. The analysis is done with respect to the laser output power p_2 but can also easily be done with respect to the SOA output power p_1 by using Equation 3.15 and Equation 3.16, as p_1 is a piecewise linear function of p_2 and vice versa. Starting from Equation 3.18 an expression for the left side boundary value can be found by taking into account that the laser diode is switched off after the right hand side boundary value of the bistable domain. This is the same as setting p_2 to 0 in Equation 3.18 yielding

$$\ln\left(\frac{p_{las}}{yp_{in}}\right) - p_{in} + \frac{p_{las}}{y} = g_0L \quad (3.19)$$

The right side boundary value of the bistable domain can be found by noting that the function $p_2(g_0L)$ has a maximum in this point. In order to obtain the right side boundary value the maximum of Equation 3.18 with respect to p_2 needs to be found. The derivative towards p_2 is taken, of course taking into account that $\frac{\partial(g_0L)}{\partial p_2} = 0$ at the extremum.

$$0 = \frac{-xy p_{in}}{x p_{las} - p_2} + x p_{las} - 2p_2 - xy p_{in} - p_{in} \quad (3.20)$$

From (3.20) a relation follows for p_2 as a function of p_{las} and p_{in} (independent of g_0L however) at the right side boundary of the bistable domain.

$$p_2 = \frac{3x p_{las} - (xy + 1) p_{in} + \sqrt{(x p_{las} + (xy + 1) p_{in})^2 + 8xy p_{in}}}{4} \quad (3.21)$$

Eq. (3.21) gives a relation for the maximum value of g_0L in Equation 3.18 as a function of p_2 . Using this value found for p_2 in Equation 3.18 leads to the right hand side boundary value of the unsaturated gain of the SOA for the bistable domain. A condition for the occurrence of bistability can be found by noting that whenever $p_2 > 0$ in Equation 3.21 the right and left hand side boundary values of the bistable domain are different, implying the existence of a bistable domain. This leads to

$$p_{las} \geq \frac{(xy + 1) p_{in} + \sqrt{(xy + 1)^2 p_{in}^2 + 4xy p_{in}}}{2x} \quad (3.22)$$

Whenever this condition is fulfilled the laser output power shows bistability as a function of the SOA drive current. Equation (3.22) can be intuitively understood if one considers that if p_{las} fulfills this condition for a fixed input power the stand alone laser diode is operating well above threshold. In that case the laser output power is high enough to saturate the gain of the SOA in such a way that the unsaturated SOA gain, for which the laser diode switches off is increased. This effectively shifts the right boundary condition of the bistable domain to higher unsaturated gain levels (and drive currents) of the SOA. The point where the laser diode switches on again is not influenced by the saturation of the SOA by the laser output power, but the left hand side boundary level of the bistable domain does shift to higher SOA gain levels for increasing stand alone laser output power. When the condition shown in Equation 3.22 is not met, the laser output power is not high enough

to maintain a high enough level of saturation in order to sufficiently saturate the gain of the SOA. This results in a monotone decrease of the laser output power as a function of the unsaturated gain of the SOA.

Changing coupling ratios

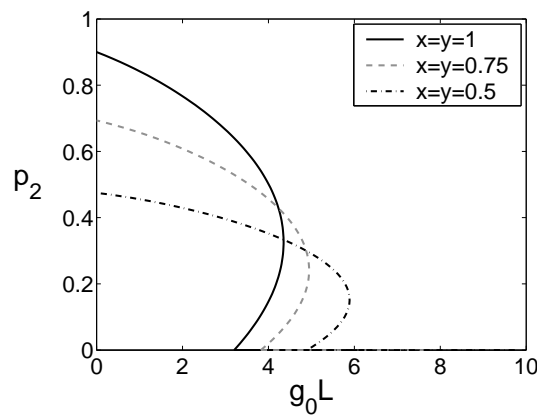


Figure 3.14: p_2 as a function of g_0L for $p_{las} = 1$, $p_{in} = 0.1$ and different $x=y$.

When the coupling ratios between the SOA and the laser diode are changed in a symmetrical way (meaning that the coupling ratio from laser diode to SOA and from SOA to laser diode remain the same) it can be seen from Figure 3.14 that the step height of the laser diode output power remains constant ($p_2 = xp_{out,las}$), but that the width of the bistable domain increases a little with decreasing coupling ratios between the SOA and the laser diode. Furthermore a shift towards higher SOA drive currents, required to operate the device in its bistable regime, can be observed when decreasing the coupling ratios. This can be explained by considering that a decrease in the coupling ratio between the SOA and the laser diode results in a smaller fraction of the SOA output power injected into the laser diode. This leads to a higher required gain in the SOA for an identical input power to obtain the SOA output power needed to switch of the laser diode. The reduced fraction of SOA power coupled into the laser diode also causes the switch on of the laser to occur at higher SOA drive currents. On the other hand a decrease in the coupling rate from laser diode to SOA leads to a faster switch off of the laser diode. This is caused by the slightly higher gain for the input signal at the same SOA drive current, due to the smaller

fraction of the laser output power injected into the SOA. In this case the effects of the decrease in coupling factor from laser diode to SOA and the other way around are counteracting each other. The effect from a change of the coupling ratio from SOA to laser diode however seems to be more important than a change in the coupling ratio from laser diode to SOA.

The effects described above can also be seen from Figure 3.15 where only one of the coupling ratios is changed each time. Here it again shows that the whole bistable domain shifts to higher unsaturated SOA gain levels when the coupling ratio (y) from SOA to laser diode is decreased. When the coupling ratio from laser diode to SOA is decreased only the right hand side boundary level is shifted towards lower unsaturated SOA gain levels.

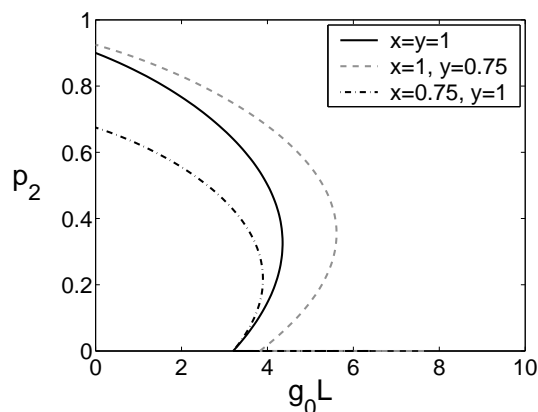


Figure 3.15: p_2 in function of g_0L for $p_{in} = 0.1$, $p_{las} = 1$ and different x and y .

Changing input power

Figure 3.16 shows that the bistable domain of the feedback scheme narrows and lowers when the input power to the SOA is increased, while the other parameters are kept constant. A shift of the bistable domain towards lower SOA drive currents can be observed as well, for increasing SOA input powers. It can be noted that the switch off point of the laser diode is dramatically reduced when the SOA input power is increased, due to the larger effect a small change in the gain of the SOA has on the absolute SOA output power for higher input powers. The switch on point of the laser diode decreases far less with decreasing in-

put power. At the switch off point the SOA is still highly saturated by the injected laser power (looking at the powers of p_2 and p_{in} this immediately becomes clear), causing a decreased gain for the input signal. The effect of this saturated gain on the actual output power of the SOA is higher for smaller input signals because more gain is required to obtain the SOA output power needed to switch off the laser diode. For the switch on operation it must be considered that only the SOA input power saturates the SOA, resulting in less saturation than in the case where the laser diode is on. The saturation in the SOA is however still input power dependent, leading to a higher gain saturation for the higher input powers. Lower input powers do require a higher gain to obtain the output power, needed to keep the laser diode quenched, but due to the lower saturation level, caused by the lower input powers, the difference in unsaturated gain for the left hand side boundary of the bistable domain is rather limited, as can be seen from Figure 3.16.

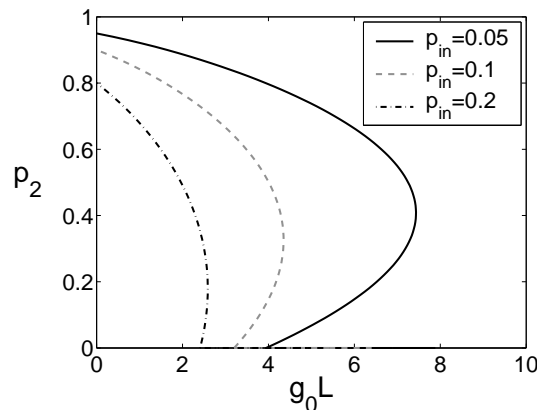


Figure 3.16: p_2 as a function of g_0L for $p_{las} = 1$, $x=y=1$ and different p_{in} .

Changing laser power

The inverse effect as for a change in SOA input power can be observed when the laser drive current (corresponding to p_{las}) is changed. This is shown in Figure 3.17. When p_{las} is decreased the position of the bistable domain shift to lower values of g_0L , while at the same time the width and the height of the bistable domain decreases. The explanation for this behaviour is analog to the case of changing SOA input powers. A higher stand alone laser power means that an identical SOA input

power needs a lot more unsaturated gain (due to the higher level of gain saturation by the higher laser output power) in the SOA in order to cause a switch off of the laser diode. For the switch on operation the effect is again less pronounced, due to the fact that only the SOA input power is present in the SOA.

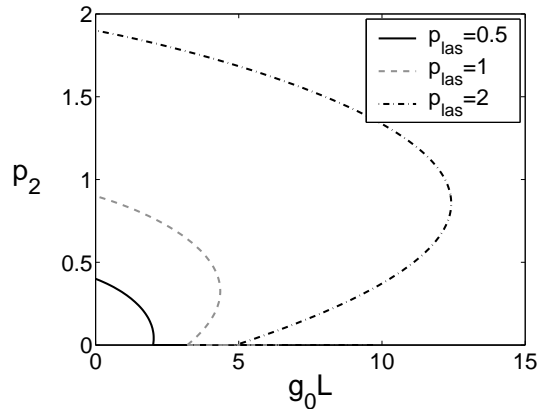


Figure 3.17: p_2 as a function of g_0L for $p_{in} = 0.1$, $x=y=1$ and different p_{las} .

3.3.2 Laser diode drive current dependency

The bistability in the laser and SOA output power can also be obtained by changing the drive current of the laser diode while keeping the other parameters constant. This is shown in Figure 3.18 for the SOA output power as a function of the stand alone laser power. For $p_{las} = 0$ the SOA works as a stand alone SOA and the output power can be calculated from Equation 3.16. As long as the stand alone laser power is below a certain threshold value the laser diode remains switched off. When the laser diode switches on eventually, for a high enough drive current (corresponding to p_{las}), the SOA gets heavily saturated, resulting in a sharp decrease in SOA output power. If the stand alone laser power is again decreased the saturation of the SOA gradually decreases, resulting in a higher SOA gain. When the SOA gain has risen enough, as to provide a high enough SOA output power, the laser diode switches off again and the gain of the SOA suddenly increases, leading to an increase in SOA output power.

Changing the drive current of the laser diode while keeping the input power and SOA drive current constant leads to bistable operation

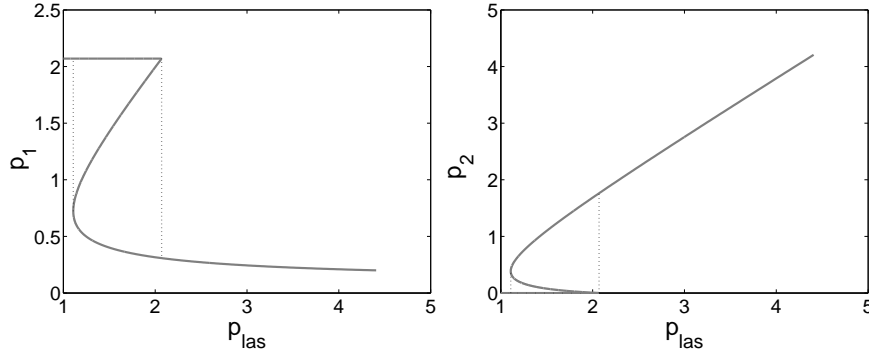


Figure 3.18: p_1 and p_2 as a function of p_{las} for $p_{in} = 0.1$, $x=y=1$ and $g_0L = 5$.

of the device, as can be seen in Figure 3.18, for both the SOA output power and the laser output power. It should be noted, as could be expected, that the bistability obtained by changing the laser drive current is a mirrored version of the one obtained when changing the SOA drive current.

An analog analysis as in the case of a changing SOA drive current can be made about the width and occurrence of the bistable domain. The right side boundary value can again be found by using Equation 3.19, while the value of p_2 at the left side boundary can be found by taking the derivative of Equation 3.18 towards p_2 , taking into account that $\frac{\partial(p_{las})}{\partial p_2} = 0$ at that point. Again the same condition as in Equation 3.21 is found. Solving Equation 3.18 for p_{las} , using Equation 3.21, provides the solution for the left side boundary value of the bistable domain.

Again bistability is only obtained when the left and right side boundary values are different. The condition to obtain bistability when changing the laser drive current can be written as a function of g_0L and p_{in} .

$$g_0L \geq \ln \left(\frac{(xy+1)p_{in} + \sqrt{(xy+1)^2 p_{in}^2 + 4xyp_{in}}}{2xyp_{in}} \right) - p_{in} + \frac{(xy+1)p_{in} + \sqrt{(xy+1)^2 p_{in}^2 + 4xyp_{in}}}{2xy} \quad (3.23)$$

From this equation it follows that the gain of the SOA has to be high enough in order to obtain bistability when changing the laser drive current. An analog analysis of the influence of p_{in} , g_0L and x and y on the width, height and position of the bistable domain, as for the case of changing SOA drive currents can easily be done using the equations

above. The behaviour of the device as a function of the laser diode drive current will show, as can already be seen from Figure 3.13 and Figure 3.18, the opposite dependence on the various parameters. The explanation for this behaviour is analog to the case where the SOA drive current is changed.

Use as an optical flip-flop

The opposite behaviour of the device as a function of the SOA drive current and the laser drive current can be used to make the device work as an optical flip-flop. When choosing both the drive current of the SOA and of the laser diode such that the device, for a given input power (and given coupling ratios) operates inside a bistable domain, switching between the stable states can be achieved by adding appropriate current pulses to both the DC SOA and laser diode drive currents. When the laser diode is in the on-state (corresponding to the off-state for the SOA output power) the state can be switched by increasing the drive current of the SOA for a short period of time in order to get the laser diode to switch off as can be seen in Figure 3.12. If the laser diode is in the off-state (corresponding to the on-state for the SOA output power) the state can be switched by increasing the drive current of the laser diode for a short period of time in order to get the laser diode to switch on as can be seen in Figure 3.18.

3.3.3 Input power dependency

The previous section showed that for a given input power bistable operation of a SOA and laser diode based optical feedback scheme could be obtained. From Figure 3.10 and Figure 3.11 it could already be seen that the device also exhibits bistability as a function of the SOA input power. In this section this all-optical bistability will be further investigated.

Condition for bistable operation

As in the previous section an expression for the left and right hand side boundary values of p_{in} can be derived from Equations 3.14 or 3.15. The left hand side boundary value can be found by using the fact that the laser is switched off at this point ($p_2 = 0$ or $p_1 = \frac{p_{las}}{y}$) in Equation 3.14.

$$g_0 L = \ln\left(\frac{p_{las}}{y p_{in}}\right) - p_{in} + \frac{p_{las}}{y} \quad (3.24)$$

The right hand side boundary value can again be found by searching for the value of p_{in} at the extremum of Equation 3.14 as a function of p_1 . To that extent the derivative of Equation 3.14 towards p_1 is taken with $\frac{\partial p_{in}}{\partial p_1} = 0$.

$$0 = \frac{1}{p_1} + \frac{xp_{las}}{p_{in}} - \frac{2xyp_1}{p_{in}} + (xy + 1) \quad (3.25)$$

From Equation 3.25 we find $p_{in}(p_1)$ for the maximum:

$$p_{in} = \frac{2xyp_1^2 - xp_{las}p_1}{(xy + 1)p_1 + 1} \quad (3.26)$$

Substituting this into Equation 3.24 results in

$$g_0L = \ln\left(\frac{(xy+1)p_1+1}{2xyp_1-xp_{las}}\right) + (xp_{las} - xyp_1) \left(\frac{(xy+1)p_1+1}{2xyp_1-xp_{las}} - 1\right) - \frac{2xyp_1^2 - xp_{las}p_1}{(xy+1)p_1+1} + p_1 \quad (3.27)$$

By solving Equation 3.27 for p_1 using Equation 3.26 leads to the right hand side boundary value of p_{in} for the bistable domain. The device becomes bistable when the left and right boundary value of the bistable domain with respect to p_{in} are different. Filling the condition for the left side boundary condition ($p_1 = \frac{p_{las}}{y}$) in into Equation 3.27 gives

$$g_0L = \ln\left(\frac{(xy + 1)p_{las} + y}{xyp_{las}}\right) - \frac{xp_{las}^2}{(xy + 1)p_{las} + y} + \frac{p_{las}}{y} \quad (3.28)$$

This equation states the minimal requirement for g_0L and p_{las} to obtain bistability. The condition to obtain bistability for g_0L and p_{las} then becomes:

$$g_0L \geq \ln\left(\frac{(xy + 1)p_{las} + y}{xyp_{las}}\right) - \frac{xp_{las}^2}{(xy + 1)p_{las} + y} + \frac{p_{las}}{y} \quad (3.29)$$

When the unsaturated gain of the SOA increases above the threshold value to obtain bistability, it follows from Equation 3.27 and Equation 3.26 that the right side boundary value of p_{in} for the bistable domain becomes higher than the left hand side boundary value. This can be understood by considering that for a higher SOA drive current, the gain for the input signal without injection of laser power is higher than

in the case of a laser in the on-state, where the laser output power injected into the SOA saturates the gain of the SOA. This difference in gain causes the left and right boundary condition to drift apart when the SOA drive current is increased. When the condition in Equation 3.29 is not fulfilled the laser diode is not switched off abruptly and instead a gradual change of the laser and SOA output power can be seen, as shown in Figure 3.19 for the SOA output power as a function of the SOA input power.

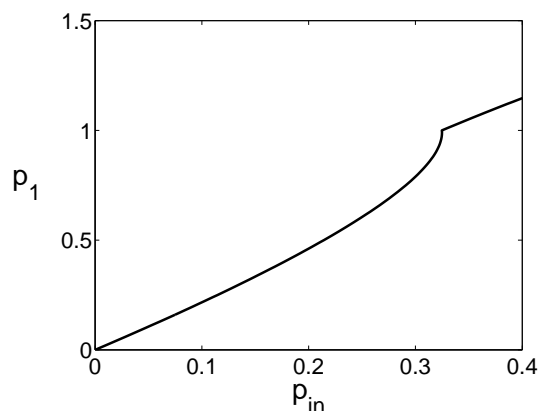


Figure 3.19: p_1 as a function of p_{in} for $p_{las} = 1$, $g_0L = 1.8$ and $x = y = 1$.

The width of the bistability can be calculated from Equation 3.24 in combination with Equations 3.26 and 3.27. The resulting SOA input power relation as a function of the unsaturated SOA gain is given in Figure 3.20 for different coupling ratios between the SOA and laser diode.

It can be clearly seen that a minimal SOA drive current is required to obtain bistability. When increasing the SOA drive current the width of the bistability increases fast initially, but saturates for higher SOA drive currents. This is due to the fact that, when the unsaturated gain of the SOA is increased further and further, the relative gain difference in the SOA between the situation with the laser diode switched on, and the situation with the laser diode switched off becomes smaller.

Changing coupling ratios

When the coupling ratios between the SOA and the laser diode are equally changed it can be seen from Figure 3.21 that the width of the

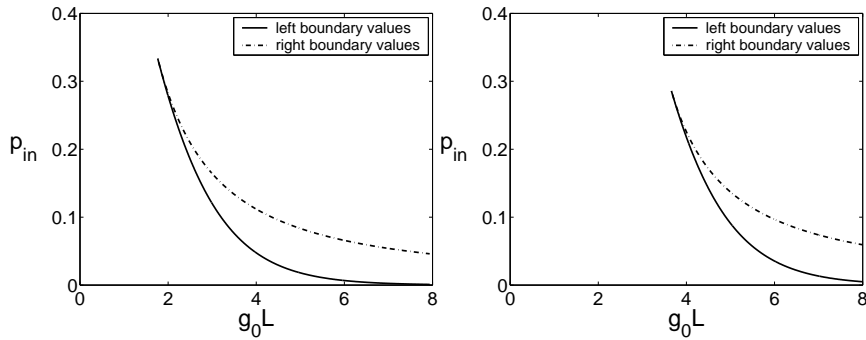


Figure 3.20: Right and left boundary values of p_{in} for the bistable domain as a function of g_0L for $p_{las} = 1$, $p_{sat} = 1$ and $x = y = 1$ (left) and $x = y = 0.5$ (right).

bistable domain decreases for decreasing coupling ratios. The height of the bistability in the SOA output power also rises with decreasing coupling factor, while the height of the bistability in the laser output power remains nearly constant (Figure 3.21 shows the fraction x of the laser output power). The position of the bistable domain shifts to higher input powers for a decreasing coupling factor.

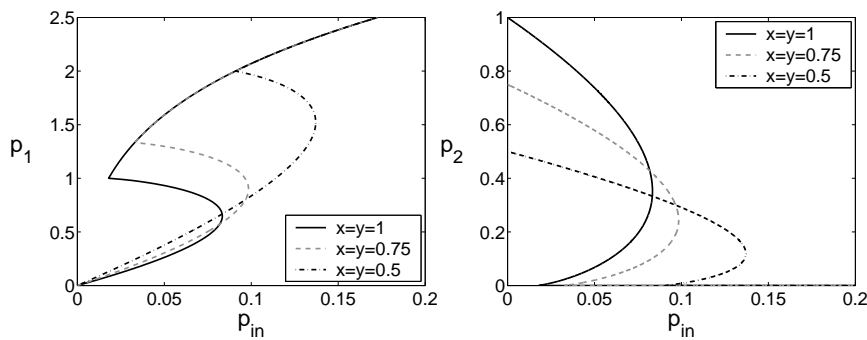


Figure 3.21: p_1 and p_2 as a function of p_{in} for $p_{las} = 1$, $p_{sat} = 1$, $g_0L = 5$ and different $x=y$.

These effects can be understood better when looking at Figure 3.22 where only one of the coupling ratios is altered at the time. When decreasing the coupling ratio from SOA to laser diode (y), while keeping the coupling ratio from laser diode to SOA (x) constant, both the right and left boundary of the bistable domain shift to higher input pow-

ers. The height of the bistability in the SOA output power also rises because a higher input power at the switching point results also in a higher output power. The step height in the bistability of the laser output power stays unaltered. Reducing the coupling ratio from SOA to laser diode (y) leads to a higher required SOA output power, as a higher input power is needed into the laser diode to switch it off. On the other hand the decrease in coupling ratio results in a decrease of the SOA output power injected into the laser diode, resulting in a shift of the left boundary value of the bistable domain to higher SOA input powers. If the coupling ratio from laser diode to SOA is decreased it can be seen that the point where the laser diode switches from the off-state to the on-state remains unchanged, whereas the right boundary of the bistable domain shifts slightly to lower input powers. This is of course due to less saturation by the actual injected laser power into the SOA as compared to the situation with a higher coupling ratio. It should also be noted that only a very small change in step height of the bistability can be observed in this case.

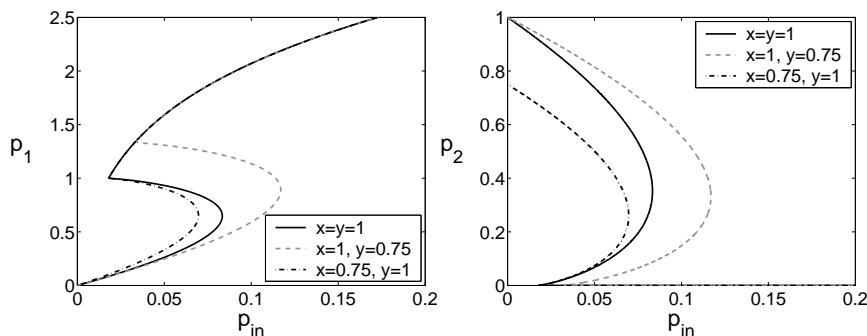


Figure 3.22: p_1 and p_2 as a function of p_{in} for $p_{las} = 1$, $p_{sat} = 1$, $g_0L = 5$ and different x and y .

Changing SOA or laser diode drive current

The influence of the drive current to both SOA and laser diode can be seen from Figures 3.23 and 3.24. When increasing the drive current of the SOA the bistable domain narrows slightly. The step height however remains almost the same, due to the fact that the SOA output power required to switch off the laser diode remains the same, when only the SOA drive current is changed. Both the left and right boundary of the

bistable domain are shifted to lower input powers due to the higher SOA gain when the SOA drive current is increased.

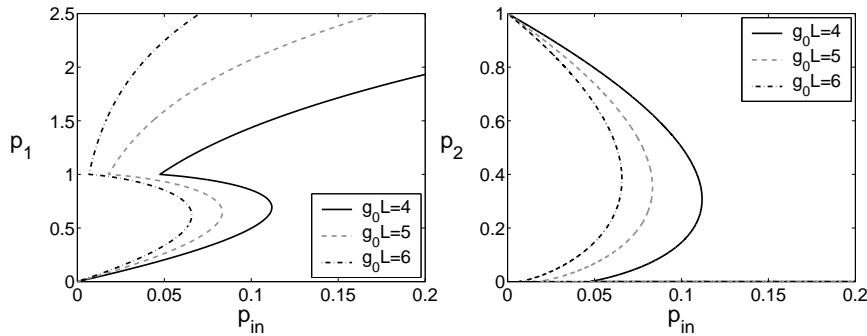


Figure 3.23: p_1 and p_2 as a function of p_{in} for $p_{sat} = 1$, $p_{las} = 1$, $x = y = 1$ and different g_0L .

Increasing the laser diode drive current leads to a big increase in the width of the bistability due to the fact that the switch off operation of the laser diode is a lot harder to achieve. More SOA output power is required to switch of the laser if the laser is driven higher above threshold. The left boundary of the bistable domain also increases because the switching point $\frac{p_{las}}{y}$ is obtained for higher input powers.

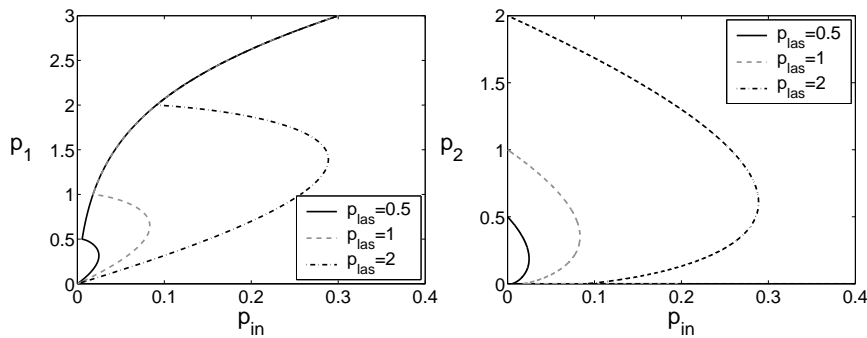


Figure 3.24: p_1 and p_2 as a function of p_{in} for $p_{sat} = 1$, $g_0L = 5$, $x = y = 1$ and different p_{las} .

Use as an all-optical flip-flop

From the analysis above it can be seen that, by selecting appropriate drive currents for both the SOA and the laser diode bistable operation

of the device can be obtained as a function of the input power. All-optical flip-flop operation can then be realized by injecting short optical pulses into the device. Setting the CW input power to a value that is situated inside the bistable domain it is possible to switch the device, by injecting short optical pulses into both sides of the SOA. When the laser diode is in the on-state (SOA output power in the off-state) a short optical pulse injected into the left side of the SOA can change the state of the device. When the optical pulse is injected the input power to the SOA is temporarily increased, and as a result so is the SOA output power. If the increase in output power due to the injected optical pulse is high enough the laser diode can be switched off (and the SOA output power switched on). When the laser diode is in the off-state (SOA output power in the on-state) the state of the device can be changed by injecting a short optical pulse into the right hand side of the SOA. Alternatively this pulse can be injected into the right hand side of the laser diode, where it gets amplified before being injected into the SOA. This optical pulse causes a short decrease in the gain of the SOA and therefore also in the SOA output power. If the decrease in the SOA output power is high enough the laser diode can switch on again, causing the SOA output power to switch off.

It can be concluded that this device can be used as a very flexible all-optical flip-flop in which the position, width and height of the bistable domain can be easily changed by varying the drive currents of the SOA and laser diode. If a tunable switch, such as a MZI-switch is used, the coupling ratio between the SOA and the laser diode can also be altered to influence the bistable domain.

3.4 Dynamic analysis

Once the static behaviour of the optical feedback combination of a SOA and a semiconductor laser diode has been investigated the dynamic nature of the device used as an all-optical flip-flop can be examined. To that extent the dynamic models describing a SOA (Equation 2.65) and a laser diode with external light injection (Equations 3.2 and 3.8) are combined.

3.4.1 Simulation method

A schematic representation of the configuration used for the simulations is shown in Figure 3.25.

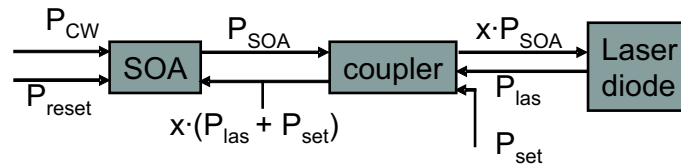


Figure 3.25: Schematic representation of the configuration of the SOA and DFB feedback combination used for the dynamic analysis of the device.

In order for the device to be used as an all-optical flip-flop an operation point has to be chosen inside the bistable domain. To that extent a CW signal is injected into the left hand side facet of the SOA. The coupler between the SOA and the laser diode ensures that the fraction of SOA output power injected into the laser diode, and also the fraction of laser output power injected into the SOA can be varied. To be able to switch between the 2 stable states in the bistable domain of the device short optical pulses are used. The set pulse, which can be used to aid the switching on of the laser diode (and therefore the switch off of the signal output power), is injected before the coupler. In the case of a 3dB splitter the set pulse could be injected through one arm of the splitter while the laser diode could be connected to the other one. The set pulse can however also be injected through the right hand side facet of the laser diode, thereby reducing the number of optical connections that have to be made to the device. The reset pulse is in our analysis injected into the left hand side of the SOA, and is used to switch the laser diode off.

The output power of the SOA is obtained as the injected power into the laser diode without the reset pulse component. The laser power is found as the laser power before the coupler. When the coupling ratio between the SOA and the laser diode equals 1, the set pulse and the laser output power are added before injection into the SOA. This is of course physically impossible but just serves to numerically show the operation of the device. In a real implementation of the device the set pulse would, in the case of butt coupled SOA and laser diode, be injected through the laser diode. As the laser diode is normally switched off in this case, and has a highly non-uniform carrier distribution, due to the power injected from the SOA, this pulse may push the carrier density in the laser diode temporarily down, while at the same time the carrier distribution shifts back towards a more symmetric situation.

In the following simulations the values of the device parameters as given in Table 2.1 and Table 3.1 are used. The SOA has a length of

500 μ m and the drive currents are 200mA and for both the SOA and laser diode. The coupling ratios used are 1 and 0.5.

3.4.2 Steady state operation

As a first step the set of dynamic equations was solved for constant input powers to obtain a steady state analysis. Both increasing and decreasing input powers are considered, meaning that the constant input power is applied after a steady state "history" of the device state has been obtained. The result of this analysis is shown in Figure 3.26.

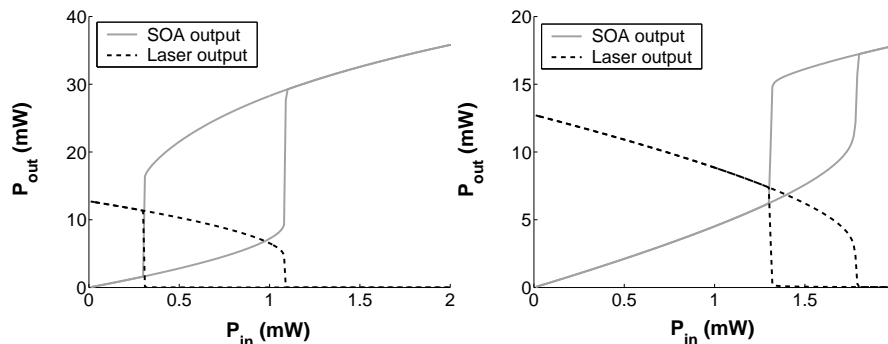


Figure 3.26: Static response of the laser and SOA output power as a function of the input power to the SOA for a coupling ratio of 1 (left) and 0.5 (right).

It can be seen that for a certain range of input powers the state of the device is dependent on the history of the device. Bistability can be observed in both the signal output power and the laser output power. A decrease in the coupling ratio leads to a shift of the bistable domain towards higher input powers. The width and height of the bistability decrease with decreasing coupling ratio.

3.4.3 Dynamic operation

Optical pulse injection

An operating point can be selected in the bistable domain by injecting an appropriate CW signal into the SOA. This CW signal ensures that the device is able to operate in the region where two stable output states are possible. In Figure 3.27 the response of the laser output power and the signal output power to optical pulses injected as shown in Figure 3.25 is shown for various combinations of pulse powers. The coupling

factor between the SOA and the laser diode is 1 and the power of the CW signal is 0.75mW corresponding to a working point in the middle of the static bistable domain shown in Figure 3.26. The used pulses are 50ps long optical block pulses.

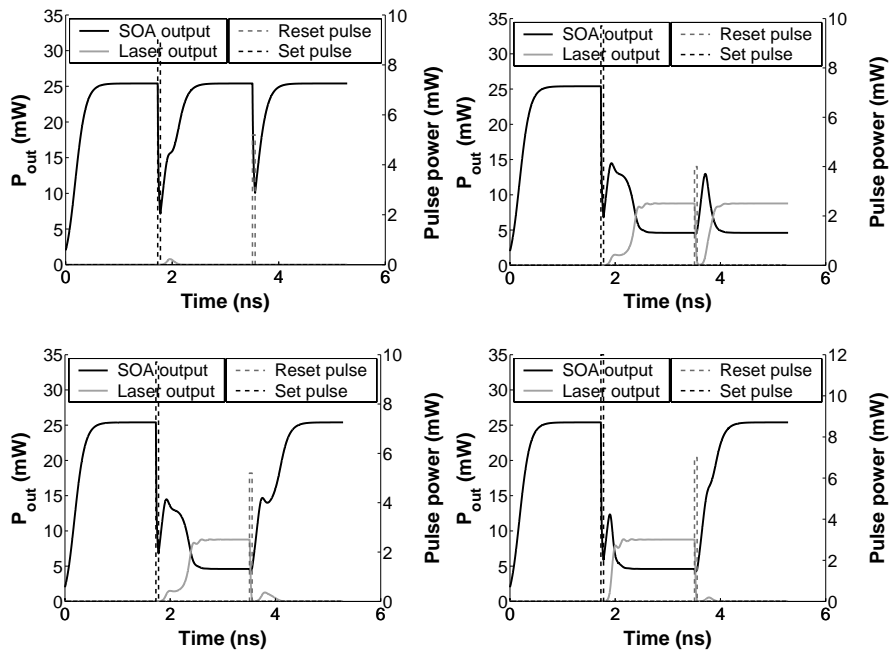


Figure 3.27: Dynamic response of the laser and SOA output power with a coupling ratio $\alpha=1$ and a CW input power of 0.75mW for various combinations of set and reset pulse powers. The pulse length is 50ps in this case. Top left: set pulse power = 9mW, reset pulse power 5.2mW. Top right: set pulse power = 9.7mW, reset pulse power 4mW. Bottom left: set pulse power = 9.7mW, reset pulse power 5.2mW. Bottom right: set pulse power = 12mW, reset pulse power 7mW.

Initially the signal output power is in the on-state and the laser diode is switched off. By injecting photons into the right hand side facet of the SOA the carrier density in the SOA can be decreased resulting in a decrease of the SOA gain and therefore less signal output power. If the decrease of the signal output power is high enough the carrier density in the laser diode can rise to the threshold carrier density leading to the switch on of the laser diode. This decrease in SOA gain has to stay low for some time to bridge the turn-on delay time of the laser diode. If the gain of the SOA recovers back to the threshold

value needed for the used CW input signal to quench the laser diode before the laser diode can exhibit enough power to sufficiently saturate the SOA, switching between the stable states does not occur.

Looking at the top 2 graphs in Figure 3.27 it can be seen that a minimal value exists for the energy of (or number of photons in) the set pulses used to switch on the laser diode. If the pulse energy is lower than this minimal required energy the gain in the SOA recovers fast enough to keep the laser diode switched off. The top right graph shows that, for a pulse power of 9.7mW (corresponding to a pulse energy of 485fJ), the signal output power starts to rise again after the set pulse has passed through the device. The laser on the other hand only switches on after some time (turn-on delay). Once the laser starts to emit power, a competition between the signal output power and the laser output power takes place. Because of the fact that the saturation of the SOA, due to the set pulse, is strong enough (and therefore the signal output power is low enough) the laser diode can, once switched on, in its turn saturate the SOA and suppress the SOA gain enough to allow the laser diode to remain switched on. It should be noted that at the boundary switching energy, which is considered to be the minimal required pulse energy to obtain switching between the stable states, the transition to the stable state occurs in different fazes. At first both the signal output power and the laser output power rise, but at a certain moment the laser diode output power is high enough to saturate the SOA and the SOA output power starts to drop again. This then in its turn allows the laser diode output power to increase further.

In order to switch the laser diode off the reset pulse also needs to be sufficiently strong as can be seen in the top right and bottom left graphs in Figure 3.27 where the set pulse energy (or power) is kept constant but the reset pulse energy (or power) increases. Again a minimal required energy is needed in order to switch the state of the device. When the reset pulse energy is too low the laser is only shortly switched off (or maybe even not switched off at all). As could be seen from Figure 3.8 an increase of the SOA output power (the amplified reset pulse power and signal input power) used to switch off the laser diode results in an increase of the turn-on delay. When the turn-on delay is long enough, to allow the SOA gain to reach a value that is high enough to allow for the amplified signal power to keep the laser diode quenched, the all-optical flip-flop can again change states. The minimal required reset pulse energy was in this case 260fJ. At the boundary reset pulse energy the transition between the states can again be seen to occur in different

phases. Initially the laser diode is switched off and the signal output power increases back to the steady state value. In a second phase the laser diode can be seen to start switching on again but the recovering gain of the SOA then leads again to the complete quenching of the laser diode.

When the pulse energy is increased above the minimal required pulse energy, needed to make the device switch, a smoother transition between the stable states can be observed. By increasing the set pulse energy beyond the minimal required reset pulse energy the gain saturation of the SOA is also further increased. This results in an additional decrease of the power injected into the laser diode. In turn this leads to a much more limited feedback time between the SOA and the DFB. This is a result of the SOA gain (and therefore also the SOA output power) remaining lower than in the boundary case, thereby allowing the output power of the laser diode to rise higher initially. Increasing the reset pulse energy leads to a longer turn-on time of the laser diode. This allows the SOA gain to recover more before the turn-on time of the laser diode has passed. This reduces the switch on effect of the laser diode and leads to a faster and smoother switching of the all-optical flip-flop. So although a minimum value exists for the pulse energies required to obtain all-optical flip-flop operation, the use of higher pulse energies may provide faster and smoother operation of the device.

Pulse length variation

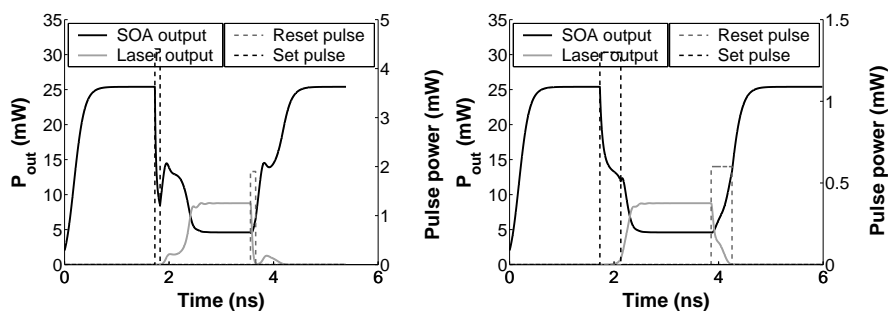


Figure 3.28: Dynamic response of the laser and SOA output power with a coupling ratio $x=1$ and a CW input power of 0.75mW for different pulse lengths. Left: 100ps pulse length, set pulse power = 4.4mW , reset pulse power 1.9mW . Right: 400ps pulse length, set pulse power = 1.3mW , reset pulse power 0.6mW .

Apart from the very short 50ps long set and reset pulses, longer pulses can also be used to switch the all-optical flip-flop as shown in Figure 3.28. For both the 100ps and 400ps long optical pulses the minimal required set and reset pulse energy are used here. As in the case of the 50ps long pulses it again can be noted that the switching occurs in different phases for 100ps long pulses. The switching in the case of the longer pulses is shown to be faster and smoother once the set and reset pulses have passed. This is caused by the fact that in the case of the set pulse the pulse reduces the gain and output power of the SOA sufficiently long for the laser diode to switch on again. After the passing of the set pulse the laser diode can immediately saturate the SOA sufficiently to reach the stable state where the laser diode is switched on. For the reset operation it holds that the reset pulse can delay the turn-on of the laser diode long enough in order to allow the gain recovery of the SOA to be sufficient to keep the laser diode switched off by the amplified CW signal once the pulse has passed.

Lower coupling ratio

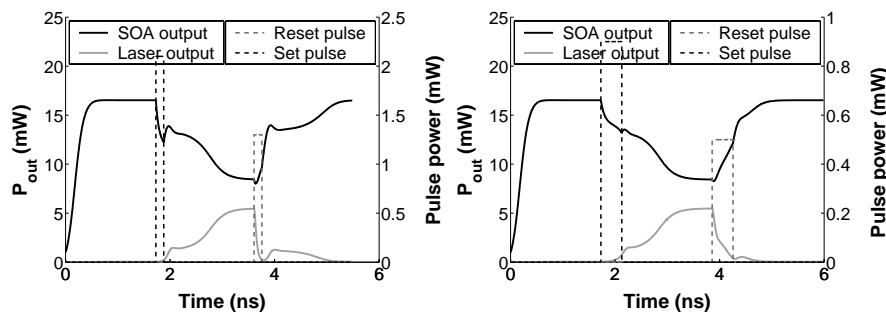


Figure 3.29: Dynamic response of the laser and SOA output power with a coupling ratio $x=0.5$ and a CW input power of 1.6mW for different pulse lengths. Left: 150ps pulse length, set pulse power = 2.1mW, reset pulse power 1.3mW. Right: 400ps pulse length, set pulse power = 0.9mW, reset pulse power 0.5mW.

When the coupling between the laser diode and the SOA is lowered it is obvious that the influence of the set and reset pulses is altered. In the case of the set pulse it is clear that due to the decrease in the coupling ratio the energy of the reset pulse injected into the SOA has to increase due to the loss in the coupler. On the other hand, since the coupling between the SOA and laser diode is lower the increase

of the SOA gain after the passage of the set pulse will be felt less by the laser diode, providing an easier turn on of the laser diode. This behaviour can be observed in Figure 3.29 where for two pulse lengths, 150 and 400ps, the minimal required set pulse energy is used to turn the laser diode on. It can be seen that the turn on of the laser diode occurs very slowly due to the feedback with the SOA output power. The set pulse causes a decrease in the SOA output power that is high enough for the laser diode to turn on. Once the laser diode has turned on the competition between the signal power and laser power in both the SOA and laser diode leads to the stable condition where the laser diode is turned on.

If the reset pulse is considered it is clear that due to the lower coupling ratio the effect of the optical pulse on the laser diode is smaller while the SOA still feels the complete pulse energy. But the lower coupling also leads to less saturation of the SOA by the laser diode. This means that while the pulse quenches the laser diode, the gain recovery of the SOA can thus be sufficiently fast to compensate for the turn on of the laser diode. This can be seen in the reset operation of the all-optical flip-flop in Figure 3.29. The laser diode is (almost) turned off by the reset pulse, while the gain of the SOA recovers fast during the pulse. After the passage of the pulse the optical feedback between the signal power and the laser power eventually lead to the laser diode remaining in the off state. It is noteworthy that again longer pulses lead to faster and smoother switching behaviour.

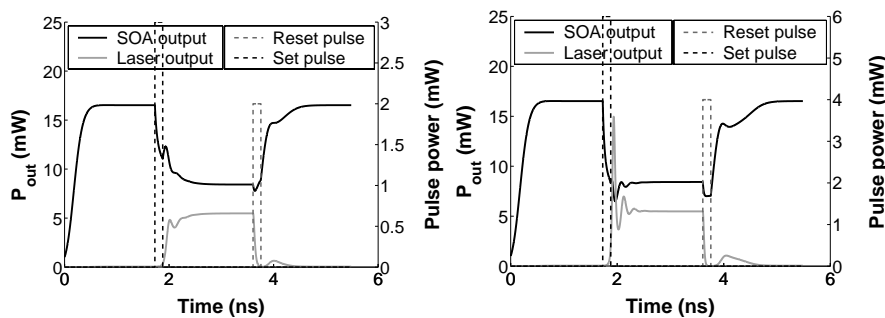


Figure 3.30: Dynamic response of the laser and SOA output power with a coupling ratio $\alpha=0.5$ and a CW input power of 1.6mW for different peak pulse powers. The pulse length is 150ps. Left: set pulse power = 3mW, reset pulse power 2mW. Right: set pulse power = 6mW, reset pulse power 4mW.

Increasing the pulse energies leads, as in the case of the coupling ratio equal to 1, to a faster and smoother switching of the all-optical flip-flop as shown in Figure 3.30. For a set pulse energy of 450fJ and a reset pulse energy of 300fJ it can be seen that the turn on and off of the laser diode happen a lot faster. Again this is due to the higher SOA gain saturation in the case of the set pulse and the higher turn on time in the case of the reset pulse. When the pulse energies are increased further, a ringing phenomena can be observed in the switch on of the laser diode. This is caused by the fact that due to the higher set pulse energy the SOA is heavily saturated beyond the saturation level that would be obtained in the stable state where the laser diode is turned on. This of course means that the feedback between the laser power and the signal does not influence the turn on of the laser diode, leading to the normal transient behaviour of a laser diode at turn on. An increase of the reset pulse energy on the other hand also causes a higher saturation of the SOA, which could give the laser diode the opportunity to switch back on after the passage of the pulse. This causes a slower switching behaviour. From these observations it can be concluded that a certain region of useable pulse energies can be found for which the switching of the all-optical flip-flop can be considered smooth and fast.

Minimal required pulse energy

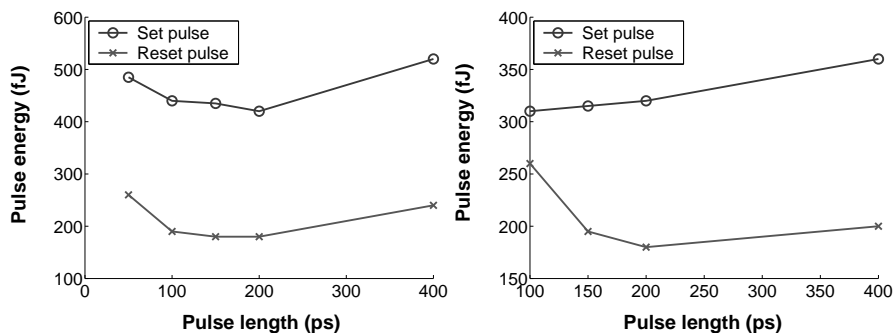


Figure 3.31: Minimal required pulse energy to obtain switching between the stable states of the SOA and laser diode combination for different pulse lengths. Left: Coupling ratio = 1, CW input power = 0.75mW. Right: Coupling ratio = 0.5, CW input power = 1.6mW.

Figure 3.31 shows the minimal required set and reset pulse energy to obtain switching of the SOA and laser diode combination for differ-

ent pulse lengths. It can immediately be seen that the required pulse energy does not differ very much as a function of the pulse length leading to the conclusion that it is in fact the energy instead of the peak power of the optical pulse that causes the state of the device to change. It can also be noted that while the reset pulse energy does not differ much from a coupling ratio of 1 to one of 0.5 the set pulse energy does. As explained above due to the lower coupling ratio between the laser diode and the SOA the gain saturation of the SOA can be lower in the case of a coupling ratio of 0.5 then in the case where the coupling ratio is 1, leading to lower set pulse energies.

3.5 Conclusions

In this chapter the behaviour of a laser diode with respect to externally injected optical power has been investigated. It has been shown that by injecting a laser diode with optical power the output power of the laser diode could be changed and the laser diode can even be quenched.

A static analytical model was presented describing the optical feedback between a SOA and a semiconductor laser diode. The device was theoretically investigated with respect to the different device parameters such as the drive current, coupling ratio and input power. It was shown that under some operation conditions the device exhibits bistability making it suitable for use as an all-optical flip-flop.

The all-optical flip-flop operation was demonstrated by combining the dynamical model of a SOA demonstrated in the previous chapter and the simple rate equations. These dynamic simulations proved that by using appropriate set and reset pulses a combination of a SOA and semiconductor laser diode could indeed be used as an all-optical flip-flop.

Chapter 4

Bistability in a SOA and DFB laser diode feedback scheme

As shown theoretically in the previous chapter it is possible to obtain bistable operation with a device consisting of a mutually and optically coupled SOA and laser diode. In this chapter more general numerical results obtained with a commercial software package will be shown as well as experimental results obtained using an integrated version of the proposed device. This chapter will only deal with the static response of the device. The dynamic behaviour of the feedback scheme will be handled in the next chapter.

4.1 Introduction

A bistable device, being electronic or optical, is a device that for certain operating conditions can operate in one of two stable states depending on the history of the device. In order to obtain any kind of bistability two requirements have to be met. These conditions are the presence of feedback and some kind of non linearity in the device. An electronic bistable device can for instance be made by connecting the output of each of a pair of operational amplifiers to the input of the other. A photonic bistable system on the other hand is constructed out of a combination of a nonlinear optical element and optical feedback.

Two types of nonlinear optical elements can be distinguished, dispersive nonlinear elements and dissipative nonlinear elements. A dis-

persive nonlinear element is based on the fact that inside the element the refractive index is a function of the optical intensity. An example is a medium with a strong optical Kerr effect ($n = n_0 + n_2 I_0$) [71]. A dissipative nonlinear element on the other hand is based on the fact that the gain or absorption coefficient is a function of the optical intensity as is the case in a saturated SOA [70].

The device under investigation here is of the latter form. The gain of both the laser diode and the SOA are dependent on and controlled by the input powers to both devices.

4.2 Simulation results

4.2.1 Simulation tool and setup

Using the commercial software package VPI Componentmaker [72], the static behaviour of the proposed device was investigated. The reason to use VPI, next to the analytical model described in the previous chapter, can be found in the more complete model used in that simulation tool. VPI for instance allows for the inclusion of amplified spontaneous emission in the SOA and laser diode, finite facet reflections, nonlinear gain coefficients,... Next to that VPI uses coupled rate equations to describe the DFB laser diode, used in these simulations and experiments, leading to a more accurate description of a real laser diode.

The scheme we used consisted of a bulk traveling wave SOA and a quarter wave shifted DFB laser diode that are connected through a bidirectional coupler as shown in Figure 4.1. Both the laser diode and the SOA are assumed to have AR coatings at both facets. These AR coatings ensure that the signal light is not reflected back to the SOA from the laser side and vice versa that the laser light is not reflected back to the laser side from the SOA side of the device. The input power to the device is injected into the left hand side facet of the SOA and the output power could in this scheme be obtained either directly after the SOA (in the case of the signal power) or at the right hand side facet of the laser diode. At this side a tunable optical filter needs to be used to separate the signal and laser power.

Some typical device parameters used in the simulations are shown in Table 4.1.

Other important parameters were default parameters from the software package and are shown in Table 4.2.

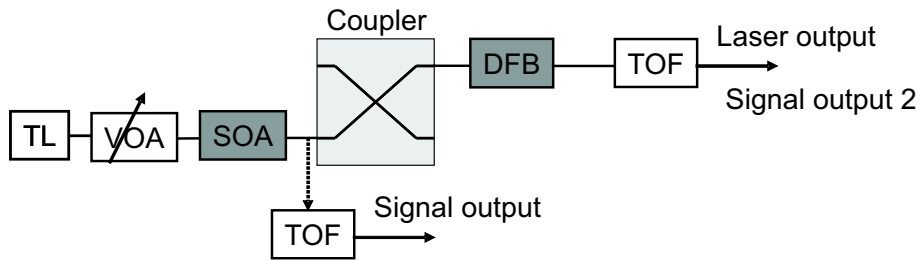


Figure 4.1: Set-up used for the numerical simulations. Used abbreviations TL: Tunable laser, VOA: Variable optical attenuator and TOF: Tunable optical filter.

SOA chip length	500 μm
Laser chip length	350 μm
Active region width	2.5 μm
Active region thickness	0.2 μm
Confinement factor laser diode	0.3
Confinement factor SOA	0.45
Laser wavelength	1552.5 nm
Signal wavelength	1537.4 nm

Table 4.1: Device properties of the scheme used in the simulations.

Internal loss	$30 \frac{1}{\text{cm}}$
Index grating coupling coefficient	$60 \frac{1}{\text{cm}}$
Linear material gain coefficient	$3e^{-16} \text{cm}^2$
Non-linear material gain coefficient	$10e^{-17} \text{cm}^3$
Material linewidth enhancement factor	3
Population inversion factor	1

Table 4.2: Default parameters of the software package used for the numerical simulations.

4.2.2 Origin of the bistability

From the analysis in chapter 3 it followed that the combination of a SOA and a (DFB) laser diode can be used as an all-optical flip-flop for certain operating conditions of both the SOA and laser diode and for certain coupling ratios between them. The bistability was found to be caused by the interplay between the signal power and the laser power due to the mutual feedback from one to another. The laser diode was approximated by using a piecewise linearized output vs input characteristic based on the simple laser rate equations. In general the static behaviour of any type of laser diode (such as a DFB laser diode) can be approximated by this piecewise linear approach. Recently it has however been numerically shown that a stand alone DFB laser diode can also exhibit bistable operation and can even be used as an all-optical flip-flop [73]. The bistable operation of this device is based on the difference in spatial hole burning in the DFB laser diode in the 2 stable states under the influence of externally injected CW light. The defining control parameters are in this case the grating coupling coefficient, which is a design and fabrication parameter, and the drive current of the laser diode. This leads to less flexibility to tune the bistable domain as compared to the approach described in this work.

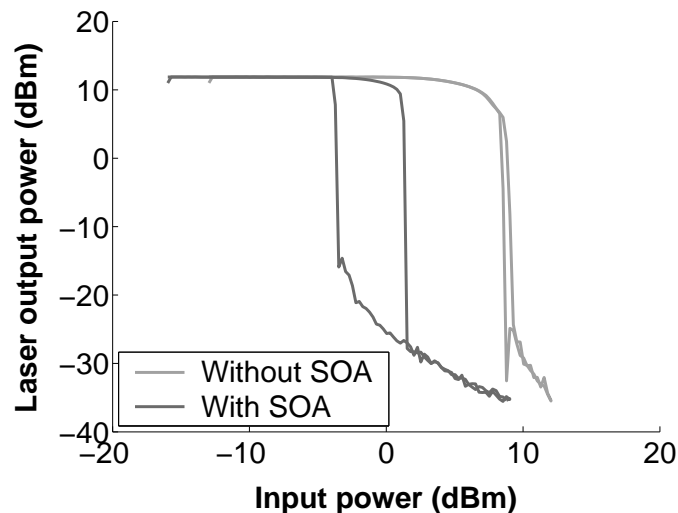


Figure 4.2: Laser output power as a function of the input power for a laser current of 80mA and a SOA current of 90mA and a coupling ratio of 0.25 between the SOA and the laser diode with and without the use of the SOA.

Since a stand alone DFB laser diode can in itself exhibit bistable operation the behaviour of the laser output power was checked by comparing the two separate devices with the same device and operating parameters. One device consists of a stand alone DFB laser diode where the input power is injected into the left hand side facet and the output power is then obtained at the right hand side facet of the laser diode. The other device is the same as in Figure 4.1. Here the input power is injected into the left hand side of the SOA and the laser output power is again obtained at the right hand side facet of the laser diode. The result of this comparison is shown in Figure 4.2. It can be seen that in the case of the stand alone DFB laser diode the laser output versus externally injected power exhibits a very small bistability that in a real device could be unnoticeable due to power fluctuations of the injected light. The response of the laser output power, with respect to the input power to the SOA, in the case of the SOA and DFB laser diode feedback scheme, results in a relatively wide (over 6dB) bistable domain. It must also be noted that the position of the bistable domain with respect to the input power is at much higher input powers for the stand alone laser diode as compared to the SOA DFB laser diode combination. This is of course caused by the gain provided by the SOA resulting in a lower switch off point of the laser diode.

From the comparison above it may be concluded that the bistability exhibited by the device consisting of both a SOA and a laser diode has a different origin than the device only consisting of a stand alone laser diode. The laser diode in the feedback scheme can of course still show some bistability (as shown in Figure 4.2) but the main cause of the possible bistability observed is the interplay between the response of the SOA and the laser diode to changing input and output powers.

4.2.3 Changing the coupling ratio

The position, width and height of the bistable domain can be changed for both the laser output power and the signal output power as shown in the following figures. When changing the coupling ratio between the SOA and the laser diode, which can be done when using a variable coupler or a MZI-switch between the SOA and the laser diode, it can be seen from Figure 4.3 that the width of the bistable domain decreases with decreasing coupling ratio, while the position of the bistable domain shifts to higher input powers. This corresponds to the results obtained in Figure 3.21. Comparing the two signal output powers, one ob-

tained directly after the coupler and the other one obtained after passing through the laser diode it can be observed that by passing through the laser diode the bistable response of the signal output power is preserved. The signal output power is however amplified while passing through the DFB laser diode. When the laser is in the on state the gain equals the threshold gain of the laser diode, while when the laser diode is in the off-state the DFB laser diode acts as a semiconductor optical amplifier for the input signal, which is heavily saturated by the injected signal light.

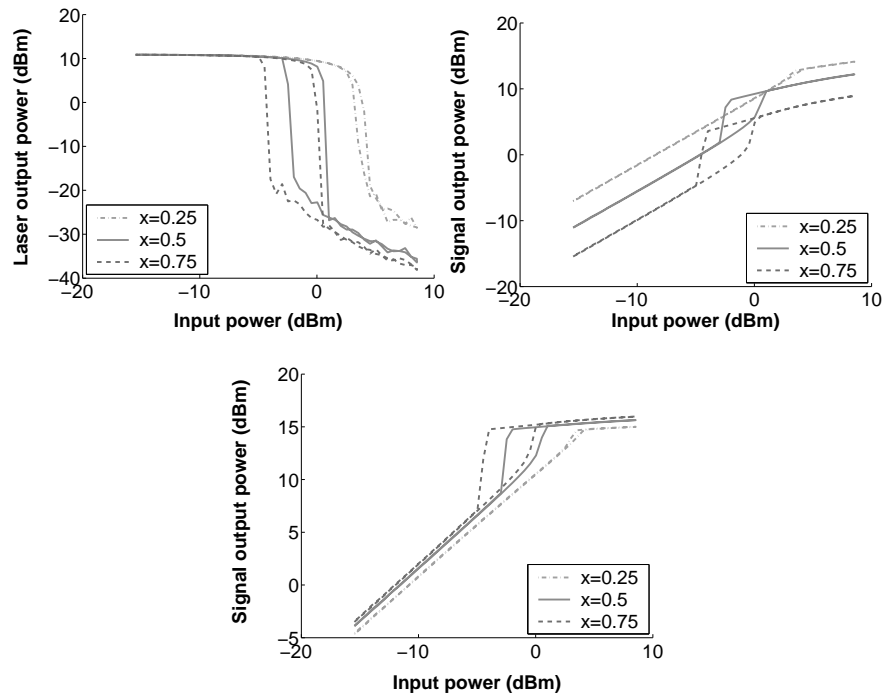


Figure 4.3: Laser, signal output power and signal output power 2 (bottom) as a function of the input power for a laser current of 80mA and a SOA current of 90mA for different coupling ratios between the SOA and the laser diode.

In Figure 4.4 the various possible output powers are shown as a function of the input power for very low coupling ratios between the SOA and the laser diode. This figure shows that while the bistability can (almost) disappear the laser diode can still be switched off, which results in a slightly steeper characteristic of the signal output power

around the switching point of the laser diode. This can clearly be seen from the signal output power measured after the coupler but also from the signal output power measured after the laser diode. This very steep response towards input power variations below the switching point and the flat output power level after the switching point can be utilized as the decision element in a 2R-regenerator. At the same time the response of the laser power might be used for wavelength conversion.

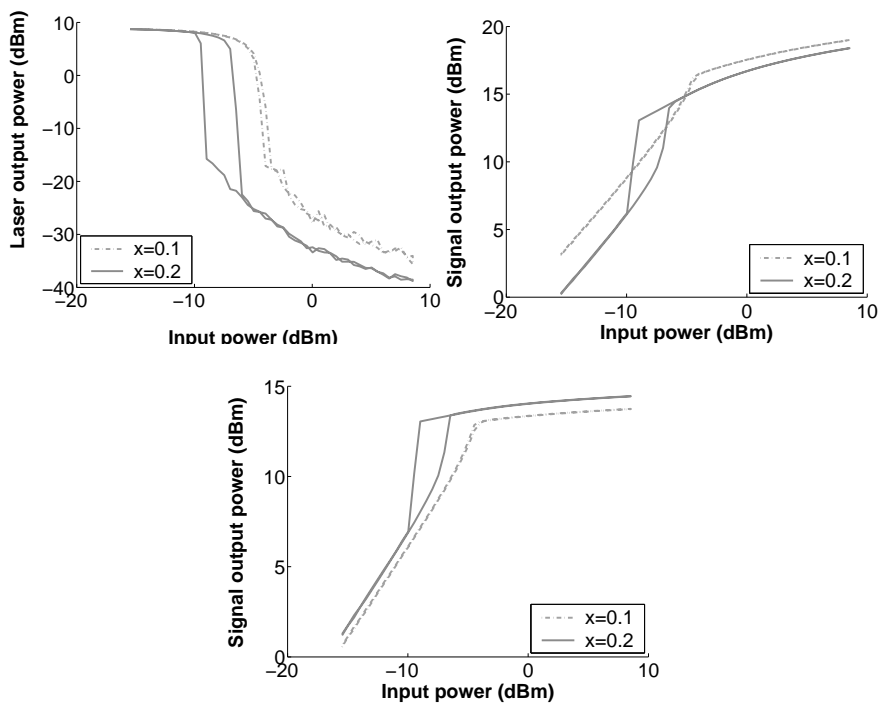


Figure 4.4: Laser and signal output power as a function of the input power for a laser current of 60mA and a SOA current of 220mA for different coupling ratios between the SOA and the laser diode.

4.2.4 Input power dependence

When a coupler with a fixed coupling ratio between the SOA and the laser diode is used, the properties of the bistable domain can still be varied by changing the drive currents of the laser diode or the SOA (or both). Figure 4.5 shows the response of the device as a function of the

input power for a fixed laser drive current and different SOA drive currents. When the SOA drive current is decreased the width and position along the input power axis of the bistable domain is also decreased. This again corresponds well with the result obtained in Figure 3.23. An increase in the SOA drive current results in a higher gain for the same input powers. This leads to more power injected into the laser diode and therefore also to a shift to lower input powers of the switch off point of the laser diode. The switch on point of the laser diode is also shifted to lower input powers because of the increased SOA gain at higher SOA drive currents. A lower input power is required for the SOA output power injected into the DFB laser diode to drop below the actual threshold injection power, at which the laser diode switches back on.

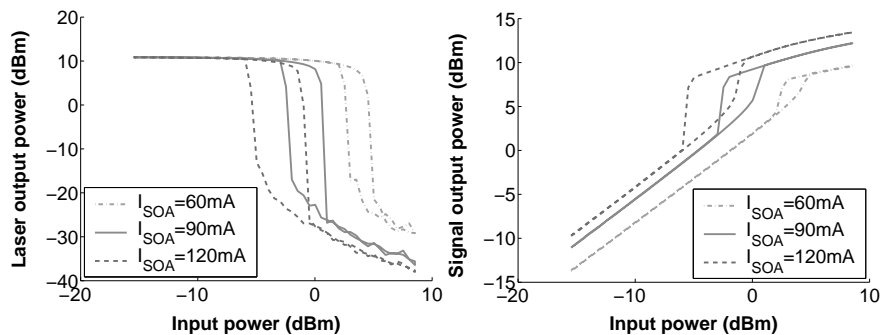


Figure 4.5: Laser and signal output power as a function of the input power for a laser current of 80mA and a coupling ratio between the SOA and the laser diode of 0.5 for different SOA currents.

In Figure 4.6 results obtained with the analytical model, described in Chapter 3, is shown for comparison with the results obtained using VPI, which are shown in Figure 4.5. The output saturation power of the SOA was in this case calculated to be 14mW (11.5dBm). The laser drive current was about 110mA. The coupling factors between the laser diode and SOA were chosen as 0.5. It can be seen that with comparable operating conditions (drive current, coupling factor) both models show similar results. The width of the bistable domain varies in both cases from around 1 to 6dB, while the step height is of the order of 10dB for the signal power and 35dB for the laser power. The power levels in both the input and output powers are also in the same range. This shows that accurate fitting between the two models could probably be performed if needed for device optimization. But since the interest of

the analytical model was primarily in finding a fast method to describe the behaviour of the device, whereas the interest in the use of VPI was primarily based on the fact that the model used there was a lot more complete, this fitting was not done.

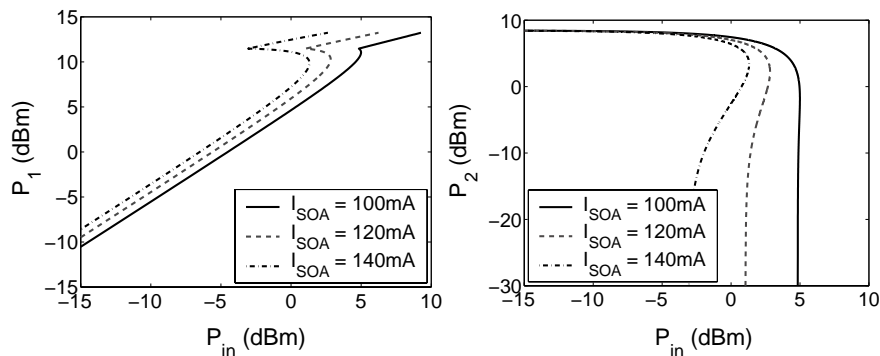


Figure 4.6: Laser and signal output power as a function of the input power, obtained from the model described in Chapter 3. The output saturation power of the SOA is 11.5dBm. The coupling ratio between laser diode and SOA is 0.5. The laser drive current is 110mA. The SOA drive current is varied.

An alternative way to vary the properties of the bistable domain when a fixed coupling ratio between SOA and laser diode is used is changing the laser diode drive current. This is shown in Figure 4.7. An increase of the width of the bistable domain accompanied with a shift of the bistable domain towards higher input powers can be observed when increasing the laser diode drive current. This can again be explained by considering the feedback between the SOA and the DFB laser diode. When the current of the laser diode is increased the input power needed to switch of the laser diode (cf Equation 3.11) also increases. This means that the right boundary of the bistable domain is shifted to higher input powers. The same thing happens for the left boundary of the bistable domain. Since the threshold input power for the laser diode to switch on increases when increasing the laser drive current, the laser diode switches on for higher input powers when the laser diode drive current is increased.

4.2.5 Wavelength dependence

An important aspect of any device used in all-optical (WDM) networks is the wavelength dependence of the device. It is always preferable if a

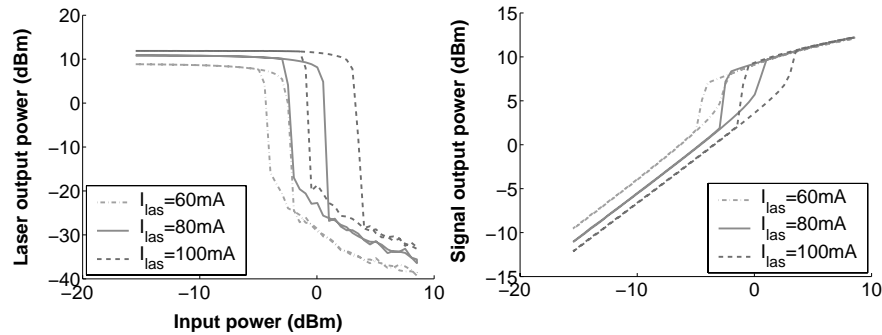


Figure 4.7: Laser and signal output power as a function of the input power for a SOA current of 90mA and a coupling ratio between the SOA and the laser diode of 0.5 for different laser currents.

single device can be used over a wide wavelength range. In that way an array of identical devices can be used to handle the different WDM channels in the light path. On the other hand this also allows for the re-configuration of the network. The information on a single channel can be switched from one wavelength to another but can still be processed by the same device. In figure 4.8 the static wavelength dependence of the SOA and DFB laser diode feedback system is shown. It can be noted that the right boundary of the bistable domain remains almost the same whereas the left boundary shifts slightly when the wavelength of the externally injected signal is altered. This can be explained by the wavelength dependence of the SOA and laser diode gain. In the case of a laser diode emitting laser power into the SOA the gain of the SOA is highly saturated resulting in a small influence of the wavelength dependence on the output power. In the case of a laser diode in the off state on the other hand the SOA is less saturated leading to slightly larger gain differences in the SOA, which in turn result in a shift in the signal input power at which the laser diode turns on again.

4.3 Experimental results

4.3.1 Device and measurement setup

For the experimental analysis of a device consisting of a mutually and optically coupled SOA and DFB laser diode a device received from NEC [63] was used. The device consists of a semiconductor optical amplifier of about $600\mu\text{m}$ long which is connected to a DFB laser diode

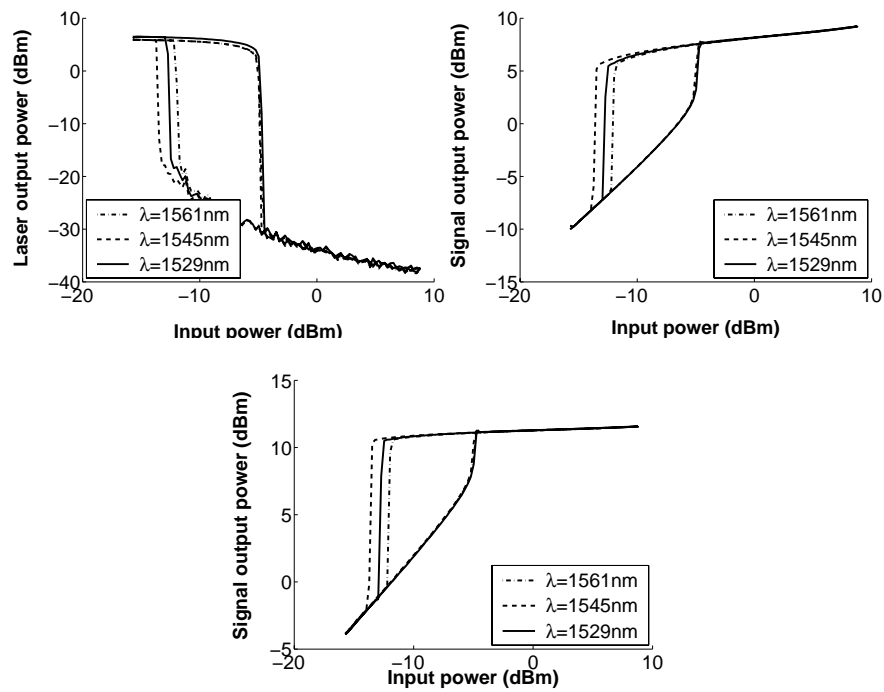


Figure 4.8: Wavelength dependence of the laser and signal output power as a function of the input power for a laser current of 80mA, a SOA current of 100mA and a coupling ratio between the SOA and the laser diode of 0.45.

array by means of a $770\mu\text{m}$ long 1 by 4 multimode interference coupler. The laser diode array consists of 4 $\frac{\lambda}{4}$ -shifted DFB laser diodes with a length of about $430\mu\text{m}$. The different laser diodes in the array each have a different grating period, which leads to a shift in lasing wavelength of 2.4nm between adjacent laser diodes. Fine tuning of the lasing wavelength can be done by thermal tuning. The output waveguide of the SOA is angled under 7° and AR coated to avoid reflections at the SOA facet. The right hand side facet of the device is AR-coated as well, to ensure single mode operation of the DFB laser diode. It also helps in avoiding reflection of the ASE generated in the SOA back to the SOA. Due to the 1 by 4 MMI-coupler the coupling between the SOA and laser diode is limited to 0.25.

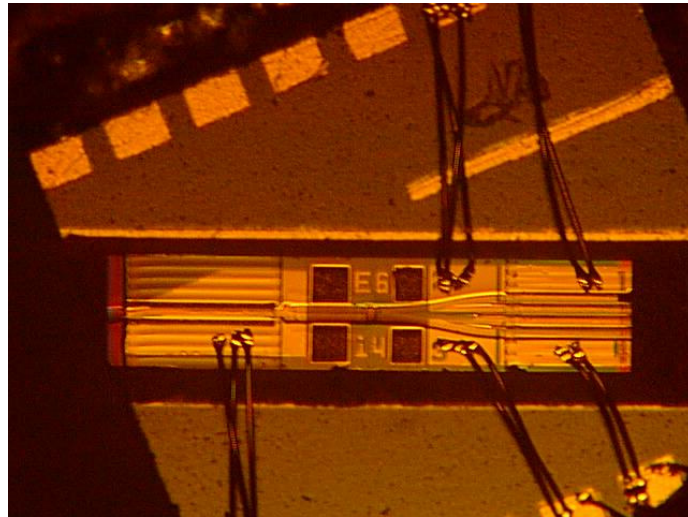


Figure 4.9: Picture of the device used for the experimental verification of the operation of a SOA and DFB laser diode combination. From left to right the SOA, MMI-coupler and laser diode array can be distinguished.

To access the device electrically probe needles are used to supply the current as shown in Figure 4.10. Optical coupling from and to the device is done by means of lensed fibers that can also be seen in Figure 4.10. The little dark square on the yellow mount corresponds to the actual device as shown in Figure 4.9. At the left side of the mount the SOA is situated and the position of the device on the mount is rotated so as to provide optical coupling with the lensed fiber at the SOA side. At the right side of the mount the output of one of the 4 laser diodes is coupled to a lensed fiber, but because of the rotation of the device

the optical coupling from waveguide to fiber will be lower than in the optimal case. Nevertheless only one of the laser diodes can be optically monitored by means of a lensed fiber. Different laser diodes can of course be driven electrically simultaneously. This can be helpful to saturate the SOA further or to obtain a device where multiple output states at different wavelengths are needed.

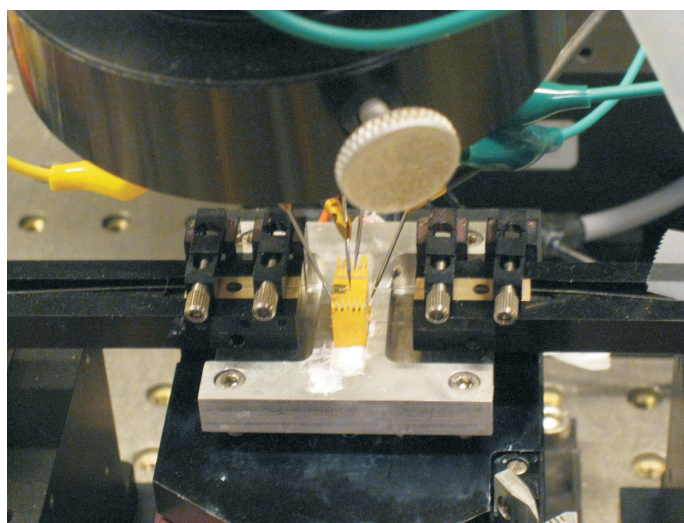


Figure 4.10: Picture of the electrical probing and coupling of the light in and out of the device.

To measure the static response of the device the setup as shown in Figure 4.11 was used. The input signal to the device was generated using a tunable laser source, allowing to change the wavelength of the injected light. The power level of the input signal could be controlled by using a variable optical attenuator. The actual injected power into the device is fed to a power meter to serve as a reference for the output versus input characteristic of the device. At the laser diode side of the device an optical switch is used to switch between one of two tunable optical filters that are tuned to the laser signal wavelength and the input signal wavelength respectively. Another optical switch is used to connect the tunable optical filter currently used to a power meter in order to measure the desired output signal. The output power of the laser diode can also be obtained from the SOA side of the device by using an optical circulator to separate the forward and backward propagating signals.

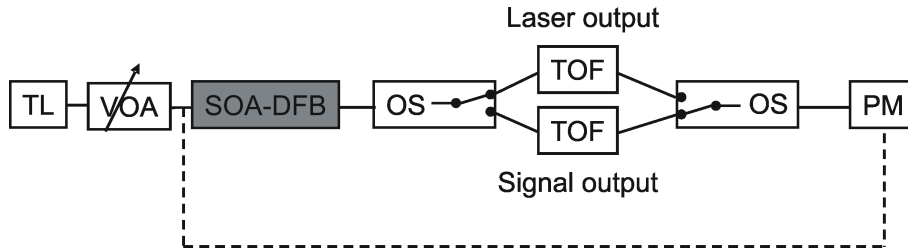


Figure 4.11: Setup used for the static characterization of the SOA and DFB laser diode combination. Used abbreviations: TL: Tunable laser, VOA: variable optical attenuator, OS: optical switch, TOF: tunable optical filter and PM: power meter.

4.3.2 SOA and laser diode drive current dependence

As shown before in the previous chapter it is possible to obtain a bistability in the laser and signal output of a SOA and DFB combination by changing the drive current of the laser diode or the SOA while keeping the other drive current and the input power constant. This is shown for a varying laser drive current in Figure 4.12 for different input powers and a SOA drive current of 80mA. The wavelength of the input power is 1550nm and the emission wavelength of the laser diode is 1541.2nm in the following results unless otherwise mentioned.

It can be observed that the width of the bistable domain decreases and the position of the bistable domain increases as a function of the laser diode drive current with increasing input power. This follows directly from the fact that a higher input power leads to a higher output power of the SOA for the same current settings. Therefore in order for the laser diode to switch on, a higher laser diode drive current is required. The switch off of the laser diode is also dependent on the input power, but due to the effect of the laser power saturating the SOA the decrease in the position of the left boundary of the bistable domain is less pronounced.

Important to note is that while the power levels of the laser output power remain fairly flat before and after the switching of the states, a positive slope can be seen in the signal output power in the case of a switched off laser. This can easily be explained by considering that in the absence of the laser field the laser diode acts as a SOA, which means that when the drive current is increased the gain in the laser diode is increased as well. Since the signal output power is obtained at the right hand side facet of the laser diode that increase in gain is reflected in the

signal output power. Once the laser diode is switched on the gain of the laser diode is clamped and the signal output power flattens out as a function of the laser diode drive current. From Figure 4.12 a bistable domain of over 20mA in laser drive current, and with a height of more than 35dB in the laser output power and 3dB in the signal output power can be observed.

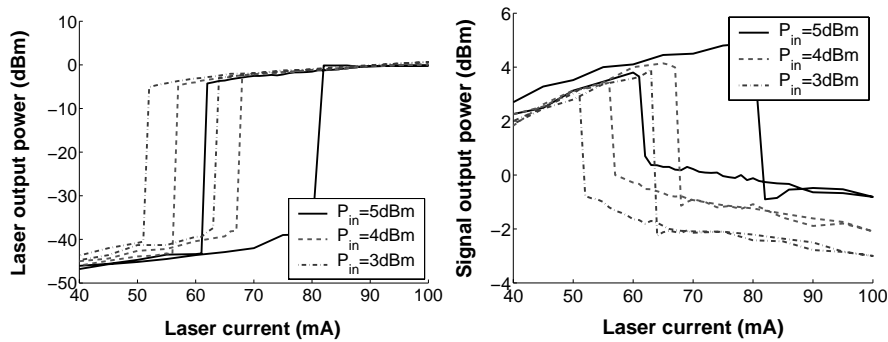


Figure 4.12: Static response of the laser output power and signal output power as a function of the laser drive current for different CW input powers and a SOA drive current of 80mA. Left: Laser output power. Right: Signal output power at the right hand side facet of the device (laser diode).

When the laser drive current is kept constant at 70mA Figure 4.13 shows that bistability can also be obtained by changing the SOA drive current. The laser drive current is kept at 70mA. The behaviour of the bistable domain corresponds well with the results obtained in Figure 3.16. The width of the bistable domain decreases with increasing CW input power and the bistable domain shifts to lower SOA drive currents when the CW input power is increased. Again this can be explained by considering that a higher CW input power requires less gain, which is equivalent to the SOA drive current, than a lower CW input power to switch off the laser diode. At the same time a higher CW input power has to receive less amplification in order for the laser diode to switch back on, which again leads to a shift of the right boundary of the bistable domain towards lower SOA drive currents. The difference in the height of the bistability in the signal output power between different CW input powers, stems from the fact that in the state with the laser diode switched on the SOA gives almost identical amplification for the same SOA drive current. This is caused by the heavy saturation by the laser power. The SOA output power is in that case amplified

by the (locked) gain of the laser diode. In the case of a switched off laser diode the output power of the SOA also saturates the laser diode leading to a characteristic resembling that of a SOA in the saturation regime.

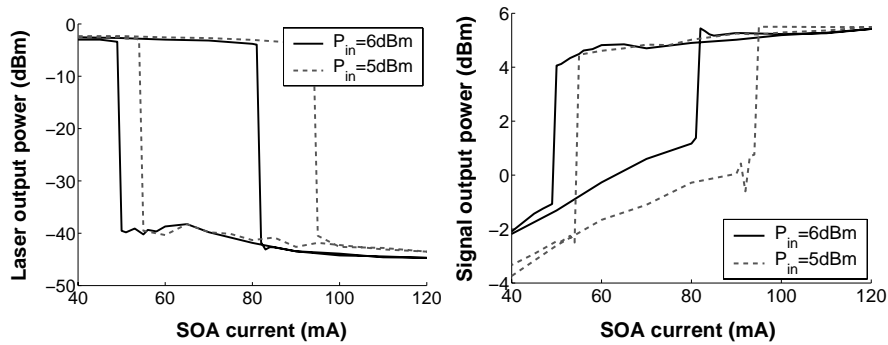


Figure 4.13: Static response of the laser output power and signal output power as a function of the SOA drive current for different CW input powers and a laser drive current of 70mA. Left: Laser output power. Right: Signal output power at the right hand side facet of the device (laser diode).

4.3.3 Input power dependence

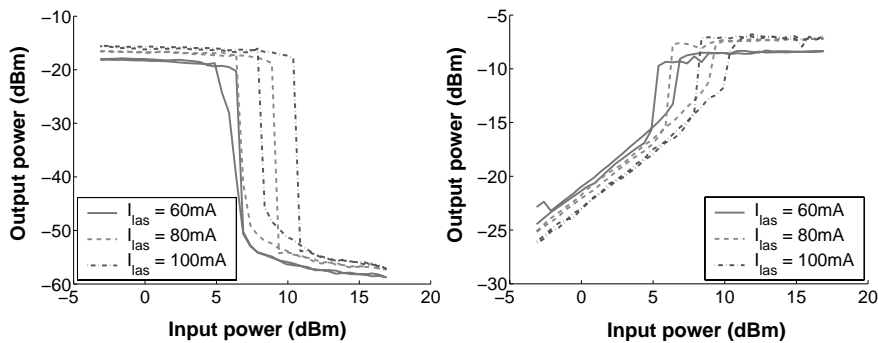


Figure 4.14: Static response of the laser output power and signal output power as a function of the input power for different laser drive currents and a SOA drive current of 120mA. Left: Laser output power. Right: Signal output power at the right hand side facet of the device (laser diode).

To be able to exploit the optical bistability present in a SOA and DFB laser diode combination all-optically the bistability has to be controlled

by means of optical signals. Statically this is shown in Figure 4.14 where the laser and signal output power of the device is shown as a function of the input power for different laser drive currents. As in Figure 3.24 it can be seen that the bistable domain shifts to higher input powers with increasing laser diode currents. The increase of the width of the bistability can also be seen, but for higher laser drive currents the width of the bistability saturates in analogy with Figure 3.20. A bistability of over 3dB wide and over 30 and 7dB high for the laser output power and the signal output power respectively can be observed.

These results correspond rather well with the simulation results shown in Figure 4.5. The main difference between the simulations and the experiments can be found in the power levels of the input and output signals. This difference can primarily be explained by considering the fiber to chip coupling loss in the experiments. Typically this loss was of the order of 6dB at the SOA side of the device, while the coupling loss at the DFB laser diode side of the device could be as high as 15dB. Taking these losses into account one can see that the experimentally obtained power levels correspond rather well with the simulation results. Since only one device was used during the experimental verification of the device's operating principle, no fitting between the experimental and simulation results was performed. This fitting however is useful in case device optimization is considered.

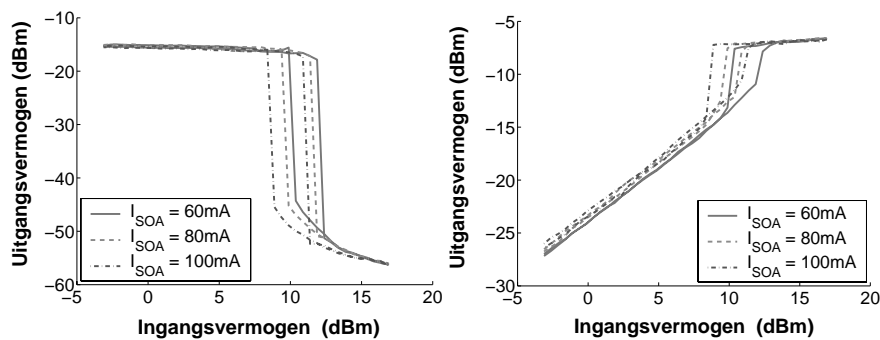


Figure 4.15: Static response of the laser output power and signal output power as a function of the input power for different SOA drive currents and a laser drive current of 100mA. Left: Laser output power. Right: Signal output power at the right hand side facet of the device (laser diode).

Another way to change the position of the bistable domain along the input power axis is to change the SOA drive current as shown in Figure 4.15 for a laser drive current of 100mA. As in Figure 3.23 the

width of the bistability can be seen to remain nearly constant with changing SOA drive current. The position of the bistable domain shifts to lower input powers for increasing SOA drive currents due to the higher SOA gain. Similar widths and heights of the bistable domain as in Figure 4.14 are shown. Again a comparison could be made with the corresponding simulation results.

4.3.4 Wavelength dependence

By changing the wavelength of the signal injected into the device the wavelength dependence of the optical bistability can be examined. Figure 4.16 shows the static bistability domain of the SOA and DFB laser diode feedback scheme for different wavelengths. The SOA drive current is 74mA and the drive current of the laser diode is 70mA. The emission wavelength of the laser diode is 1541.2nm. It can be seen that bistability in the laser output can be obtained over a wavelength range of at least 25nm. Broader wavelength operation is limited by the gain curve of the SOA and laser diode and the wavelength dependence of the coupler between the SOA and the laser diode. The difference in width and position of the bistable domain between the different wavelengths may be explained by the wavelength selectivity in the laser diode, due to the grating and the wavelength dependence of the coupling ratio in the MMI-coupler.

Special care has to be taken when the wavelength of the input signal approaches the laser wavelength. When the signal wavelength nears the Bragg wavelength of the laser diode the relative coupling from signal power into the laser diode increases, disrupting the optical feedback scheme. Due to the increasing reflectivity of the grating of the laser diode for signal wavelengths approaching the Bragg wavelength a fraction of the input signal, after amplification in the SOA and laser diode, couples back into the SOA. This reflected signal power acts as a saturating term, reducing the gain of the SOA and making it harder to switch the laser diode off. This can be seen in Figure 4.17 where the response of the laser output power is shown for wavelengths near the laser emission wavelength (1541.2nm). It is clear that for signal wavelengths as close as 1.5nm to the laser wavelength the laser diode can not be quenched for the input powers obtainable with the used setup. For a signal wavelength of 1542.7 the laser diode can be quenched but bistable operation of the device can not be guaranteed.

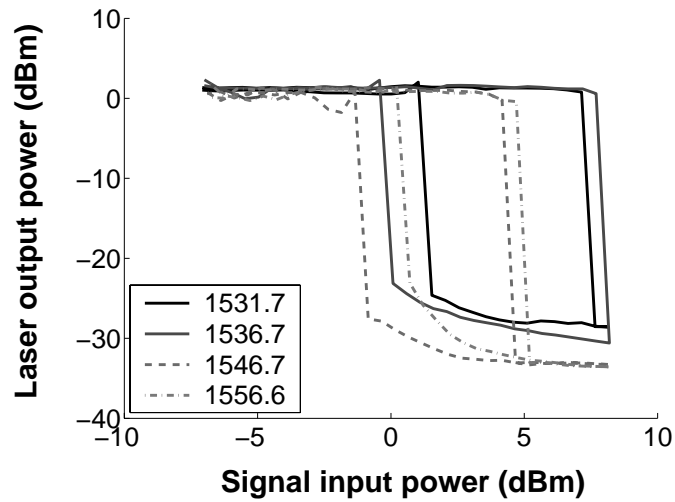


Figure 4.16: Static response of the laser output power and signal output power as a function of the input power for different SOA drive currents and a laser drive current of 100mA. Left: Laser output power. Right: Signal output power at the right hand side facet of the device (laser diode).

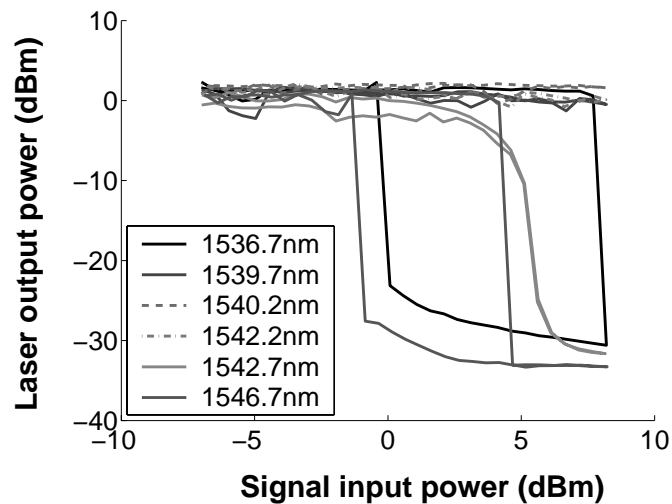


Figure 4.17: Static response of the laser output power and signal output power as a function of the input power for different SOA drive currents and a laser drive current of 100mA. Left: Laser output power. Right: Signal output power at the right hand side facet of the device (laser diode).

4.4 Conclusions

In this chapter the static behaviour of a feedback scheme consisting of a DFB laser diode and a SOA was investigated both by means of simulations using a commercial software package as by means of experiments using an integrated SOA with DFB laser array. The device was shown to exhibit bistable operation in both the signal output power and laser output power under external optical signal injection. The flexibility of operation of the device was demonstrated by looking into the dependence on the drive current of both laser diode and SOA, the coupling ratio between laser diode and SOA and the wavelength and power of the input signal. The obtained results were compared with the results from the theoretical study in the previous chapter showing good correspondence.

The device was shown to be optically bistable, both when changing one of the drive currents (while keeping the other drive current and the input power constant) and when changing the input power (while keeping the drive currents constant). Operation over a wavelength range of over 25nm was demonstrated. For signal wavelengths near the Bragg wavelength of the laser diode the bistable behaviour of the device can however not be guaranteed.

To prove that the bistability in this device originates from the feedback between the signal power and the laser power in both the laser diode and the SOA simulations were performed indicating the validity of the model in the previous chapter.

Chapter 5

Dynamic analysis of an all-optical flip-flop based on a SOA and DFB laser diode

The bistability in the output power of a device consisting of an optically coupled SOA and DFB laser diode will be used in this chapter to obtain all-optical flip-flop operation. Again both simulations and experiments are carried out. An analysis of the dependence of the required switching energy on the pulse length and other device parameters is made.

5.1 All-optical flip-flops

As already mentioned in chapter 1, the ever increasing network traffic drives a demand for more bandwidth in the network. All-optical networks, and in particular all-optical packet- and burst-switching networks are starting to become viable competitors to standard networks employing optical-electronic-optical (OEO) conversions [74]. In packet-switched all-optical networks, there is a need for all-optical flip-flops (AOFFs) that show latching capabilities to implement switching, routing, packet header buffering and optical memory operations.

Bistable devices such as the one shown in the previous chapter are important in the digital circuits used in communications, signal processing and computing. They can be used as all-optical flip-flops in switches, logic gates and memory elements [75]. As a switch the AOFF can be used to provide the additional power needed to reduce the absorption in a saturable absorber. If the bistable device is in the upper

branch state the signal passes through the saturable absorber if not the signal can get (partly) blocked by the saturable absorber. An AOFF can also be used as a logic gate, such as an AND-port by using it in such a way that switching can only occur when two signals are simultaneously present. It is known from digital electronics, that any digital device can be constructed from combinational and sequential logic gates [76]. In combinational logic gates the output of the device is only dependent on the current input to the device. Thus far several schemes showing both high processing speeds and low power consumption have been demonstrated [17, 77, 78]. Sequential logic requires that the output of the logic gate depends on previous inputs to the device. The history of the device is taken into account in such devices. In order to come to all-optical sequential logic all-optical flip-flops are a key element. An all-optical replication of the combinational and sequential logic components from electronics, combined with a scalable and flexible manufacturing process, will allow the construction of sophisticated optical circuits using the powerful design techniques of digital electronics. The motivation for realizing digital logic in optics is a potential increase in processing speed and a significant reduction of power consumption.

Finally a bistable device can be used as a memory element when considering that the state of the device is defined by its history and only changes due to external control. This makes that an all-optical flip-flop can be considered as a one bit optical memory.

AOFFs have been used as building blocks in several packet switching demonstrations at 40 Gb/s and beyond [79, 10, 80, 81, 82, 83]. Typically, the AOFFs are used as continuous wave (CW) inputs to wavelength converters, hence controlling the target wavelength of the converted data packet. Current demonstrations of optical flip-flops are focused on the switching fabric of optical network nodes, where the requirements for processing speed and power consumption are highly critical. In the future, one could envisage that the entire control plane functionality could be realized in all-optical logic or even all-optical general purpose computers, provided that the control plane load justifies a switch from electrical to optical technology.

5.1.1 All-optical flip-flops in literature

In this section a short overview of the most common types of all-optical flip-flops currently presented in literature will be given along with their principle of operation.

Bistable laser diodes

Depending on the configuration, different types of bistable laser diodes can be distinguished. Possibly the most documented to date is the multimode interference bistable laser diode (MMI-BLD). This device consists of an active multimode interference 2×2 coupler inside a laser cavity [84, 85, 86]. Saturable absorbers are added to the two output ports to provide for the non-linearity and feedback required to obtain the bistable operation. Both cross states of the MMI coupler can support lasing oscillations, but they are mutually exclusive due to cross-gain saturation and bleaching of the absorbers. The lasing cross state of the MMI-coupler defines the state of the AOFF and state changes can be forced by injecting an optical pulse in the non-lasing mode of the device. A variant of this device with distributed Bragg reflectors on the output waveguide showed a contrast ratio of 16dB between the on and the off state [87].

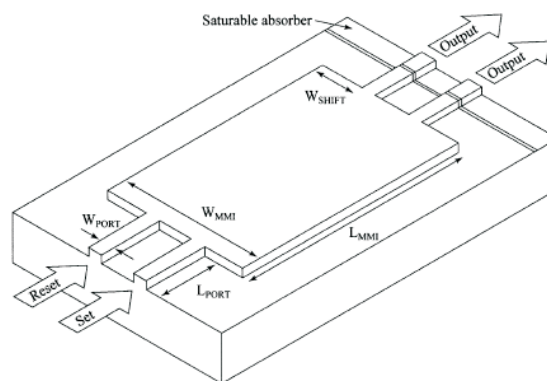


Figure 5.1: Schematic representation of the multimode interference bistable laser diode based all-optical flip-flop [84].

Another approach uses a cavity consisting of a saturable absorber and a nonlinear directional coupler to come to a bistable laser diode [88].

Using a DFB laser diode bistable operation can also be obtained [73]. The bistability is in this case based on the difference in threshold carrier density for the laser diode between the two states as has been explained in section 4.2.2.

Coupled laser diodes

By coupling two laser diodes (CLC), each lasing at a different wavelength, all-optical flip-flop operation can be obtained. At any time only one of the two laser diodes can be switched on. The other laser diode is then quenched by the output power of the switched on laser diode. Switching between the states can be done by injecting a pulse at the switched off laser wavelength into the device. In addition to in-line laser diodes [89] also ring laser based devices can be used to construct the all-optical flip-flop [90].

Using microring lasers very fast (20ps switching time) and low switching energy (5.5fJ) operation has been demonstrated [91]. The output power of these devices is however rather limited, making it useful for optical memory purposes but less for switching purposes.

Recently it has been shown that (micro)ring or (micro)disk lasers can exhibit bistability on their own by taking advantage of the bimodal nature of the devices. Due to gain non-linearities in the ring or disk, only one of both clockwise or counter-clockwise modes will lase at any time. By using optical pulses the preferred lasing mode can be changed [92]. Recent advances in the development of microdisk lasers lead to believe that very fast devices could be made with very low switching energies [93].

Coupled Mach-Zehnder interferometers

A coupled Mach-Zehnder interferometer (CMZI) consists of two Mach-Zehnder interferometers with SOA's in one arm and passive phase shifters in the other, connected by a 3dB coupler [94, 95]. Depending on the phase difference in the arms of one MZI, it can dominate the other MZI by switching an externally generated CW signal through the 3dB coupler into the active (SOA-equipped) arm of the opposite MZI. The injected light perturbs the phase shift in the MZI locking it in the "dominated" state. Since the setup is symmetric, the situation can also be reversed by injecting a pulse into the active arm of the dominating MZI [96, 97]. The state of the AOFF is defined by the dominating SOA and can be detected either by the wavelength of the CW output or the port

where it appears. A schematic representation of the coupled Mach-Zehnder interferometers based all-optical flip-flop is given in Figure 5.2.

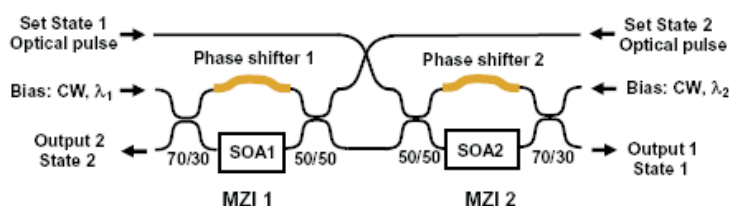


Figure 5.2: Schematic representation of the coupled Mach-Zehnder interferometers based all-optical flip-flop [96, 97].

All-optical flip-flop operation has also been demonstrated using a single Mach-Zehnder interferometer with a feedback loop [98, 99].

Polarization bistable lasers

Polarization bistable lasers (PBL) have two lasing modes in orthogonal polarizations, defining the two states of the AOFF [100]. The state can be switched by injecting a light pulse with the desired polarization into the laser. Cross-gain modulation between the two polarization states is responsible for the bistability. Typically these lasers are of the vertical cavity surface-emitting laser (VCSEL) type.

DFB SOA's

DFB SOA'S are devices where a DFB laser diode is driven below threshold. In that case the DFB laser diode can be considered as a sort of resonant SOA with respect to injected signals. The all-optical flip-flop operation in these devices is based on the dispersive bistability present in such devices for input signals close to the resonance wavelength of such devices [101, 102].

Optical feedback scheme between a SOA and DFB laser diode

In this device, which will be explained later in this chapter, the DFB laser diode in contrast to the previous case is driven above threshold [70, 103, 104].

Comparison of different devices

Each type of AOFF has advantages and drawbacks, and no optimal choice has emerged yet. Here, a comparison will be given of some AOFFs reported in the literature. The most common used properties to describe an all-optical flip-flop are the switching time, contrast ratio, repetition rate, pulse energy and the pulse length. The switching time is defined as the 10%-90% transition time between the different states. The contrast ratio is defined as the difference in output power level between the stable states. The set and reset pulses are defined by their energy and length. The repetition rate can be defined in several ways. The most logical would be to define the repetition rate as the rate at which two equal transition between states (set-set or reset-reset) occur. In that way the actual speed of the device can be determined. Most commonly however the time between two different transitions (being set-reset or reset-set) is taken as the repetition rate of an all-optical flip-flop. The different possible conventions for the repetition rate are shown in Figure 5.3.

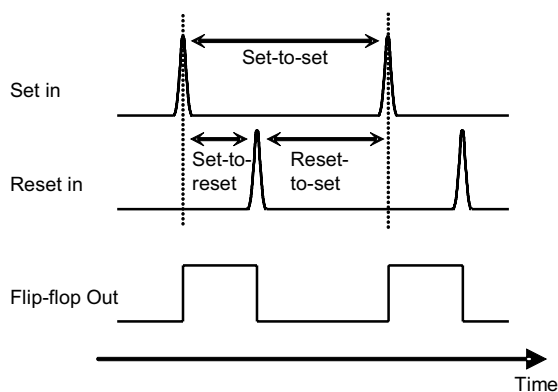


Figure 5.3: Different definitions of the repetition rate of all-optical flip-flops.

In this work the repetition rate is defined as the rate between two equal transitions. In Table 5.1 the repetition rate is however defined by the time between two different state transitions for comparison reasons. Table 5.1 shows the most important device parameters for all-optical flip-flops presented in literature.

Table 5.1 shows large variations in the key parameters of different AOFFs reported in the literature. The maximum clock speed of all-optical logic circuits is bound by the switching time of the AOFFs as

Type	Switching time	Contrast ratio	Repetition rate	Pulse energy	Pulse length
PBL [100]	100ps	n/a	10GHz	2-3.5fJ	50ps
PBL [100]	n/a	n/a	540MHz	0.2-0.3fJ	900ps
MMI-BLD [87]	300ps	16dB	3.25GHz	40pJ	10ns
CLC [89]	n/a	n/a	30kHz	n/a	4 μ s
CLC [91]	20ps	9dB	90MHz	5.5fJ	13ps
CMZI [94]	200ps	12dB	67MHz	20pJ	200ps
CMZI [96]	200ps	13dB	31MHz	600pJ	150ps
DFB SOA [102]	1ns	8dB	1MHz	36pJ	15ns
SOA and DFB LD [104]	50ps	19dB	3GHz	0.9-1.6pJ	50ps
SOA and DFB LD [105]	100ps	15dB	330MHz	0.24-0.34pJ	100ps

Table 5.1: Device properties of different all-optical flip-flops presented in literature.

well as the repetition rate. Specifically, the inverse of the clock frequency must stay below the switching time so the AOFF can switch states in each clock period. In practice, the devices in Table 5.1 have been demonstrated with repetition rates much lower than the bound given by the switching time. The only exception is [100], which achieves the upper bound at 10GHz repetition rate with a switching time of 100ps. [104] comes close to the limit with 3GHz repetition rate and 50ps switching times. The reason for the gap between reported repetition rates and switching times are not necessarily intrinsic to the devices. Generating sufficiently short set and reset pulses along with a high pulse repetition rate can be difficult and may be the limiting factor for some experiments. Judging from the control pulse width and switching time of the micro-ring laser in [91], it should have a potentially much higher repetition rate than the reported 90MHz. Another factor may be the intended application of the AOFFs. Papers [87] and [96] propose to use the AOFFs for optical packet switching, and thus only require a repetition rate on the order of the inverse of the packet duration.

The needed switch pulse energy is a main differentiator of the compared AOFFs. Ranging from tens of pJ using coupled laser cavities [89] to a fraction of a fJ using coupled micro-ring lasers [91], the switching energies span 5 decades. Low switching energies is a primary requirement as it will directly influence the power consumption of the device. The contrast rate is generally good, at approx. 10dB or more for all types.

It should be noted that some all-optical flip-flops mentioned here require the presence of a continuous input power to make the device work in its bistable regime. This however is not a big problem as a single laser diode could be used to provide this CW power for several all-optical flip-flops at the same time, leading to only a minor additional cost. The AOFF should however still accept a wide range of CW input powers and control pulse energies to allow integration with other flip-flops and to form logic gates. In a complicated digital design, the signal paths will be varied and the signal qualities on each input cannot be expected to be ideally suited to each AOFF. Every device has optimal operating conditions, but deviating slightly from these should not degrade the device performance to an unacceptable level.

5.2 Principle of operation

In order to use any bistable device as a flip-flop, being all-optical or not, some method to change between the different stable states is required. In the case of a bistable device consisting of a SOA and a DFB laser diode, as shown in the previous chapter, the switching between the stable states can be done by injecting appropriate optical pulses into the SOA and laser diode respectively.

The working principle of the device can be explained as follows. From the static output versus input power response, as for instance shown in Figure 4.13, a CW input power can be chosen that forces the device to operate inside the optical bistable domain. The initial state of the device is assumed to be the one with the DFB laser diode emitting power as schematically shown in Figure 5.4. In this state both the CW input power and the DFB output power saturate the SOA resulting in limited gain for the signal power. The low signal power injected into the laser diode in its turn has little influence on the laser output power allowing the device to remain in the same state when the operating conditions of the device remain the same.

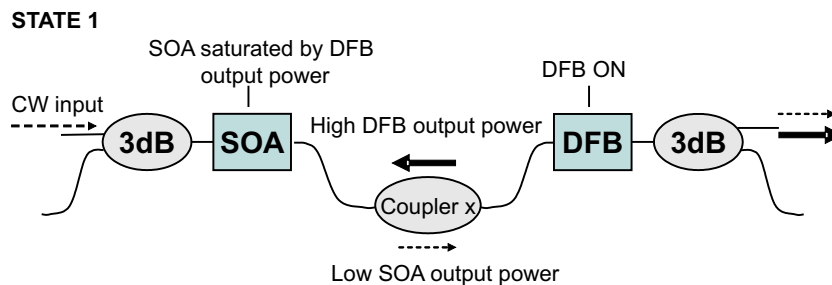


Figure 5.4: Schematic overview of the SOA-DFB all-optical flip-flop in the stable state with a turned on DFB laser diode. Coupler x represents a coupling device with a coupling ratio equal to x , while the other couplers used are 3dB couplers. The dashed line represents the signal power, the full line the laser power.

When a reset pulse is applied to the left hand side facet of the SOA the state of the device can be changed. The response of the device to the reset pulse is schematically shown in Figure 5.5. After passing through the SOA the reset pulse quenches the DFB laser diode. This leads to a sudden decrease of the total power injected into the SOA, resulting in gain recovery in the SOA. When the reset pulse is chosen properly (both in terms of length and energy) the higher gain in the SOA allows

for the amplified signal power to keep the laser diode quenched. This effectively changes the state of the device to the situation as shown in Figure 5.6.

RESET

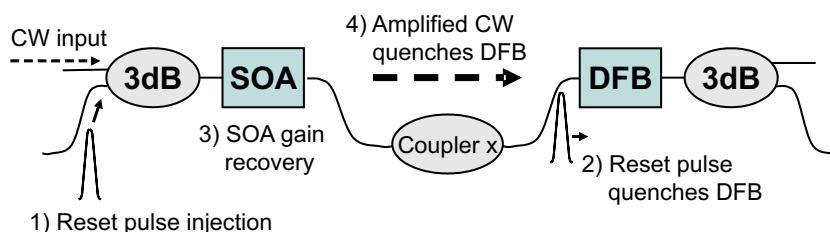


Figure 5.5: Schematic overview of the response of the SOA-DFB all-optical flip-flop during the reset operation. The dashed line represents the signal power.

STATE 2

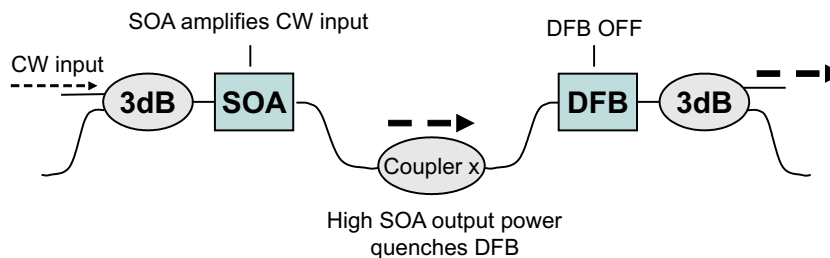


Figure 5.6: Schematic overview of the SOA-DFB all-optical flip-flop in the stable state with a quenched DFB laser diode. The dashed line represents the signal power.

As a final step to come to an all-optical flip-flop a set pulse, injected at the right hand side of the DFB laser diode, can be used to change the state back to the one shown in Figure 5.4. The set pulse upon arrival in the SOA saturates the SOA, leading to a decrease in gain for the signal power, which in its turn results in less signal power injected into the DFB laser diode. When the decrease of the signal power injected into the laser diode is large enough the laser diode can switch on again. The output power of the laser diode can then keep the SOA heavily saturated leading to stable operation of the device with a switched on laser diode. This is schematically shown in Figure 5.7.

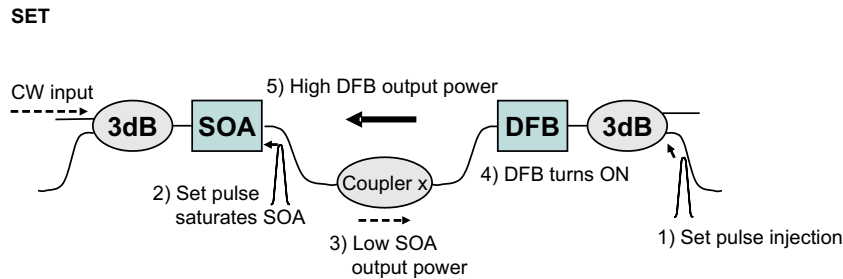


Figure 5.7: Schematic overview of the response of the SOA-DFB all-optical flip-flop during the set operation. The dashed line represents the signal power, the full line the laser power.

5.3 Simulation results

5.3.1 Setup

The SOA/DFB-laser diode feedback scheme was first numerically investigated using the commercial software package VPI [72]. The setup used in the simulations is shown in Fig. 5.8. A $500\mu\text{m}$ long SOA is connected through a bidirectional 3dB coupler with a $350\mu\text{m}$ long quarter wave shifted DFB laser diode.

In the results shown below the wavelength of the laser output power is 1553nm and the signal wavelength is 1538nm . The signal wavelength can be varied as long as it is sufficiently distant from the Bragg wavelength of the DFB laser diode. The optical pulses used for the switching of the device are first order Gaussian pulses (with a certain full width at half maximum (FWHM) and peak power). A CW input power is injected into the SOA and the optical set and reset pulses can be injected at port 2 and port 1 respectively. Alternatively they can also be injected at port 4 and port 3 (at the coupler). In this way the propagation of the pulse through the SOA (reset pulse) and DFB-laser diode (set pulse) can be avoided. The set and reset pulse train used in the simulations were periodical with a period of 6.4ns and shifted over 3.2ns with respect to each other.

5.3.2 Static bistability domain

In order to be able to use the combination of a SOA and DFB laser diode as an all-optical flip-flop the static response of the device as a function of the input power to the SOA has to be obtained first. The static

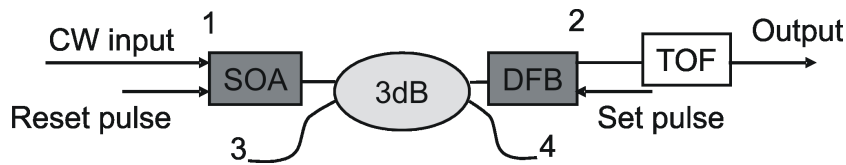


Figure 5.8: Schematic setup used for the simulations

bistable domain for the device described above with a SOA drive current of 120mA and a DFB laser diode drive current of 100mA is shown in Figure 5.9. The laser output power is obtained at the right hand side of the laser diode, while the signal output power is obtained directly after the 3dB coupler.

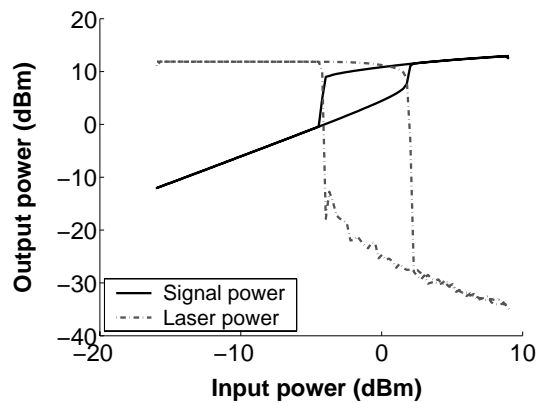


Figure 5.9: Static bistable domain in the signal and laser output power of the all-optical flip-flop used in the simulations for a SOA drive current of 120mA and a DFB laser diode drive current of 100mA.

A bistable domain with a width of over 7dB can be observed in both the signal output power and the laser output power. It is noteworthy that the contrast ratio between the different stable states is a lot larger for the laser output power than for the signal output power, around 30dB and around 10dB respectively. This difference in contrast ratio makes the laser output power more suitable for further use in other signal processing devices than the signal output power.

The fact that the signal output power is obtained after the coupler instead of after the laser diode, as would be the case in an integrated version of the device, only leads to a shift along the output power axis, as shown in Figure 5.10. The overall response of the device remains practically identical.

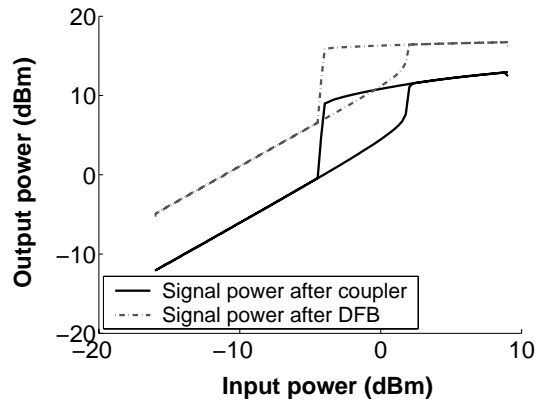


Figure 5.10: Static bistable domain in the signal power of the all-optical flip-flop used in the simulations for a SOA drive current of 120mA and a DFB laser diode drive current. The signal power right after the 3dB coupler and after the laser diode is shown.

5.3.3 All-optical flip-flop operation

Starting from the static bistability domain, shown in Figure 5.9, all-optical flip-flop operation in the laser and signal output power can be obtained by injecting optical pulses into the device. The set pulses used to switch on the DFB laser diode are injected into the SOA from port 4, while the reset pulses used to switch the laser diode off are injected into the laser diode from port 3. This approach allows for the effect of the set and reset pulses only to be felt directly by the SOA and laser diode respectively as compared to pulse injection into port 1 and 2.

In the latter case the set pulse first depletes the carriers in the laser diode further before the (amplified) pulse can deplete the SOA gain. This results in a slightly slower switch on of the laser diode. When the reset pulse is injected into the left hand side facet of the SOA instead of in port 3, the SOA gain is depleted first after which the amplified reset pulse can switch the laser diode off. Due to the amplification of the pulses in either the laser diode or the SOA, when the pulse injection is done through port 1 and 2, the peak pulse power and pulse energy can be lower than when the pulses are injected through port 3 and 4. On the other hand this can also lead to an upper limit to the pulse power. This happens because the carrier depletion in laser diode and SOA at injection through port 2 and 1 respectively may cause the device to return to the initial state after the passage of the reset and set pulse. The general behaviour of the device is however the same for both optical

pulse injection schemes albeit at different pulse energy levels as can be seen from Figures 5.11 and 5.12 where for the same CW input power of -0.5dBm and for a set and reset pulse length of 400ps all-optical flip-flop operation in the laser output power is demonstrated for both pulse injection schemes.

The pulse energy used to obtain the switching between the stable states is minimized in both cases. The minimal required pulse energy to obtain switching is lower when the set and reset pulse are first injected through the DFB laser diode and SOA respectively then when only injected into the SOA and the laser diode. What also can be observed from Figures 5.11 and 5.12 is that the laser turn on is slightly delayed with respect to the set pulse arrival in the case of pulse injection through port 3 and 4, as compared to the pulse injection through port 1 and 2. This may be caused by the additional amplification received by the set pulse in the latter case in the DFB laser diode, which may lead to a deeper saturation of the SOA and therefore a faster turn on of the laser, due to less amplified signal power injected into the laser diode. Another notable effect is the higher overshoot when the set pulse is injected into port 2. This again can be explained in the same way. Due to the amplification of the set pulse in the laser diode the SOA is pushed deeper into saturation resulting in less amplification of the input signal, which in its turn leads to a larger decrease in the signal power injected into the DFB laser diode, eventually causing the larger overshoot in the laser output power.

All-optical flip-flop operation for pulse injection at port 3 and 4 and for 50ps long pulses is shown in Figure 5.13 for the laser output power along with the corresponding set and reset pulses. The CW input signal power is -0.5dBm and the 50ps long set and reset pulses have a peak power of 46mW and 90mW respectively. Clear and fast transition between the different states can be observed. The stable states are shown to be maintained for over 3ns each.

The signal output power corresponding with the laser output power from Figure 5.13 is shown in Figure 5.14. The pattern of the signal output power is clearly inverted with respect to the laser output power pattern.

A more detailed look at the behaviour of the laser and signal output power around the time of the arrival of the set and reset pulses is given in Figure 5.15. The switch off operation of the DFB laser diode is almost instantaneous after the injection of the reset pulse. The switch on operation of the DFB laser diode shows some delay between the ac-

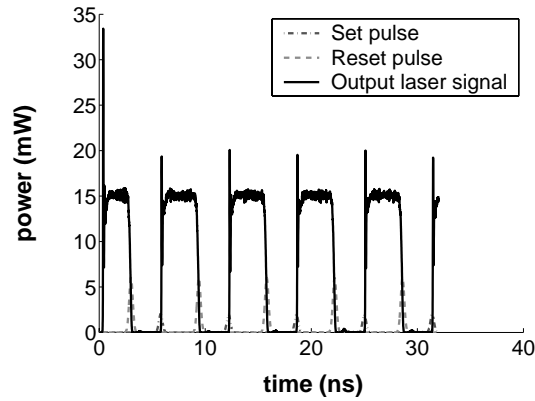


Figure 5.11: Laser output power during the all-optical flip-flop operation for pulse injection through port 1 and 2 as shown in Figure 5.8. The pulse length was 400ps and the CW input signal power is -0.5dBm. The set pulse peak power is 2mW and the reset pulse peak power is 6mW.

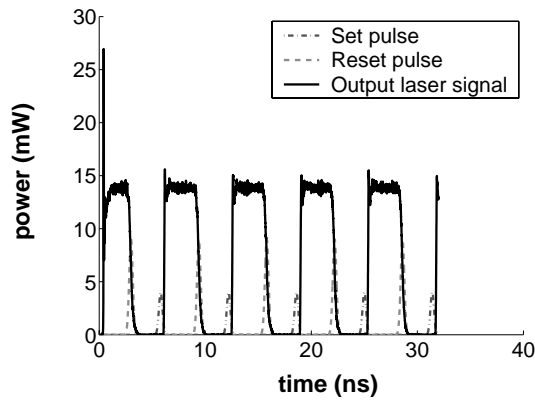


Figure 5.12: Laser output power during the all-optical flip-flop operation for pulse injection through port 3 and 4 as shown in Figure 5.8. The pulse length was 400ps and the CW input signal power is -0.5dBm. The set pulse peak power is 4mW and the reset pulse peak power is 9mW.

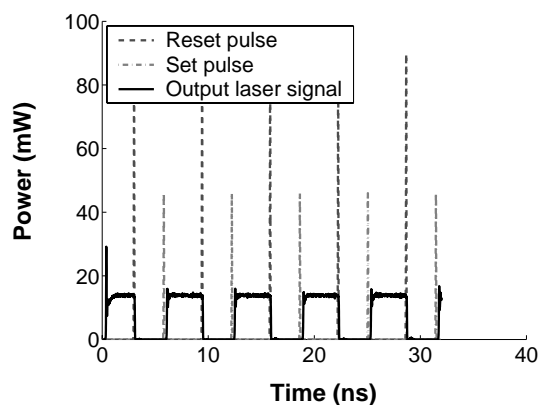


Figure 5.13: Simulated all-optical flip-flop operation in the laser output power for a CW input signal power of -0.5dBm . The pulse length is 50ps for both the set and reset pulses. The peak power of the set pulses is 46mW and it is 90mW for the reset pulses.

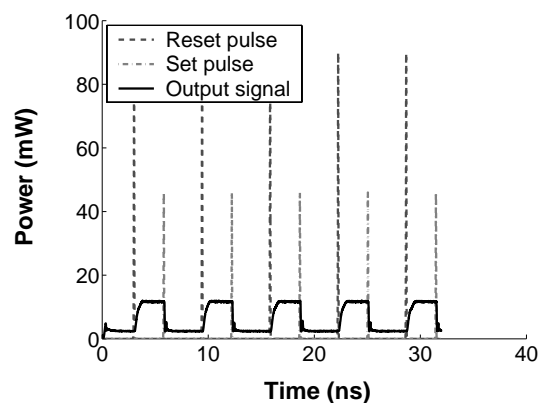


Figure 5.14: Simulated all-optical flip-flop operation in the signal output power corresponding with the laser output power response shown in Figure 5.13.

tual switch on of the laser diode and the arrival of the set pulse. This is partly caused by the optical path length this pulse has to travel before arriving at the laser diode. The remainder of the delay between the turn on of the laser diode and the injection of the set pulse can be explained by the turn-on delay time of the laser diode. After the switch on of the laser diode a small ringing phenomena can be observed representing the relaxation oscillations.

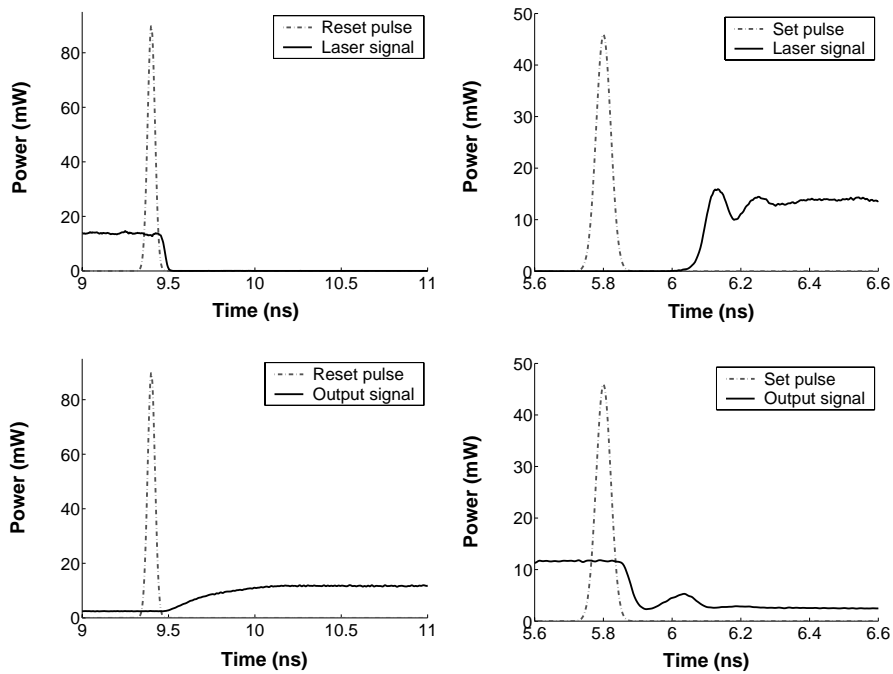


Figure 5.15: Detailed view of the laser and signal output power as a function of the time around the arrival of the set and reset pulse. Top: laser output power. Bottom: signal output power. Left: Reset pulse arrival. Right: Set pulse arrival.

The response of the signal output to the reset pulse happens almost instantaneously but the actual transfer to the eventual stable state happens more gradually than is the case for the laser output power. This gradual stabilization originates from the time needed for the carriers in the SOA to recover to the level corresponding to the actual power distribution in this case. Considering the behaviour of the signal output power to the set pulse a fast decline of the signal output power can be observed followed by an inverted ringing phenomena as the one

caused by the relaxation oscillations originating from the switch on of the laser diode.

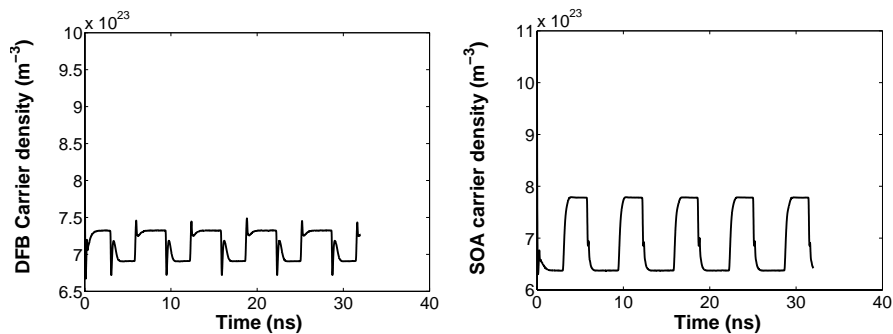


Figure 5.16: Average carrier density during the all-optical flip-flop operation as shown in Figure 5.13 and 5.14 for the laser diode (left) and the SOA (right).

The average carrier density inside the SOA and DFB laser diode during the all-optical flip-flop operation is shown in Figure 5.16. The carrier density in the DFB laser diode shows an overshoot at the time of the set operation as expected from the turn on behaviour of a laser diode. At the turn off of the laser diode a transient can be observed where the carrier density at first is highly depleted due to the reset pulse. After the passage of the reset pulse the carrier density partly recovers but then decreases again due to the increased amplification of the input signal in the SOA. When looking at the average carrier density inside the SOA the relatively slow rising carrier density after the reset pulse can be seen, which was also reflected in Figure 5.15. During the switch on operation of the laser diode resulting in an increase in the laser power injected into the laser diode, the ringing phenomena seen in Figure 5.15 can also partly be seen in the decreasing carrier density of the SOA.

5.3.4 Pulse energy dependence

In Figures 5.17 and 5.18 the minimal required set and reset pulse energies to obtain all-optical flip-flop operation are shown as a function of the pulse length for different CW input powers to the SOA. The minimal required pulse energy is defined as the pulse energy minimally required to make the device switch between stable states.

Ideally the energy required to switch the device between the two stable states is the same for the set and reset operation. This holds best

for CW input powers chosen in the center of the bistable domain. When shifting the CW input power towards one of the edges of the bistable domain a growing asymmetry between the set and reset pulses can be observed.

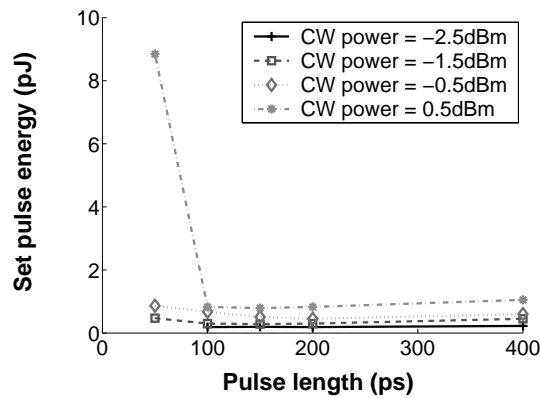


Figure 5.17: Minimal required set pulse energy to obtain all-optical flip-flop operation as a function of the pulse length for different CW input powers.

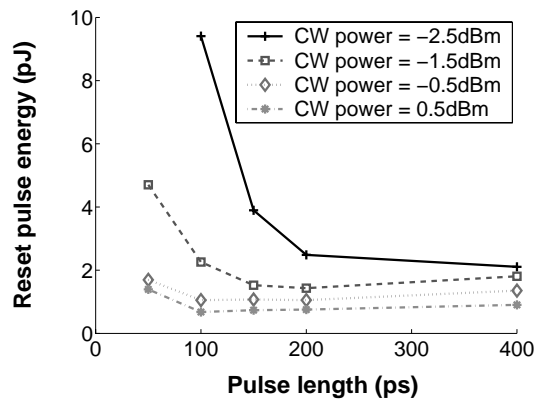


Figure 5.18: Minimal required reset pulse energy to obtain all-optical flip-flop operation as a function of the pulse length for different CW input powers.

It can be noted that when the SOA input power moves towards the left boundary of the bistable domain in Figure 5.9 the set pulse energy becomes lower while the reset pulse energy rises. The opposite holds when the CW input power nears the right boundary of the bistable domain. This can be explained by considering that for a given CW input power inside the bistable domain shown in Figure 5.9 the set and reset

pulses have to push the device temporarily outside this bistable domain in order to make the device switch between states. Near the right boundary of the bistable domain it is clear that less energy is required to push the laser diode from the on to the off state than the other way around as the working point of the device is already closer to the operating region where the laser diode is always switched off. The opposite of course applies for CW input signals near the left boundary of the bistable domain.

From Fig. 5.17 it can also be seen that the required pulse energy rises with decreasing pulse length. Due to the optical feedback present between the SOA and the DFB laser diode, the effect of a set or reset pulse needs to be long enough to enable the feedback to switch the state of both the SOA and the DFB laser diode. As the set and reset pulses essentially lead to a carrier depletion in the SOA (set) or DFB laser diode (reset) it is clear that shorter pulses need to result in a higher carrier depletion in order to make the deviation from the original state last longer.

Comparing the minimal required set and reset pulse energies obtained using VPI with the ones shown in Figure 3.31 it can be seen that the energy levels are mostly similar. In both cases set and reset pulse energies of around or below 1pJ can be observed. The static bistable domains corresponding with these results are also comparable (see Figures 3.26 and 5.10).

5.4 Experimental results

5.4.1 Setup

The experimental setup used for the demonstration of all-optical flip-flop operation of the device, consisting of an optically coupled DFB laser diode and a SOA, is shown in Fig. 5.19. To provide and control the constant input power into the SOA, needed to make the device operate inside the bistable domain, a wavelength tunable laser is used that is followed by an attenuator. The set and reset pulse trains are generated using another wavelength tunable laser and a 40Gbit/s NRZ-bit pattern generator that drives an electro-optical modulator. After generation of a single pulse train it is split using a 3dB coupler giving identical set and reset pulse trains. Using an EDFA and an attenuator for both the set and reset pulse trains the power of the set and reset pulses can be independently varied. The delay between the set and re-

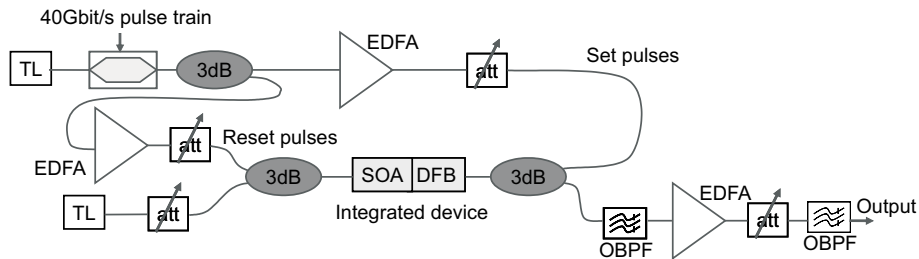


Figure 5.19: Experimental setup used for the measurements of the SOA/DFB laser diode based all-optical flip-flop. Used abbreviations: TL: tunable laser diode, 3dB: 3dB splitter/combiner, EDFA: Erbium doped fiber amplifier, att: variable optical attenuator, OBPF: tunable optical bandpass filter.

set pulse train is obtained by using an optical fiber delay line along one of the paths. By changing the length of the delay line the delay between the arrival of the set and reset pulse train could be varied. At the SOA side a 3dB coupler is used to combine the CW input power and the reset pulse train, while at the DFB laser diode side a 3dB coupler is used to inject the set pulse train into the device and to extract the output power of the laser diode or the signal output power after the laser diode at the same time. A tunable optical bandpass filter is used to separate the laser output power from the CW power.

The receiver used is a pre-amplified receiver consisting of an EDFA used to amplify the signal, a variable optical attenuator to control the power incident on the photo-detector of the digital sampling scope and an optical bandpass filter used to filter out part of the ASE noise from the EDFA. After this final signal handling the signal is fed to an optical digital sampling scope.

The device used is the integrated version of the feedback scheme consisting of a SOA connected to a DFB-laser diode array through a 1X4-coupler as shown in Figure 4.9. The coupling ratio between the SOA and each DFB-laser diode is then 25%. The fiber to chip coupling is done by means of lensed fibers as shown in Figure 4.10.

For each measurement of the all-optical flip-flop operation of the device the set and reset pulse energy was minimized to the point where the switching between the stable states was possible first.

Several measurements setups (at different research institutes) have been used to come to the results shown below. The different setups can however all be described by the setup shown in Figure 5.19. The only differences between the different setups are the different discrete

devices used to build the setups. This may lead to slightly different operating conditions and therefore also some differences in the obtained results. This difference is however only quantitative, as will also be shown below.

5.4.2 All-optical flip-flop operation

The static response of the laser output power as a function of the input power into the SOA for different wavelengths of that input power is shown in Fig. 5.20. The drive current of the SOA is 103.5mA and the drive current of the laser diode is 101.4mA. The wavelength of the laser signal is 1538.7nm.

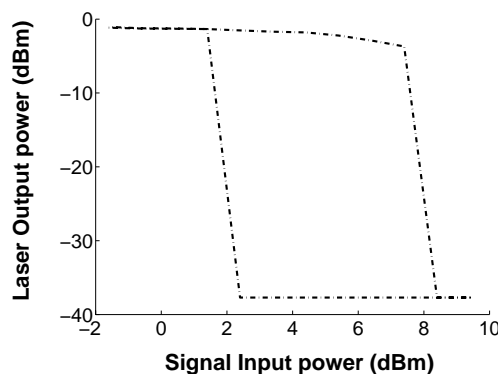


Figure 5.20: Laser output power as a function of signal input power into the SOA for a SOA drive current of 103.5mA and a laser diode drive current of 101.4mA. The wavelength of the input signal is 1555nm.

The contrast ratio in the bistable domain is over 35dB. From Fig. 5.20 it can be seen that the CW input power can be chosen anywhere between 2 and 7.5dBm.

However, because of the CW power present in the generated pulse train, as can be seen in Fig. 5.21, the actual part of the bistable domain to be used is smaller. This CW component causes the total CW power injected into the SOA to rise due to an additional CW component in the reset pulse train, causing the working point inside the bistable domain to shift to higher CW input powers. The presence of a CW component in the set pulse train leads to a slightly deeper saturation of the SOA but at the same time also to a constant power injection into the laser diode. These two effects are counteracting and lead to only minor deviations from the situation without CW component in the set pulse train. The

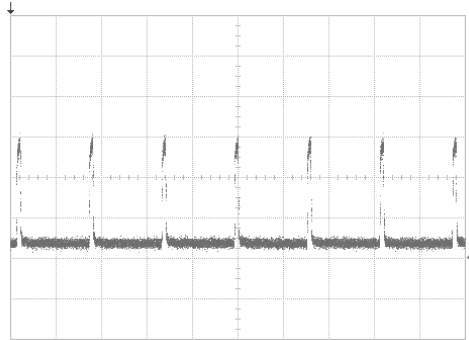


Figure 5.21: Pulse train of 150ps long pulses with a period of 1.6ns. The axis scales are 2ns/div for the horizontal and $500\mu\text{W}/\text{div}$ for the vertical axis.

pulse train shown in Figure 5.21 is periodical with a 1.6ns period. The pulses are 150ps long. The period and pulse length of the pulse train can be varied by changing the bit pattern generated by the 40Gbit/s NRZ-bit pattern generator.

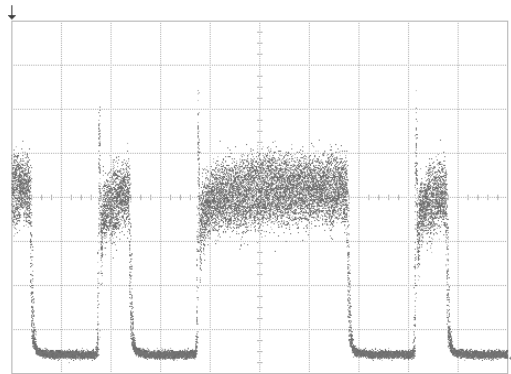


Figure 5.22: Dynamic flip-flop operation for 150ps set and reset pulses and a CW input power of 6.4dBm. The axis scales are 1ns/div for the horizontal and 1mW/div for the vertical axis.

An example of all-optical flip-flop operation of the SOA/DFB laser-diode feedback scheme is shown in Fig. 5.22. The set and reset pulses are 150ps long and the wavelength of the CW input power and the pulses is 1555nm. The set pulse energy is 10.6pJ and the reset pulse energy is 4.4pJ. The period of the set and reset pulse train is 6.4ns. In each period 2 pulses are present, one at the start of the period and one 2ns later, as can also be seen from the sequence of set and reset oper-

ations in Figure 5.22. The contrast ratio between the ON-state and the OFF-state of 11.6dB is lower than expected from Fig. 5.20 but might be explained by the limited sensitivity of the receiver resulting in an overestimation of the zero level (due to the shot noise of the receiver). The relatively high noise on the one-level is probably caused by the noise addition in the pre-amplified receiver. Another factor contributing to this noise factor is again the CW component in the pulse trains as these are amplified by means of an EDFA before injection into the device leading to addition of noise to the pulse train due to amplified spontaneous emission. The repetition rate (defined as the rate at which two equal transitions (being on to off or off to on occur)) is as high as 500MHz.

The set and reset switch time of the AOFF is in this case as low as 150ps as can be seen in Fig. 5.23. The transient in the switch on of the AOFF is caused by the relaxation oscillation of the DFB laser diode.

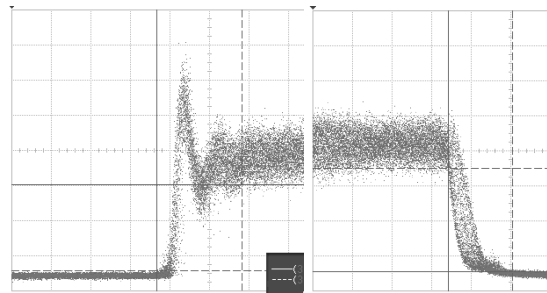


Figure 5.23: Set and reset switch times for 150ps set and reset pulses and a CW input power of 6.4dBm. The axis scales are 100ps/div for the horizontal and 600 μ W/div for the vertical axis.

Figure 5.24 shows all-optical flip-flop operation for different pulse lengths for a CW input power of 6.5dBm. The operating conditions are the same as in Figure 5.23. The set and reset energies used to obtain the state switching are shown in Table 5.2.

Pulse length (ps)	Set Pulse energy (pJ)	Reset Pulse energy (pJ)
200	9.67	4.92
300	11.02	6.22
400	12.04	7.0

Table 5.2: Set and reset pulse energy corresponding with the all-optical flip-flop operation shown in Figure 5.24.

The changing width of the set and reset pulses is reflected in the shift of the switching timing. A longer set pulse also keeps the laser diode turned off a little longer since it passes through the laser diode as well. The switch off of the laser still starts at the same time, but due to the fact that a lower peak pulse power is used for the switching, the switching is a little more gradual.

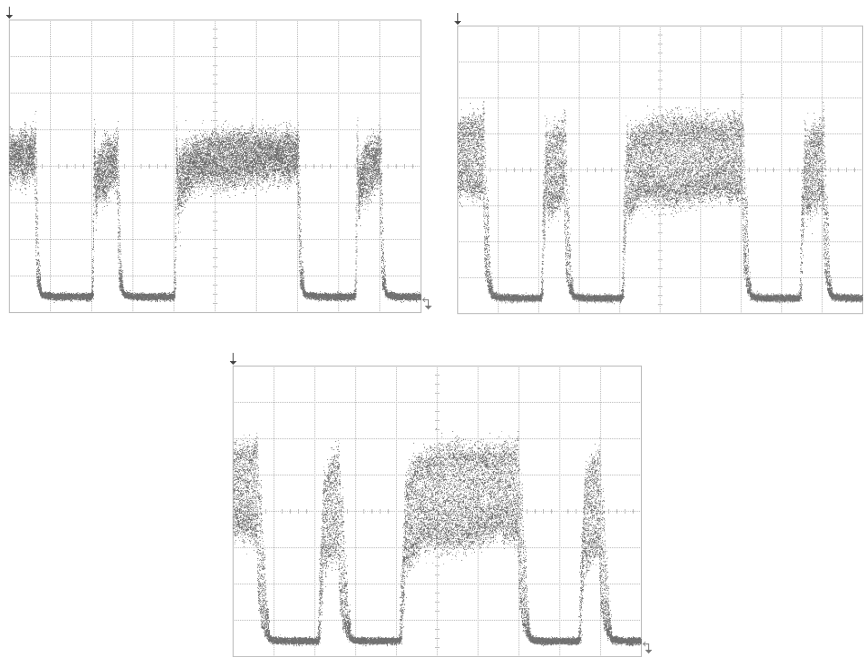


Figure 5.24: Dynamic flip-flop operation in the laser output power for different set and reset pulse lengths and a CW input power of 6.4dBm. The axis scales are 1ns/div for the horizontal and 1mW/div for the vertical axis. Top left: 200ps long pulses. Top right: 300ps long pulses. Bottom: 400ps long pulses.

The optical power incident on a device in an all-optical network can change over time due to variations in the signal handling prior to the arrival at the device. Furthermore in tightly meshed packet switched all-optical networks packets are not necessarily routed along the same path, making the power control at intermediary nodes more difficult. In order to compensate for these power variations the device should be flexible enough to handle these changes. In Figure 5.25 the minimal required set and reset pulse energy is shown as a function of the pulse length for different CW input powers chosen inside the bistable do-

main of Figure 5.20. Minimal set and reset pulse energies of below 5pJ can be observed, albeit not for the same CW input power. The minimal required set pulse energy to switch the AOFF on rises for a fixed pulse length with increasing CW input power, which corresponds to the numerical results shown in Figure 5.17. At the same time the minimal required reset pulse energy to switch the AOFF off decreases with increasing CW input power for fixed pulse lengths again corresponding with the results shown in Figure 5.18.

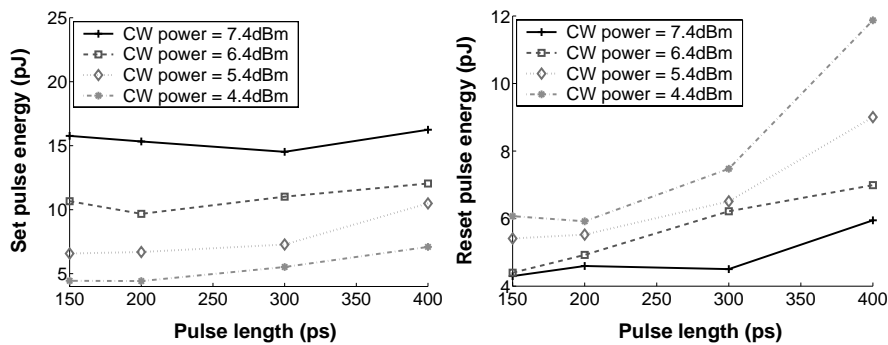


Figure 5.25: Minimal required set (right hand side) and reset (left hand side) pulse energy to obtain switching as a function of the pulse length for different CW input powers chosen inside the bistable domain shown in Figure 5.20.

The increase of the required reset pulse energy for increasing pulse length may be caused by the decrease of the CW component in the reset pulse train when the pulse length grows longer (as a result of the use of an EDFA for the amplification of the pulses the average power is kept constant but by increasing the pulse length the duty cycle of the signal changes, thereby actually decreasing the amplification of the CW component). Due to the decrease of this CW component the operating point of the all-optical flip-flop inside the bistable domain shifts towards the left edge of the domain resulting in a higher pulse power required to switch the AOFF. The energy of the set pulses remains almost equal, corresponding with the simulation results obtained in Fig. 5.17.

From Figure 5.25 it can be concluded that all-optical flip-flop operation can be guaranteed over almost the entire static bistable domain, which makes the device robust to input power variations.

The evolution of the switching times in the laser output power as a function of the set and reset pulse length for different CW input powers is shown in Figure 5.26. The set and reset pulse energy used for these

measurements can be found in Figure 5.25. The switching times are defined and calculated as the time needed for the 10%-90% transition between the states. Both the switch on and switch off time of the laser diode can be seen to increase with increasing pulse length while being nearly independent from the CW input power level. The switching times are tightly related to the pulse length used, indicating that the switching of the all-optical flip-flop is really controlled by the set and reset pulses.

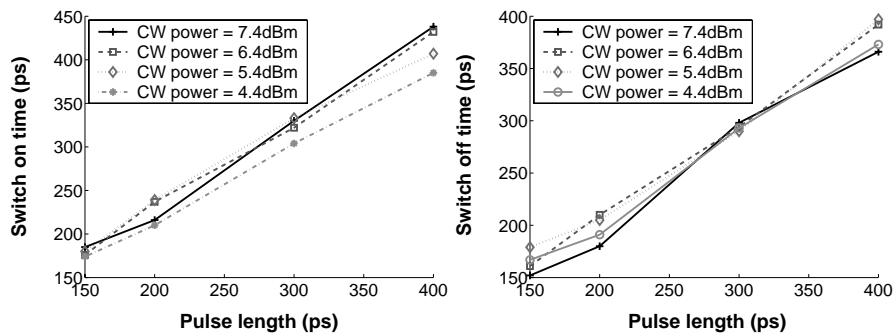


Figure 5.26: Switch on and switch off times for the laser output power corresponding with the set and reset pulse energies from Figure 5.25. The switch time is defined as the 10%-90% transition between the states.

The contrast ratio between the two states in the laser output power remains, as can be seen in Figure 5.27, reasonably constant as a function of the pulse length and CW input power. A deviation of about 1dB can be seen around the mean contrast ratio of 11.5dB.

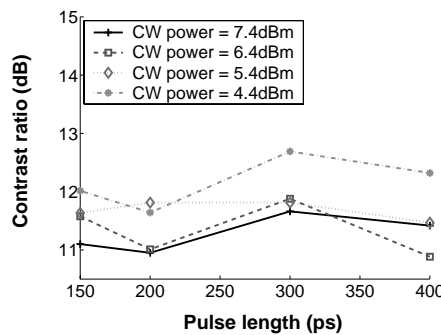


Figure 5.27: Contrast ratio between the two states in the laser output power corresponding with the set and reset pulse energies from Figure 5.25.

5.4.3 Wavelength dependence

In this section the experimental wavelength dependence of the all-optical flip-flop is investigated. The measurements shown are performed with a drive current for the SOA of 114.81mA and a drive current for the DFB laser diode of 79.86mA. The operation of the device has been investigated for different wavelengths (1547,1553 and 1557nm), different CW input powers and different pulse lengths (from 100 to 400ps). The wavelength of the DFB laser diode is 1542nm. Note that although the wavelength of CW power and the pulses change all other parameters, including polarization are kept unchanged throughout the whole experiment.

In Figure 5.28 the static bistability curves of both the laser and signal output power as a function of the input power are shown for different wavelengths. The right boundary value of the bistable domain can be seen to coincide for the different input wavelengths but the left boundary of the bistable domain is shifted as a function of the wavelength corresponding with the results obtained in Figure 4.8. This can again be explained by the wavelength dependence of the SOA and laser diode gain. In the case of a laser diode emitting laser power into the SOA the gain of the SOA is highly saturated. This results in a small influence of the wavelength dependence on the output power. In the case with a laser diode in the off state on the other hand the SOA is less saturated leading to slightly larger gain differences in the SOA. This in turn results in a shift in the signal input power at which the laser diode turns on again.

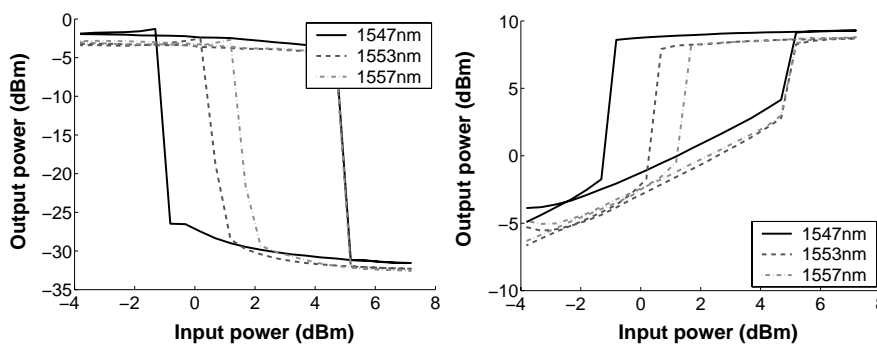


Figure 5.28: Static laser and signal output power as a function of the signal input power for different input signal wavelengths. Left: laser output power. Right: Signal output power.

A bistable domain of about 25dB high in the laser output power and about 10dB high in the signal output power, with a width ranging from 3 to 6dB can be observed.

As compared to the previous section the CW component in the set and reset pulse train was minimized, as shown in Figure 5.29, due to the use of a different measurement setup. The figure shows an example of the set and reset pulse trains used to obtain all-optical flip-flop operation. The pulses demonstrated are 100ps long and the period of a pulse train is 6.4ns. The relative delay between the arrival of the two pulse trains at the device is about 3.2ns. The lower CW component in these pulse trains leads to less deviation away from the operating point due to the pulse trains and can result in lower minimal required set and reset pulse energies, leading to the switching of the device.

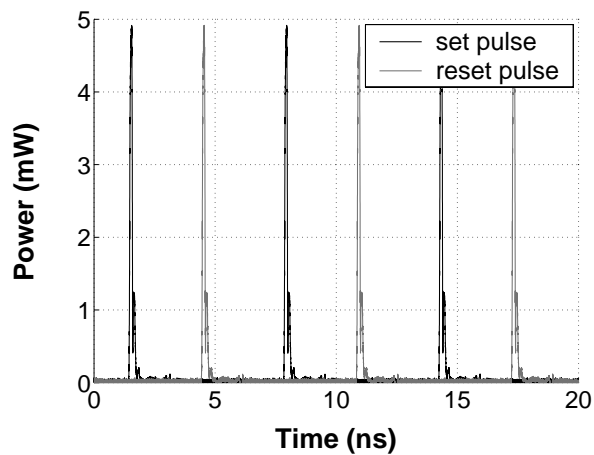


Figure 5.29: Set and reset pulse train used to obtain all-optical flip-flop operation. The pulse trains consist of 100ps long pulses and are periodical with a period of 6.4ns. The pulse trains are shifted relatively over 3.2ns.

In Figure 5.30 the all-optical flip-flop operation in the laser and signal output power for different input signal wavelengths is shown for a CW input power of 3.9dBm. The pulse energies corresponding with the results shown in Figure 5.30 are given in Table 5.3. The signal and laser output power are obtained simultaneously. A splitter and tunable optical filters are then used to separate the signal and laser output power. The power levels of the obtained signals are then adjusted by means of an optical attenuator in order to obtain the same output conditions for the different measurements. This attenuation prevents the saturation of the optical receiver.

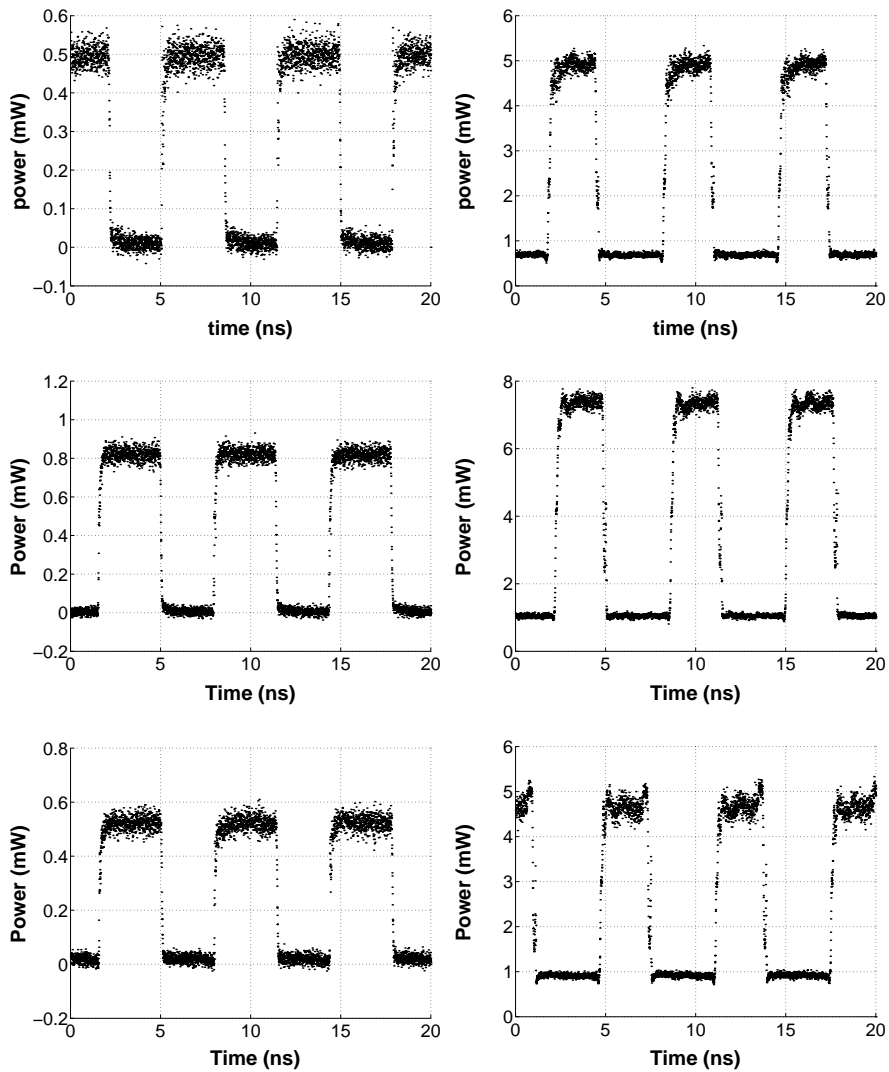


Figure 5.30: All-optical flip-flop operation in the laser and signal output power for different input signal wavelengths. From top to bottom the wavelength of the input signal is 1547, 1553 and 1557nm. The laser output power is shown on the left and the signal output power is shown on the right each time. The corresponding set and reset pulse energy of the 100ps long pulses used is shown in Table 5.3. The CW input power is 3.9dBm for each input signal wavelength.

All-optical flip-flop operation in both the laser and signal output power can be obtained over a wavelength range of at least 10nm . The laser output shows a higher contrast ratio than the signal output, mainly caused by the better suppression of the zero level in the laser output as compared to the signal output. The contrast ratio in the laser output power is around 11dB and the contrast ratio in the signal output power is around 7dB for all input signal wavelengths shown in Figure 5.30. Switch times of the order of 100ps can be observed for the set and reset operation in both the laser and the signal output power.

Input wavelength (nm)	Set Pulse energy (pJ)	Reset Pulse energy (pJ)
1547	1.2	0.85
1553	2.2	0.8
1557	1.45	0.6

Table 5.3: Set and reset pulse energy corresponding with the all-optical flip-flop operation shown in Figure 5.30.

The set and reset pulse energy, shown in Table 5.3, used to obtain the all-optical flip-flop operation seen in Figure 5.30 demonstrates that by using set and reset pulse trains with higher extinction ratio switching of the all-optical flip-flop can be achieved with lower pulse energies than in the case of Figure 5.25. The set and reset energy does differ between the chosen input wavelengths, a fact that can be explained by the difference in coupling into the device, as well as the wavelength dependence of the gain region of both the SOA and laser diode. The set and reset pulse energy remain however of the same order when changing the input wavelength of both the pulses and the CW signal. Important to note is that the assumption that the set and reset pulse trains and the CW input signal operate at the same wavelength is not binding. The pulses and the CW signal can be at different wavelengths as long as those wavelengths are chosen sufficiently distant from the Bragg wavelength of the DFB laser diode.

The evolution of the minimal required set and reset pulse energy to obtain switching is given in Figure 5.31 as a function of the pulse length for different CW input signals and different input wavelengths. In general the same behaviour for the different input wavelengths can be observed. For CW input powers near the left hand side boundary of the bistable domain, as shown in Figure 5.28, the set pulse energy decreases while the reset pulse energy increases. When the CW input power is increased the opposite happens and the set pulse energy in-

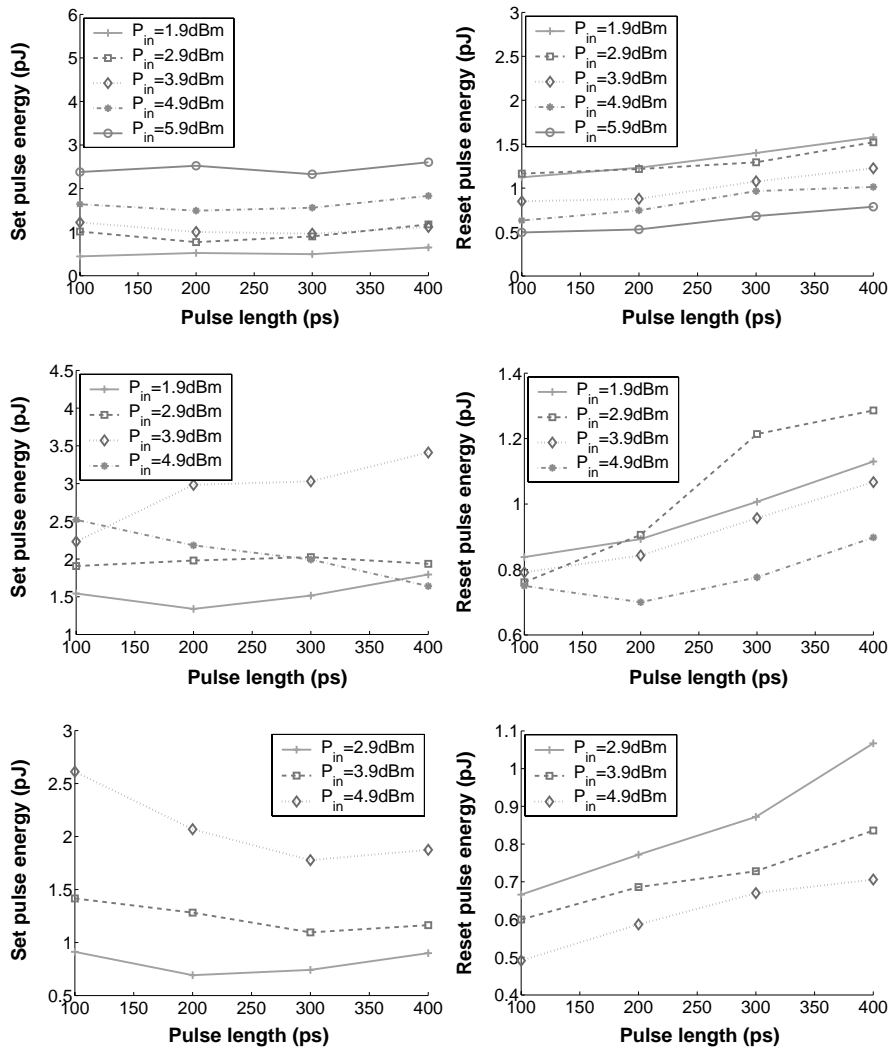


Figure 5.31: Minimal required set and reset pulse energy as a function of the pulse length for different CW input powers chosen inside the bistable domain. The results are shown for different wavelengths of the input signals (CW input power and pulses). From top to bottom the wavelength of the input signals is given as 1447, 1553 and 1557nm. The left graph each time shows the minimal required set pulse energy and the right hand side graph shows the minimal required reset pulse energy.

creases while the reset pulse energy decreases. The minimal set and reset pulse energy required to obtain switching is for each CW input power the additional energy (or power) needed to push the operating point of the device temporarily outside the static bistable domain. It is clear that when nearing a boundary value of the bistable domain a growing asymmetry between the required set and reset pulse energy can arise.

The set and reset pulse energy can be seen to be relatively constant as a function of the pulse length. A slight increase in the reset pulse energy can be observed for increasing pulse lengths. As the pulse length increases the reset pulse power needed to quench the laser diode, and to additionally deplete the carrier density in the laser diode, can be lower, due to the fact that the switch off of the laser enables the carrier density of the SOA to partly recover during the passage of the set pulse. The reset pulse energy can therefore remain almost constant with increasing pulse length. When the pulse length keeps on increasing however the pulse power can not be decreased indefinitely because a certain level of carrier depletion in the laser diode has to be obtained in order for the switching of the device to occur. This leads to a small increase of the reset pulse energy for increasing pulse lengths. In the case of the set pulse energy the increase is much less obvious because of the fact that the set pulse only has to cause a slight decrease in the gain of the SOA, which can allow the laser diode to switch back on again. As the set pulse also travels through the DFB laser diode the energy (and power) of the set pulse can not be too high in order to avoid strong carrier depletion in the DFB laser diode.

In the case of an input wavelength of 1557nm all-optical flip-flop operation can be observed with sub-pJ set and reset pulse energies over different pulse lengths for a CW signal power of 2.9dBm.

Comparing the results shown in Figure 5.31 with the numerical results from Figures 3.31, 5.18 and 5.17 shows that, apart from the coupling losses associated with the experimental results (of the order of 6dB), a good agreement between the simulations and experiments can be found. Exact fitting of the experimental results, using either the analytical model from chapter 2 or the simulation tool VPI, does not make a lot of sense, due to for instance the unknown coupling efficiency of the pulses into the device. With more devices at hand this fitting could however be worthwhile.

The switching times of both the laser output power and the signal output power show the same dependence on the pulse length as shown

in Figure 5.26. The switch times increase with increasing pulse lengths but differ only little for different CW input powers. The same holds for the extinction ratio of the signal and laser output power. The average extinction ratio of the laser output power is of the order of 11.5dB while that of the signal output power is about 7dB. The deviations in the extinction ratio are in both cases limited to about 1dB as a function of the pulse length, CW input power and wavelength of the input signals.

5.4.4 Pulse energy dependence

Just as the power of the CW input signal can change over time so can the pulse energy variate. In this section the response of the laser and signal output power to a change in the set and reset pulse energy will be shown. The drive currents of the laser diode and SOA are 79.86mA and 114.81mA respectively. The wavelength of the input signals is 1547nm and the CW input power is 3.9dBm. The static bistability curve is the same as in Figure 5.28.

The minimal required set and reset pulse energy needed to obtain all-optical flip-flop operation with the chosen pulse length and CW input power is 1.12pJ for the set pulse and 1.23pJ for the reset pulse as can be seen for the laser output power in the top left graph of Figure 5.32. When the reset pulse energy is increased it can be seen from the top right graph that the switching off operation of the laser diode is much sharper, due to the fact that the pulse itself can already turn off the laser diode. The feedback between laser and SOA then only acts to maintain the state, whereas for the lower reset pulse energy the feedback between the laser diode and the SOA aids in the switching of the device.

When the set pulse energy is increased above the minimal required energy 2 different states can be observed. At first when the set pulse energy is increased to 6.23pJ, it can be seen that due to the higher saturation of the SOA the laser diode can start to switch on a bit earlier. But because the higher set pulse energy is also injected into the laser diode the laser field can not build up fast enough and the feedback between the laser diode and SOA kicks in to aid in the switching of the device once the set pulse has passed through the device. The time at which the set pulse has passed the device can be seen as the point where the laser output power drops again after the initial first attempt to switch on.

If the set pulse energy is further increased the carrier depletion in the laser diode is high enough to keep the laser switched off during the

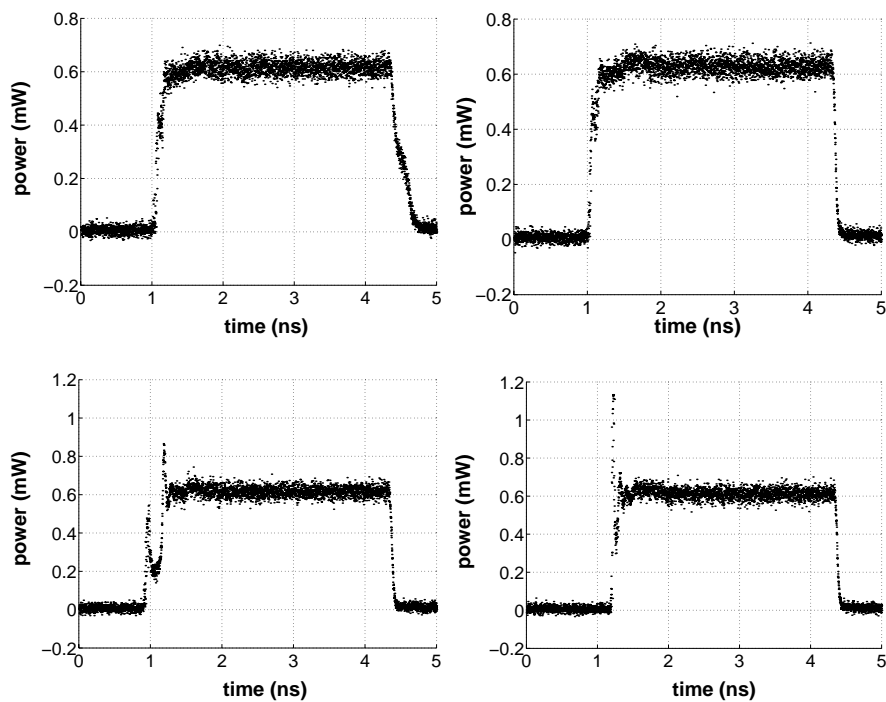


Figure 5.32: All-optical flip-flop operation in the laser output power for different combinations of set and reset pulse energies. The input signals wavelength is 1547nm and the CW input power is 3.9dBm. The pulses are 400ps long. Top left: 1.12pJ set pulse energy and 1.23pJ reset pulse energy. Top right: 1.14pJ set pulse energy and 5.64pJ reset pulse energy. Bottom left: 6.23pJ set pulse energy and 5.64pJ reset pulse energy. Bottom right: 10.39pJ set pulse energy and 5.64pJ reset pulse energy.

passage of the set pulse. Once the set pulse has passed the laser diode switches on after a certain turn-on delay as can be seen from the bottom right graph in Figure 5.32.

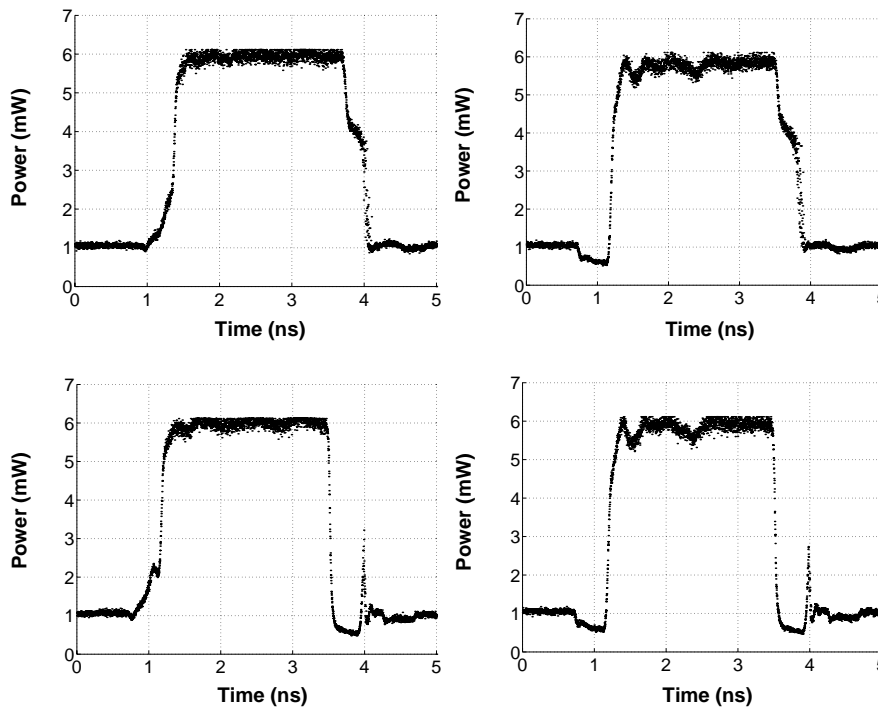


Figure 5.33: All-optical flip-flop operation in the signal output power for different combinations of set and reset pulse energies. The input signals wavelength is 1547nm and the CW input power is 3.9dBm. The pulses are 400ps long. Top left: 1.12pJ set pulse energy and 1.23pJ reset pulse energy. Top right: 1.14pJ set pulse energy and 5.64pJ reset pulse energy. Bottom left: 10.69pJ set pulse energy and 1.44pJ reset pulse energy. Bottom right: 10.69pJ set pulse energy and 5.64pJ reset pulse energy.

The similar behaviour as in the case of the laser output power can be observed in the signal output power, as is shown in Figure 5.33. Again 400ps long pulses and a CW input power of 3.9dBm are used. The input signal wavelength is 1547nm. When the reset pulse energy is increased above the minimal required energy the signal output power can be seen to increase more rapidly corresponding to a faster switch off of the laser diode. This can be seen when comparing the top two graphs in Figure 5.33. When on the other hand the set pulse energy is increased, as shown in the bottom left graph, it can be seen that the

signal output initially shifts to a lower output power, due the gain saturation caused by the set pulse. After the passage of the pulse however a short but sharp increase in the signal output power can be observed. When the set pulse has passed the SOA, the total power incident on the SOA suddenly drops, resulting in fast carrier recovery before the laser diode switches on and saturates the SOA again. When both the set and reset pulse energy is increased sufficiently above the minimal required set and reset pulse energy the timing of the pulses can be observed from the signal output power, as shown in the bottom right graph of Figure 5.33.

5.4.5 Fast all-optical flip-flop operation

Up to now the all-optical flip-flop operation shown was relatively slow with the stable states of the device maintained from 1 to a couple of nanoseconds. Here in this section it is shown that the device can operate at relatively high switching speeds up to 1.25GHz between 2 identical switch operations.

The SOA was driven at 83mA and the DFB laser diode at 105.8mA. The wavelength of the CW input power and the pulses was 1550nm, while the wavelength of the laser output was 1542nm. The CW input signal to the SOA, used to operate the device inside the bistable domain shown in Figure 5.34, was set at 4.5dBm. The pulses were generated at a 1.25GHz repetition rate, resulting in a pulse each 800ps, and then split along 2 different paths to form the set and reset pulse trains. The difference in time between the arrival of a set and reset pulse was determined by the different optical path length and was measured to be about 400ps. This results in a switching of the state of the device at a rate of 2.5GHz.

Figure 5.35 shows the all-optical flip-flop operation of the device for a set pulse energy of 1pJ and a reset pulse energy of 1.3pJ. The CW input power was 4.5dBm and the pulses used were 50ps long. It can be seen that the switching of the device occurs at 1.25GHz when the repetition rate is measured as the time between two set or 2 reset operations. This makes the device suitable for applications where high-speed switching is required. The contrast ratio between the two states in the laser output power is as high as 18dB.

When looking more carefully at the set and reset operation it can be noted from Figure 5.36 that the switch times again scale with the length of the pulses used. The set and reset switch time can be seen to be as

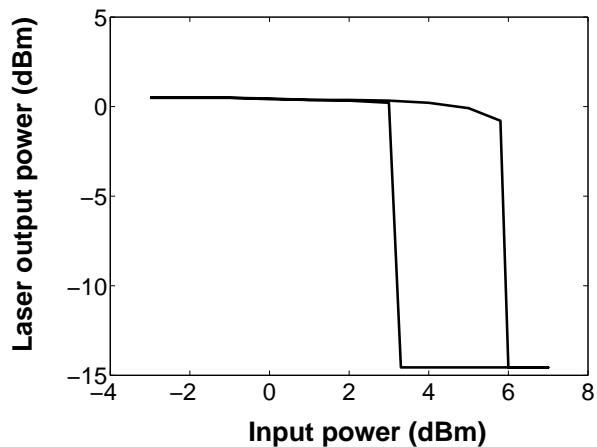


Figure 5.34: Static bistable response of the laser output power as a function of the input power. The drive currents of the laser diode and the SOA are 105.8mA and 83mA respectively. The input signal wavelength was 1550nm.

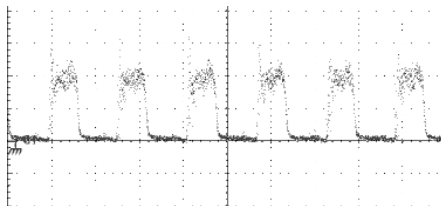


Figure 5.35: All-optical flip-flop operation in the laser output power for a CW input power of 4.5dBm and a set and reset pulse energy of 1pJ and 1.3pJ respectively. The pulses are 50ps long. The axis scales are 500ps/div for the horizontal and 1mW/div for the vertical axis.

low as 50ps. In the set operation the relaxation oscillations of the laser diode can be observed.

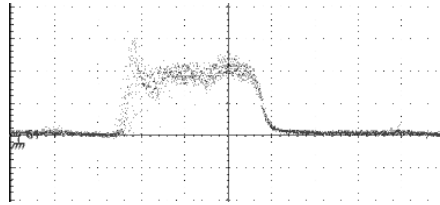


Figure 5.36: Zoom in around the set and reset operation shown in Figure 5.35. The axis scales are 100ps/div for the horizontal and 1mW/div for the vertical axis.

When the length of the set and reset pulses is increased, as is shown in Figure 5.37, the fast operation of the device can still be achieved. The switching times can however be seen to increase to around 150ps. The set and reset energy is 0.8 and 0.9pJ respectively.

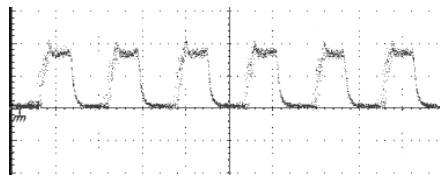


Figure 5.37: All-optical flip-flop operation in the laser output power for a CW input power of 4.5dBm and a set and reset pulse energy of 0.8pJ and 0.9pJ respectively. The pulses are 150ps long. The axis scales are 500ps/div for the horizontal and 1mW/div for the vertical axis.

5.4.6 Simultaneous multiple wavelength output operation

Thus far all the experiments shown have been performed using only one of the laser diodes that are present in the device shown in Figure 4.9. In this section results will be demonstrated where two of the laser diodes are simultaneously driven. The experimental setup used in these measurements is a variant of the measurement setup demonstrated in Figure 5.19 and can be seen in Figure 5.38. Since only one of the laser diodes can be optically connected at any time by means of a lensed fiber a circulator is used at the SOA side to obtain both of the laser output powers simultaneously at the left hand side of the device. A tunable optical bandpass filter is then used to separate both laser

signals from each other. The reset pulse is still injected into the SOA together with the CW input power. The set pulse is injected in only one of the driven DFB laser diodes as can be seen from Figure 5.38.

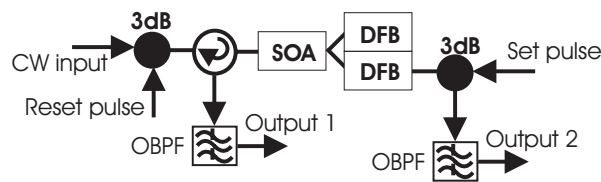


Figure 5.38: Experimental setup used for the all-optical flip-flop operation of the SOA and DFB laser diode feedback scheme where two laser diodes are driven at the same time.

The laser diodes, further on denominated by LD1 and LD2, are emitting light at a wavelength of 1541 and 1543nm respectively. The input signal wavelength is 1547nm. The drive currents of LD1 and LD2 are 46mA and 56mA respectively. The drive current of the SOA is 120mA. The drive currents are chosen such that the static bistable domain is situated in the input power range obtainable with the setup shown in Figure 5.38. The static bistable domain in both the laser output powers is shown in Figure 5.39. It can be seen that bistable operation can be obtained simultaneously in both the laser diodes. The width of the bistable domain is about 3dB while the height is of the order of 20dB.

The use of 2 laser diodes driven at almost the same drive current actually can be considered as a doubling of the coupling ratio from the DFB laser diode power into the SOA. This means that for the same operating conditions the SOA can be saturated more in the case where both laser diodes are switched on. When the laser diode drive currents are too high, the SOA can not deliver enough gain to keep the laser diodes quenched in the off-state, due to the very high level of gain saturation. Therefore the drive currents of the laser diode are chosen at a lower value, which also implies that the reset pulse energy needed to cause the laser diodes to switch off will be lower than in the previous cases. On the other hand the set pulse energy can be somewhat higher due to the lower amount of amplification received by the set pulse upon the passage in the laser diode. This effect is however countered by considering that since the set pulse only travels through one of the 2 laser diodes the other laser diode does not experience a carrier depletion, which leads to a faster turn on of the laser diode.

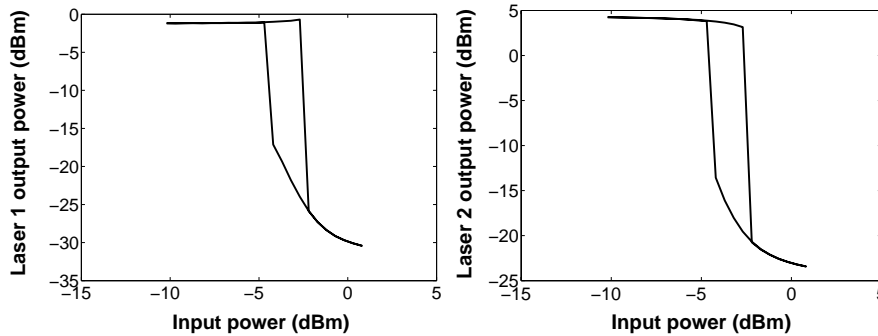


Figure 5.39: Static bistable domain in both driven laser output powers as a function of the input power.

The simultaneous multiple wavelength output operation of the device with two laser diodes driven at the same time is shown in Figure 5.40. The set and reset pulses are 100ps long and their corresponding pulse energy is 340fJ and 240fJ respectively. The CW input power is 0.5dBm. The difference in the output power between the two signals is caused by the different coupling losses in the filters used to separate the two signals. It can be seen that the switching in both laser output powers occurs simultaneously making the device capable of acting as a multi-cast element. The extinction ratio of both the output signals is over 15dB. The signal output power again shows the inverted response of the laser output powers and can be obtained at the right hand side of the laser diode that is connected to a lenzed fiber.

The same dependence of the set and reset pulse energy as a function of the pulse length and CW input power as shown above can also be obtained in this case, as well as operation over an input signal wavelength range of 10nm.

5.5 Conclusions

In this chapter the all-optical flip-flop operation of the device consisting of a SOA and 1 or more DFB laser diodes has been investigated extensively. Both the results obtained by means of simulations using a commercial software package, as experimental results using an integrated version of the device show the excellent operation of the device. Good agreement was obtained between the simulations and experimental results.

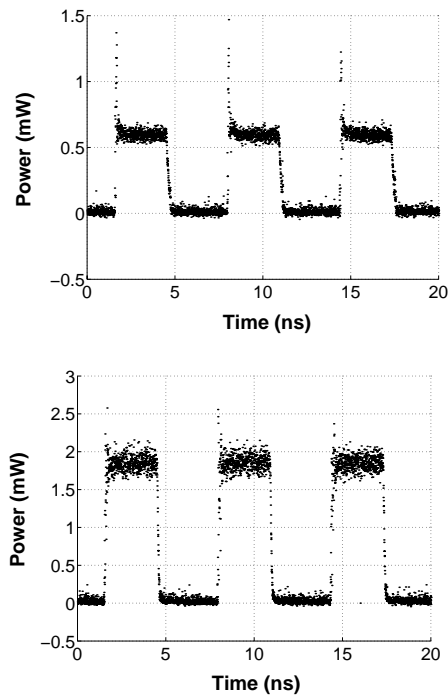


Figure 5.40: Simultaneous all-optical flip-flop operation at the wavelengths of the two laser diodes used. The pulse length is 100ps and the CW input power is 0.5dBm. The set and reset pulse energy is 340fj and 240fj respectively.

The wavelength dependence shows that the device can be used for input signal wavelengths ranging over at least 10nm. The evolution of the minimal required energy to obtain switching as a function of the pulse length and the CW input power shows, together with the dependence of the all-optical flip-flop operation on the pulse energy, that the device is robust with respect to variations of the pulse length, pulse energy and CW input power, making it very suitable for use in real network environments. The extinction ratio has been shown to remain relatively constant as a function of changing operating conditions. The switch times on the other hand are highly dependent on the length of the pulses used to perform the switching. Switching times as low as 50ps and set to set (or reset to reset) operation at a repetition rate up to 1.25GHz has been demonstrated.

By using two DFB laser diodes at the same time simultaneous multiple wavelength output operation can be obtained with very low set and reset pulse energies.

Chapter 6

Optical decision element

In this chapter the use of the optical feedback scheme, consisting of a SOA and DFB laser diode, as an optical decision element will be demonstrated. As shown in the previous chapter very sharp transfer characteristics could be obtained in the signal and laser output power as a function of the input power, albeit combined with bistable operation. However it has also been shown that, by changing the drive currents of both SOA and laser diode (see Figures 4.14 and 4.15), the width of the bistability can be changed. For certain drive current combinations the width of the bistability can be small enough for both switching operations to occur at the same input power to the device when taking small input power fluctuations into account. In this chapter the operation of the device under these operating conditions is investigated and extinction ratio improvement is demonstrated at 10Gbit/s. In addition to that wavelength conversion at 2.5Gbit/s is also presented.

6.1 Measurement setup

The setup used in the 2R-regeneration and wavelength conversion measurements is shown in Figure 6.1. Light coming from a tunable laser diode is modulated using a 10Gbit/s optical modulator. The modulated signal can then be controlled in terms of the signal to noise ratio by means of a succession of a variable optical attenuator and an EDFA. By reducing the power incident on the EDFA the relative noise added onto the signal by the ASE generated in the EDFA can be increased. After the signal has passed through the device an optical bandpass filter is used to obtain the signal at the laser or input signal wavelength.

This signal is then detected using a pre-amplified receiver. In this pre-amplified receiver the signal power incident on the actual optical receiver is adjusted by means of a variable optical attenuator and an EDFA. The signals used in these experiments are 2.5Gbit/s or 10Gbit/s non-return-to-zero (NRZ) signals, generated using a $2^{31} - 1$ pseudo random bit sequence (PRBS) generator.

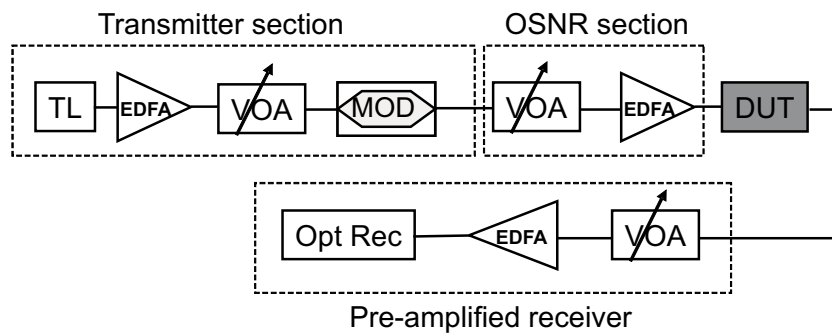


Figure 6.1: Experimental setup used for the 2R-regeneration and wavelength conversion measurements. TL: tunable laser. VOA: variable optical attenuator. MOD: 10Gbit/s modulator. DUT: device under test. Opt Rec: Optical receiver.

Two types of measurements are performed. The first one, eye diagram measurements, result in a qualitative characterization of the device. By comparing the eye diagram of the input and output signal of the device on a high speed optical sampling scope, an idea can be formed of the signal improvement obtained by using the device. Typically this improvement is characterized by the change in extinction ratio between the two signals. The second type of measurements that can be performed offers a quantitative characterization of the device performance. This type of measurements constitutes of bit error rate (BER) measurements. To that extent, the BER of the signal before and after passage through the device, as a function of the actual power incident on the pre-amplified receiver, is compared. The signal improvement is measured as the difference in required received power to obtain a BER of 10^{-9} . The measurement of the BER of the input signal is referred to as the back to back measurement (implying the bypassing of the device under test).

The device under consideration is the same as shown in Figure 4.9. The input signal is injected into the left hand side of the SOA. The output power is obtained at the right hand side of the laser diode, or in

reflection mode again at the left hand side facet of the laser diode. The input and output signal are in that case split by means of an optical circulator. As could be seen from Figures 4.14 and 4.15 the width, position and height of the bistable domain observed in the optical feedback scheme consisting of a SOA and DFB laser diode can be changed by variation of the drive currents to the laser diode and SOA. For certain current combinations the width of the bistable domain can be narrowed down to a value below the measurement accuracy of the used experimental setup. In that case the static output versus input transfer function exhibits a very sharp optical decision characteristic in both the signal and laser output power. Such characteristics can be used as part of an all-optical 2R-regenerator or wavelength converter.

The wavelength of the input signal is 1553nm and the DFB laser output wavelength is 1541nm.

6.2 2R-regeneration

For a SOA and laser diode drive current of 45mA and 65mA respectively the static characteristic as shown in Figure 6.2 can be obtained. For this current combination the static output versus input transfer function exhibits no observable bistability. A step of over 7dB can be observed in the output power for an input power variation of less than half a dB. An extinction ratio of at least 7dB can therefore be obtained based on this static characteristic, resulting in a good possible signal reshaping.

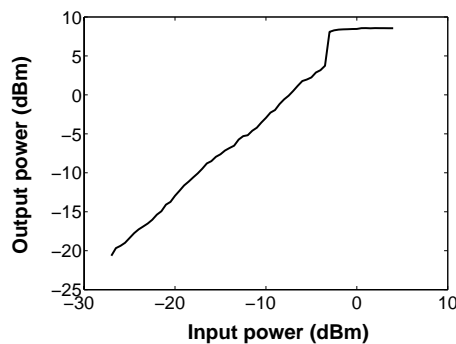


Figure 6.2: Static signal output versus input power transfer function of the SOA and DFB laser diode feedback scheme. The drive currents of the laser diode and SOA are 65mA and 45mA respectively.

In Figure 6.3 an example of ER improvement is shown for a 10Gbit/s modulated signal with an extinction ratio at the input of the device of 3.4dB. The resulting output of the device can be seen to exhibit an extinction ratio of 10.3dB. This results in an extinction ratio improvement of almost 7dB corresponding with the static transfer function shown in Figure 6.2. The zero level suppression observed in the output signal is caused by the additional attenuation added to the signal in order to avoid the receiver to get saturated by the signal power.

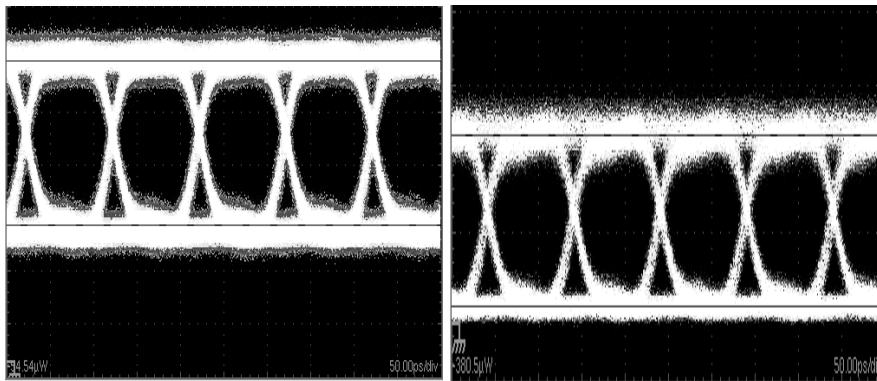


Figure 6.3: Measured eye diagrams of a 10Gbit/s NRZ signal. The output signal considered is the output signal at the right hand side facet of the laser diode. The left graph shows the input signal with an ER of 3.4dB. The right graph shows the output graph 10.3dB. The division along the x-axis is 50ps/div. The division along the y-axis is $200\mu\text{W}$ and $500\mu\text{W}$ for the left and right graph respectively. The zero power level is depicted by the ground symbol.

From this result a qualitative signal improvement can be concluded. However in order to get a quantitative idea of the signal quality improvement a BER measurement is required. The BER measurement corresponding with the input and output signal shown in Figure 6.3 can be seen in Figure 6.4. It can be seen that the two BER curves corresponding with the input and output signal are almost identical indicating that no clear signal improvement is obtained when using the device. The reason for the discrepancy between the eye diagram measurements and the BER measurements can be sought in the low OSNR of the eventually measured output signal (large noise component in the signal) caused by the noise addition in the SOA and (pre-amplified) receiver.

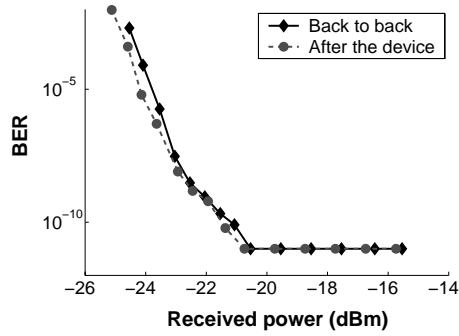


Figure 6.4: Measurement of the BER as a function of the signal power incident on the pre-amplified receiver. Both the back to back signal and the output signal after passage through the device are considered.

From Figure 6.4 it can be seen that no quantitative improvement of the signal can be obtained with the investigated device. By improving the fiber to chip coupling from and to the device the noise addition in the pre-amplified receiver can be reduced. This can lead to BER improvement. ER improvement can however be obtained for a wide range of input signal extinction ratios as shown in Figure 6.5. For an input ER ranging from 2dB to 6.5dB an output ER around 9.5dB can be obtained.

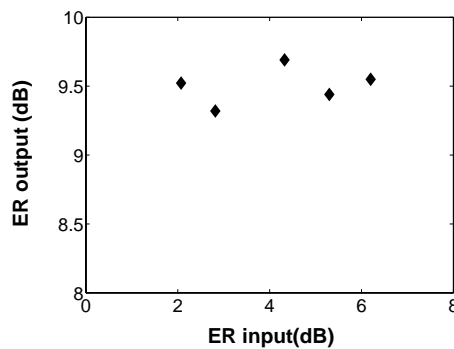


Figure 6.5: Extinction ratio of the output signal as a function of the extinction ratio of the input signal.

The device can also be used as an all-optical decision element in the reflection mode. Although the right hand side of the DFB laser diode is AR coated a small part of the signal power can still be reflected back to the SOA. The grating in the DFB laser diode also causes a fraction of

the signal power to reflect back to the SOA. After amplification in the SOA this reflected signal power can be measured at the left hand side facet of the SOA. The static output power versus input power transfer function for the signal output power at the left hand side of the SOA is shown in Figure 6.6. The corresponding drive currents of the SOA and laser diode are in this case 73mA and 87mA respectively. A step of over 15dB in the output power can be observed for an input power variation of 1dB. The power levels of the output power in reflection mode are a lot smaller than the power levels in the transmission mode. This is caused by the limited reflections.

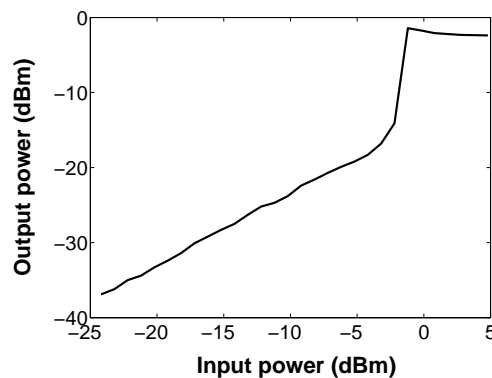


Figure 6.6: Static signal output versus input power transfer function of the SOA and DFB laser diode feedback scheme. The output signal considered is the output signal at the left hand side facet of the SOA. The drive currents of the laser diode and SOA are 65mA and 45mA respectively.

In Figure 6.7 the eye diagrams for the input and output signal at 10Gbit/s are shown. The ER of the input signal is 3.9dB while the ER of the output signal is 9.1dB. Again the zero level suppression observed is mainly caused by the attenuation of the output signal, needed to avoid the saturation of the optical receiver. It can be seen that apart from the ER improvement the overall signal quality has decreased. This can be noted from the noise level in the one level as well as the slow zero to one transition, which is caused by the relatively slow response of the SOA in this case. This slow response may be a result of the strong interaction between the laser output power and the signal power due to a lower injected input power. This effect could in some way also be observed as a function of the pulse energies in for instance Figure 3.27.

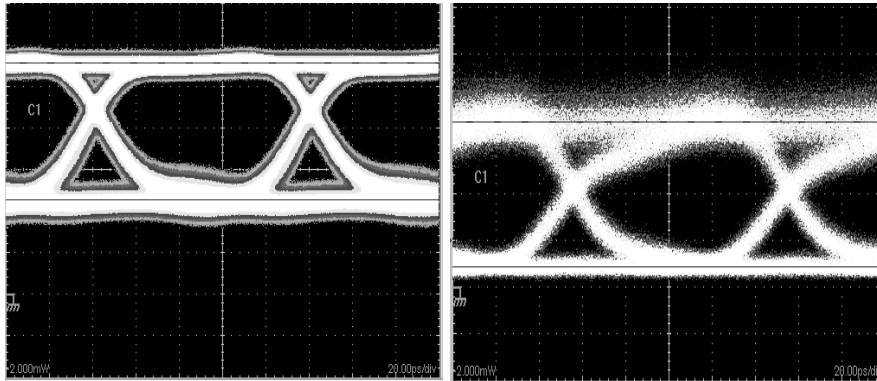


Figure 6.7: Measured eye diagrams of a 10Gbit/s NRZ signal. The output signal considered is the output signal at the left hand side facet of the SOA. The left graph shows the input signal with an ER of 3.9dB. The right graph shows the output graph 9.1dB. The division along the x-axis is 20ps/div. The division along the y-axis is 1mW/div. The zero power level is depicted by the ground symbol.

6.3 Wavelength conversion

As has already been shown in the previous chapters the laser output power shows the inverted response, with respect to the input power, as the signal output power. This can be exploited to obtain wavelength conversion with the device. The static transfer function of the laser output power as a function of the input power is shown in Figure 6.8. The SOA and laser diode drive current is 100mA and 125mA respectively. The laser wavelength is again 1541nm while the wavelength of the input signal is 1553nm.

A sharp decision characteristic can be observed with a step of over 20dB high for an input power variation of about 1dB. Based on this decision characteristic all-optical wavelength conversion from the input signal wavelength to the laser wavelength should be possible, albeit in an inverted way. Eye diagram measurements showing the input signal with an ER of 6.9 and the corresponding laser output signal with an ER of 18.5dB are demonstrated in Figure 6.9. The resulting ER improvement of over 11dB shows good agreement with the static transfer function as seen in Figure 6.8.

The slow response observed in the laser output power can be explained by the optical feedback and the delay caused by the switch on of the laser diode. The transition from zero to one output bit is slightly

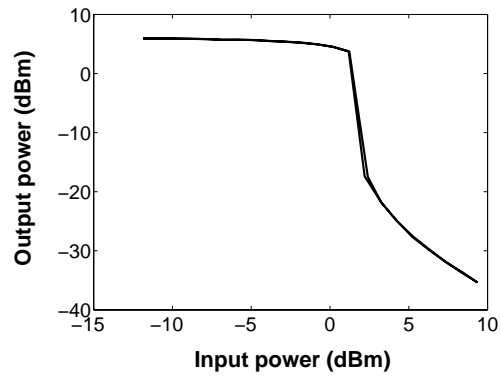


Figure 6.8: Static laser output versus input power transfer function of the SOA and DFB laser diode feedback scheme. The drive currents of the laser diode and SOA are 100mA and 125mA respectively.

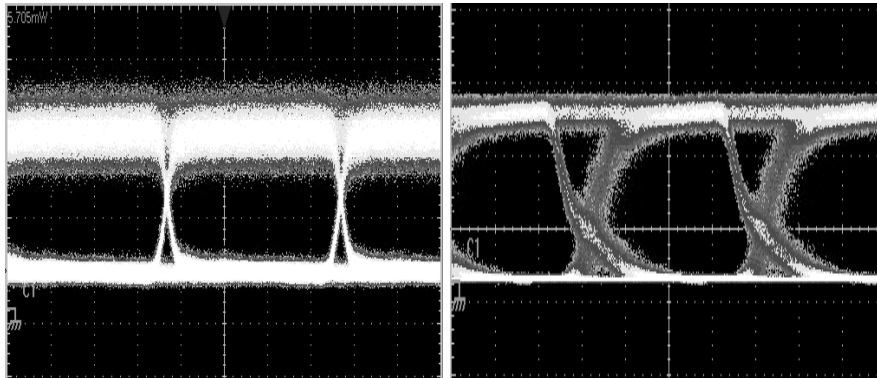


Figure 6.9: Measured eye diagrams of a 2.5Gbit/s NRZ signal. The output signal considered is the laser output signal at the right hand side facet of the DFB laser diode. The left graph shows the input signal with an ER of 6.9dB. The right graph shows the output graph 18.5dB. The division along the x-axis is 50ps/div. The division along the y-axis is 1mW/div. The zero power level is depicted by the ground symbol.

delayed with respect to the opposite transition corresponding with the turn on delay of the laser diode. The subsequent slow rising slope is a result of the relaxation phenomena in a laser diode during the switch on operation. The transition from one to zero output bit can also be seen to be relatively slow. This is caused by the strong interaction between the laser output power and the signal power due to a low injected input power during the switch off operation of the laser diode. A higher input power would lead to a faster switch off of the laser diode. The ER of the output signal corresponds rather well with the step height observed in Figure 6.8. The suppression of the zero level, that can be observed in Figure 6.9, also corresponds with the steep drop of the laser output power seen in the static transfer function of Figure 6.8.

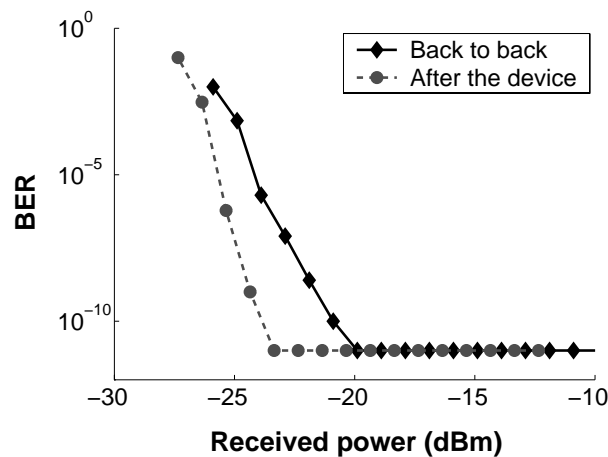


Figure 6.10: Measurement of the BER as a function of the signal power incident on the pre-amplified receiver. Both the back to back signal and the wavelength converted laser output signal are considered.

In Figure 6.10 the BER as a function of the signal power incident on the (pre-amplified) receiver is shown for both the input signal (back to back) and the wavelength converted signal corresponding with the eye diagrams shown in Figure 6.9. A clear improvement of the receiver sensitivity can be observed of up to 3dB for a BER value of 10^{-9} .

6.4 Conclusions

In this chapter the possibility of using the device consisting of a SOA and DFB laser diode in an optical feedback scheme as an all-optical de-

cision element has been demonstrated. Clear extinction ratio improvement has been shown for the device operating as a 10Gbit/s 2R regenerator. The obtained output extinction ratio corresponds well with the static transfer function of the device.

A BER measurement performed showed no actual improvement of the receiver sensitivity. This may be explained by the relatively large noise component in the signal caused by noise addition in the regenerator and pre-amplified receiver. The evolution of the output ER as a function of the input ER indicates that ER improvement can be obtained for a variety of input signals and input signal quality.

Furthermore it has also been shown that the device might also work in reflection mode when the output signal of the device is obtained at the left hand side facet of the SOA and separated from the input signal by means of an optical circulator. Again the ER improvement of the signal corresponds with the static transfer function obtained. The slow effects observed in the output eye diagram can be explained by the limited feedback between the laser diode and the SOA.

The device can also be used as a wavelength converter when using the output of the laser diode as the output power. Measurements performed at a bitrate of 2.5Gbit/s show a large ER improvement of over 11dB. The relatively slow effects observable in the wavelength converted signal are again partially caused by the limited feedback between the laser diode and the SOA. But also the transient phenomena observed during the switch on of a laser diode are a cause of these effects. A BER measurement showed that the receiver sensitivity could be improved with about 3dB for a BER value of 10^{-9} .

Chapter 7

Conclusions

7.1 Overview and conclusions

The explosive growth of the amount of users connected to global telecommunications systems, such as the internet and the continuously growing bandwidth of the used applications created a need for ever faster and higher bandwidth telecommunication networks. This trend has led to the development of all-optical networks, which can overcome the electrical bottleneck imposed by the numerous optical-electrical-optical conversions needed in current networks to route the data from point to point. These all-optical networks are however not yet completely viable, and a lot of research is still going on to implement the necessary signal processing functionalities in the optical domain. In the special subset of all-optical packet switched networks all-optical flip-flops, 2R regenerators and wavelength converters are very important devices.

This work concentrated on the use of a feedback scheme consisting of a semiconductor optical amplifier and a laser diode as an all-optical flip-flop but also as an all-optical 2R regenerator or wavelength converter.

In order to come to a good description of the device an analytical SOA model was first presented in Chapter 2. This model was derived from the standard traveling wave SOA equations in which some approximations were made, such as neglecting the amplified spontaneous emission. The static solution of these equations yielded a simple description of a SOA for both the lossy and lossless case and showed good qualitative agreement with experimental results, obtained with a commercially available SOA. For the dynamic solution of the SOA traveling wave equations the SOA was considered to be lossless, which results in

an overestimation of the SOA gain and output power but still leads to qualitative correct results. The response of the dynamic solution obtained with the analytical model presented in Chapter 2 showed good (qualitative) agreement with results presented in literature. Based on this model a fast qualitative approximation can be made of the behavior of a SOA under different operating conditions.

In Chapter 3 the model obtained in Chapter 2 was combined with the simple rate equation model of a DFB type laser diode to study the behavior of the SOA and laser diode optical feedback scheme. In the static treatment of the device it was theoretically shown that such a device can exhibit bistability for certain operating conditions. The condition for this bistability was derived as a function of the coupling ratios between the SOA and laser diode, the input power and the drive currents of the laser diode and the SOA. It was demonstrated that the width, height and position of the bistable domain could be varied as a function of the device operating parameters. By solving the dynamic set of equations corresponding with this device all-optical flip-flop operation could be demonstrated. The operation of the device as an all-optical flip-flop was shown for a variety of pulse lengths, coupling ratios and CW input powers. The dependence of the device operation on the pulse energies was investigated showing that a minimal value for the pulse energies exists in order to obtain all-optical flip-flop operations for a certain operating condition.

As a next step the static bistability observed in a SOA and DFB laser diode pair was investigated using both a commercial software tool and experiments. For the experiments a device consisting of a SOA and an array of 4 laser diodes connected by means of a 1x4 coupler was used. As in the results obtained with the theoretical model it was concluded that this device can show bistable operation for certain operating conditions in both the laser and signal output power, when a CW input signal is injected into the SOA. The width, height and position of the bistable domain was again shown to be dependent on the drive currents of SOA and laser diode, the coupling ratio between them and the input power to the SOA. Bistable operation was experimentally demonstrated over an input signal wavelength range of over 25nm. This makes a single device useable for several different wavelength channels reducing the complexity and cost of all-optical networks.

In order to verify the origin of the optical bistability observed in this device simulations were performed, which indicated the validity of the proposed model describing the origin of the bistability. A clear

distinction with the bistability found in a stand alone DFB laser diode was found.

The dynamic simulation and experimental results presented in Chapter 5 showed the operability of the device as an all-optical flip-flop device. Good agreement was obtained between the simulations and experimental results. The wavelength dependence measurements showed that the device can be used as an all-optical flip-flop for input signal wavelengths ranging over at least 10nm. The evolution of the minimal required energy needed to obtain switching as a function of the pulse length and the CW input power showed, together with the dependence of the all-optical flip-flop operation on the pulse energy, that the device is robust with respect to variations of the pulse length, pulse energy and CW input power. This makes it very suitable for use in real network environments. The extinction ratio has been shown to remain relatively constant as a function of changing operating conditions. The switch times on the other hand are highly dependent on the length of the pulses used to perform the switching. Switching times as low as 50ps and set to set (or reset to reset) operation at a repetition rate up to 1.25GHz has been demonstrated. Set and reset pulse energies have been demonstrated below 1pJ. By using two DFB laser diodes at the same time simultaneous multiple wavelength output operation can be obtained with very low set and reset pulse energies of 340fJ and 240fJ respectively for 100ps long pulses. The extensive characterization of the all-optical flip-flop presented in this work shows both the robustness of the device and the excellent operating conditions (primarily the required pulse energy). The presented investigation of the flexibility of the device is to our knowledge one of the most complete of an all-optical flip-flop to date.

After seeing the steep boundaries of the bistable domain, possible in the SOA and DFB laser diode feedback scheme, in combination with the possibility to adjust the width, height and position of the bistable domain by means of different control parameters, the use of the device as an all-optical decision element and wavelength converter was investigated. The device was shown to operate as a 2R regenerator with clear ER improvement up to 7dB for NRZ signals for a bitrate of 10Gbit/s in both transmission and reflection mode. BER measurements showed that an improvement of the receiver sensitivity could not yet be obtained with this device.

All-optical wavelength conversion has also been demonstrated at a bitrate of 2.5Gbit/s showing both an ER improvement of over 11dB and a receiver sensitivity improvement of 3dB for a BER of 10^{-9} .

All in all it can be concluded that the device discussed in this work can be used for various applications, the foremost being the use as an all-optical flip-flop where very low switching energies in combination with a large robustness to environmental changes has been demonstrated. This device can be used as a building block of all-optical packet switching nodes or other network elements where the need arises for short or long term all-optical memory elements.

7.2 Future work

While it has been shown that the optical feedback combination of a SOA and DFB laser diode can be used as an all-optical flip-flop, 2R regenerator or wavelength converter some questions and possible improvements still remain:

- **The device performance** can be increased by improving the efficiency as well as the stability of the fiber to chip coupling. This can be done by packaging the device or by integrating the device on a photonic circuit with other devices in order to form a higher level network element (possibly even a complete all-optical switch). Another device improvement might be the incorporation of a tunable coupling section between the SOA and the laser diode. Devices have been developed with this purpose but fabrication problems halted this part of the research. The extra degree of freedom gained with a variable coupling between the laser diode and the SOA may reduce the restriction put on the minimal required energy and CW input power in the case of operation of the device as an all-optical flip-flop.
- **System experiments** where the device is used as part of a small all-optical network could show the real operating properties of this device. Using the device as an all-optical flip-flop that delivers the pump power for an all-optical wavelength converter, when the address of the packet header changes the state of the flip-flop, is an example of such an experiment. These experiments are approximations of the intended large scale all-optical networks and can lead to a better understanding of the requirements imposed on the different devices in these networks. To

that extent collaboration with a group focused on higher level all-optical network architectures could also be favorable.

- **A multi-stable device** could be obtained by using the device as shown in Figure 4.9, which is the device used for the experiments, in such a way that more than 1 laser diode in the array of laser diodes is used but only one is switched on at any time. This can be done by adding an additional reflector section at the left hand side of the SOA (either by means of a high reflection coating or a broad wavelength grating). In this way the power from the switched on laser gets reflected at the left hand side facet of the SOA, and also amplified during the double passage through the SOA enabling one laser diode to keep the other laser diodes quenched. By injecting pulses with the correct wavelength into a switched off laser diode this laser diode can switch on and quench the other laser diodes. By combining this device with an AWG a multi-stable all-optical flip-flop can be obtained in which the output state of the device is determined by the wavelength.

Figures

1.1	Estimated number of hosts in the internet as a function of time [2]	2
1.2	Schematic view of a simple all-optical network. IP: internet protocol. OADM: Optical add-drop multiplexer. AO: All-optical.	3
1.3	Schematic representation of an all-optical packet switch.	5
2.1	Schematic view of the SOA and the various input and output signals.	16
2.2	Output power (P_4) and gain for the backward propagating signal as a function of the right hand side input power (P_3) with $P_1 = 0\text{dBm}$ and $I_{SOA} = 200\text{mA}$ for different values of α_i	22
2.3	Output power (P_2) and gain for the forward propagating signal as a function of the right hand side input power (P_3) with $P_1 = 0\text{dBm}$ and $I_{SOA} = 200\text{mA}$ for different values of α_i	23
2.4	Output power (P_4) and gain for the backward propagating signal as a function of the right hand side input power (P_3) with $P_1 = 0\text{dBm}$ and $I_{SOA} = 400\text{mA}$ for different values of α_i	24
2.5	Static single pass gain of the SOA as a function of the left hand side input power (P_1) for different values of the right hand side input power (P_3).	25
2.6	Comparison of the output power (P_2) for the forward propagating signal as a function of the right hand side input power (P_3) with $P_1 = 0\text{dBm}$ and $I_{SOA} = 200\text{mA}$ for different values of α_i . Both the solution obtained by solving equation 2.29 as the numerical solution of the traveling rate equations is shown.	26

2.7	Measurement setup for the static characterization of a SOA. C TL: Tunable laser source, EDFA: Erbium Doped Fiber Amplifier, VAO: variable optical attenuator and circ: optical circulator.	28
2.8	Output power (P_2) and gain for the forward propagating signal as a function of the left hand side input power (P_1) with the backward injected power (P_3) set to -1.8dBm for different values of the SOA drive current (I_{SOA}).	29
2.9	Gain of the SOA as a function of the left hand side input power (P_1) with the backward injected power (P_3) set to 1.46dBm for different values of the SOA drive current (I_{SOA}).	29
2.10	Gain of the SOA as a function of the left hand side input power (P_1) with $I_{SOA} = 200\text{mA}$ for different values of α_i	31
2.11	Comparison of the gain of the SOA as a function of the left hand side input power (P_1) with $I_{SOA} = 200\text{mA}$ for different values of α_i . Both the solution obtained by solving equation 2.44 as the numerical solution of the traveling rate equations is shown.	31
2.12	Experimentally obtained gain of the SOA as a function of left hand side input power (P_1) for different values of the SOA drive current (I_{SOA}).	32
2.13	Simulated small signal gain in the counter-propagating scheme for different CW input powers and a SOA drive current of 200mA.	37
2.14	Comparison between the analytical solution of the dynamic response of a SOA and the standard traveling wave rate equation approach for the counter-propagating scheme for different CW input powers and a SOA drive current of 200mA.	38
2.15	Simulated small signal gain in the co-propagating scheme for different CW input powers and a SOA drive current of 200mA.	39
2.16	Measurement setup for the static characterization of a SOA. Used abbreviations are TL: Tunable laser source, EDFA: Erbium Doped Fiber Amplifier, VAO: variable optical attenuator and circ: optical circulator.	40
2.17	Experimentally obtained small signal gain in the counter-propagating region for different CW input powers and a SOA drive current of 300mA.	41

2.18	Measurement setup for the static characterization of a SOA. Used abbreviations are TL: Tunable laser source, EDFA: Erbium Doped Fiber Amplifier, VAO: variable optical attenuator and circ: optical circulator.	41
2.19	Experimentally obtained small signal gain in the co-propagating region for different CW input powers and a SOA drive current of 300mA.	42
2.20	Right hand side output power (P_2) of the SOA as a function of time. The CW input power is 0dBm. A 100ps (left) and 400ps (right) long optical pulse is injected into the r.h.s. facet at $t=1.2$ ns. The SOA current is 120mA. . .	43
2.21	Right hand side output power (P_2) of the SOA as a function of time. The CW input power is 0dBm. A 100ps (left) and 400ps (right) long optical pulse is injected into the l.h.s. facet at $t=1.2$ ns. The SOA current is 120mA. . .	44
2.22	Right hand side output power (P_2) of the SOA as a function of time. The CW input power is 0dBm. A 100ps long optical pulse is injected into the l.h.s. (left) or r.h.s. (right) facet at $t=1.2$ ns. The SOA current is 120mA. . . .	44
2.23	Right hand side output power (P_2) of the SOA as a function of time calculated using the lossless solution of Equation 2.65 and the traveling wave rate equations with $\alpha_i = \frac{30}{cm}$. The CW input power is 0dBm. A 100ps long optical pulse is injected into the r.h.s. (right) and l.h.s. (left) facet at $t=1.2$ ns. The SOA current is 120mA.	45
3.1	Schematic view of a semiconductor laser diode.	48
3.2	Laser output power as a function of the input current. . .	50
3.3	Laser output power as a function of injected power for a laser current of 200mA.	52
3.4	Dynamic response of the laser output power as a function of the externally injected power for for a laser current of 200mA.	53
3.5	Dynamic response of the laser output power as a function of the externally injected power for for a laser current of 200mA. Zoom in around the switch on and off of the laser diode.	54

3.6	Dynamic response of the laser output power and carrier density as a function of the time with external power injected as in Figure 3.5 for a laser current of 200mA. Zoom in around the switch on and off of the laser diode.	54
3.7	Dynamic response of the laser output power as a function of the input power for a laser current of 200mA.	55
3.8	Dynamic response of the laser output power as a function of time for varying input powers as in Figure 3.7 for a laser current of 200mA.	55
3.9	Schematic view of a semiconductor laser diode mutually and optically coupled to a SOA.	56
3.10	Static response of the laser output power p_2 as a function of the input power p_{in} for $p_{las} = 1$, $g_0L = 5$ and $x = y = 1$	58
3.11	Static response of the SOA output power p_1 as a function of the input power p_{in} for $p_{las} = 1$, $g_0L = 5$ and $x = y = 1$	59
3.12	p_2 as a function of g_0L for $p_{las} = 1$, $p_{in} = 0.1$ and $x = y = 1$	61
3.13	p_1 as a function of g_0L for $p_{las} = 1$, $p_{in} = 0.1$ and $x = y = 1$	61
3.14	p_2 as a function of g_0L for $p_{las} = 1$, $p_{in} = 0.1$ and different $x=y$	63
3.15	p_2 in function of g_0L for $p_{in} = 0.1$, $p_{las} = 1$ and different x and y	64
3.16	p_2 as a function of g_0L for $p_{las} = 1$, $x=y=1$ and different p_{in}	65
3.17	p_2 as a function of g_0L for $p_{in} = 0.1$, $x=y=1$ and different p_{las}	66
3.18	p_1 and p_2 as a function of p_{las} for $p_{in} = 0.1$, $x=y=1$ and $g_0L = 5$	67
3.19	p_1 as a function of p_{in} for $p_{las} = 1$, $g_0L = 1.8$ and $x = y = 1$	70
3.20	Right and left boundary values of p_{in} for the bistable domain as a function of g_0L for $p_{las} = 1$, $p_{sat} = 1$ and $x = y = 1$ (left) and $x = y = 0.5$ (right).	71
3.21	p_1 and p_2 as a function of p_{in} for $p_{las} = 1$, $p_{sat} = 1$, $g_0L = 5$ and different $x=y$	71
3.22	p_1 and p_2 as a function of p_{in} for $p_{las} = 1$, $p_{sat} = 1$, $g_0L = 5$ and different x and y	72
3.23	p_1 and p_2 as a function of p_{in} for $p_{sat} = 1$, $p_{las} = 1$, $x = y = 1$ and different g_0L	73
3.24	p_1 and p_2 as a function of p_{in} for $p_{sat} = 1$, $g_0L = 5$, $x = y = 1$ and different p_{las}	73

3.25	Schematic representation of the configuration of the SOA and DFB feedback combination used for the dynamic analysis of the device.	75
3.26	Static response of the laser and SOA output power as a function of the input power to the SOA for a coupling ratio of 1 (left) and 0.5 (right).	76
3.27	Dynamic response of the laser and SOA output power with a coupling ratio $x=1$ and a CW input power of 0.75mW for various combinations of set and reset pulse powers. The pulse length is 50ps in this case. Top left: set pulse power = 9mW, reset pulse power 5.2mW. Top right: set pulse power = 9.7mW, reset pulse power 4mW. Bottom left: set pulse power = 9.7mW, reset pulse power 5.2mW. Bottom right: set pulse power = 12mW, reset pulse power 7mW.	77
3.28	Dynamic response of the laser and SOA output power with a coupling ratio $x=1$ and a CW input power of 0.75mW for different pulse lengths. Left: 100ps pulse length, set pulse power = 4.4mW, reset pulse power 1.9mW. Right: 400ps pulse length, set pulse power = 1.3mW, reset pulse power 0.6mW.	79
3.29	Dynamic response of the laser and SOA output power with a coupling ratio $x=0.5$ and a CW input power of 1.6mW for different pulse lengths. Left: 150ps pulse length, set pulse power = 2.1mW, reset pulse power 1.3mW. Right: 400ps pulse length, set pulse power = 0.9mW, reset pulse power 0.5mW.	80
3.30	Dynamic response of the laser and SOA output power with a coupling ratio $x=0.5$ and a CW input power of 1.6mW for different peak pulse powers. The pulse length is 150ps. Left: set pulse power = 3mW, reset pulse power 2mW. Right: set pulse power = 6mW, reset pulse power 4mW.	81
3.31	Minimal required pulse energy to obtain switching between the stable states of the SOA and laser diode combination for different pulse lengths. Left: Coupling ratio = 1, CW input power = 0.75mW. Right: Coupling ratio = 0.5, CW input power = 1.6mW.	82

4.1	Set-up used for the numerical simulations. Used abbreviations TL: Tunable laser, VOA: Variable optical attenuator and TOF: Tunable optical filter.	87
4.2	Laser output power as a function of the input power for a laser current of 80mA and a SOA current of 90mA and a coupling ratio of 0.25 between the SOA and the laser diode with and without the use of the SOA.	88
4.3	Laser, signal output power and signal output power 2 (bottom) as a function of the input power for a laser current of 80mA and a SOA current of 90mA for different coupling ratios between the SOA and the laser diode. . .	90
4.4	Laser and signal output power as a function of the input power for a laser current of 60mA and a SOA current of 220mA for different coupling ratios between the SOA and the laser diode.	91
4.5	Laser and signal output power as a function of the input power for a laser current of 80mA and a coupling ratio between the SOA and the laser diode of 0.5 for different SOA currents.	92
4.6	Laser and signal output power as a function of the input power, obtained from the model described in Chapter 3. The output saturation power of the SOA is 11.5dBm. The coupling ratio between laser diode and SOA is 0.5. The laser drive current is 110mA. The SOA drive current is varied.	93
4.7	Laser and signal output power as a function of the input power for a SOA current of 90mA and a coupling ratio between the SOA and the laser diode of 0.5 for different laser currents.	94
4.8	Wavelength dependence of the laser and signal output power as a function of the input power for a laser current of 80mA, a SOA current of 100mA and a coupling ratio between the SOA and the laser diode of 0.45.	95
4.9	Picture of the device used for the experimental verification of the operation of a SOA and DFB laser diode combination. From left to right the SOA, MMI-coupler and laser diode array can be distinguished.	96
4.10	Picture of the electrical probing and coupling of the light in and out of the device.	97

4.11 Setup used for the static characterization of the SOA and DFB laser diode combination. Used abbreviations: TL: Tunable laser, VOA. variable optical attenuator, OS: optical switch, TOF: tunable optical filter and PM: power meter. 98

4.12 Static response of the laser output power and signal output power as a function of the laser drive current for different CW input powers and a SOA drive current of 80mA. Left: Laser output power. Right: Signal output power at the right hand side facet of the device (laser diode). 99

4.13 Static response of the laser output power and signal output power as a function of the SOA drive current for different CW input powers and a laser drive current of 70mA. Left: Laser output power. Right: Signal output power at the right hand side facet of the device (laser diode). 100

4.14 Static response of the laser output power and signal output power as a function of the input power for different laser drive currents and a SOA drive current of 120mA. Left: Laser output power. Right: Signal output power at the right hand side facet of the device (laser diode). . . . 100

4.15 Static response of the laser output power and signal output power as a function of the input power for different SOA drive currents and a laser drive current of 100mA. Left: Laser output power. Right: Signal output power at the right hand side facet of the device (laser diode). . . . 101

4.16 Static response of the laser output power and signal output power as a function of the input power for different SOA drive currents and a laser drive current of 100mA. Left: Laser output power. Right: Signal output power at the right hand side facet of the device (laser diode). . . . 103

4.17 Static response of the laser output power and signal output power as a function of the input power for different SOA drive currents and a laser drive current of 100mA. Left: Laser output power. Right: Signal output power at the right hand side facet of the device (laser diode). . . . 103

5.1 Schematic representation of the multimode interference bistable laser diode based all-optical flip-flop [84]. . . . 107

5.2	Schematic representation of the coupled Mach-Zehnder interferometers based all-optical flip-flop [96, 97].	109
5.3	Different definitions of the repetition rate of all-optical flip-flops.	110
5.4	Schematic overview of the SOA-DFB all-optical flip-flop in the stable state with a turned on DFB laser diode. Coupler x represents a coupling device with a coupling ratio equal to x , while the other couplers used are 3dB couplers. The dashed line represents the signal power, the full line the laser power.	113
5.5	Schematic overview of the response of the SOA-DFB all-optical flip-flop during the reset operation. The dashed line represents the signal power.	114
5.6	Schematic overview of the SOA-DFB all-optical flip-flop in the stable state with a quenched DFB laser diode. The dashed line represents the signal power.	114
5.7	Schematic overview of the response of the SOA-DFB all-optical flip-flop during the set operation. The dashed line represents the signal power, the full line the laser power.	115
5.8	Schematic setup used for the simulations	116
5.9	Static bistable domain in the signal and laser output power of the all-optical flip-flop used in the simulations for a SOA drive current of 120mA and a DFB laser diode drive current of 100mA.	116
5.10	Static bistable domain in the signal power of the all-optical flip-flop used in the simulations for a SOA drive current of 120mA and a DFB laser diode drive current. The signal power right after the 3dB coupler and after the laser diode is shown.	117
5.11	Laser output power during the all-optical flip-flop operation for pulse injection through port 1 and 2 as shown in Figure 5.8. The pulse length was 400ps and the CW input signal power is -0.5dBm. The set pulse peak power is 2mW and the reset pulse peak power is 6mW.	119
5.12	Laser output power during the all-optical flip-flop operation for pulse injection through port 3 and 4 as shown in Figure 5.8. The pulse length was 400ps and the CW input signal power is -0.5dBm. The set pulse peak power is 4mW and the reset pulse peak power is 9mW.	119

5.13 Simulated all-optical flip-flop operation in the laser output power for a CW input signal power of -0.5dBm. The pulse length is 50ps for both the set and reset pulses. The peak power of the set pulses is 46mW and it is 90mW for the reset pulses. 120

5.14 Simulated all-optical flip-flop operation in the signal output power corresponding with the laser output power response shown in Figure 5.13. 120

5.15 Detailed view of the laser and signal output power as a function of the time around the arrival of the set and reset pulse. Top: laser output power. Bottom: signal output power. Left: Reset pulse arrival. Right: Set pulse arrival. 121

5.16 Average carrier density during the all-optical flip-flop operation as shown in Figure 5.13 and 5.14 for the laser diode (left) and the SOA (right). 122

5.17 Minimal required set pulse energy to obtain all-optical flip-flop operation as a function of the pulse length for different CW input powers. 123

5.18 Minimal required reset pulse energy to obtain all-optical flip-flop operation as a function of the pulse length for different CW input powers. 123

5.19 Experimental setup used for the measurements of the SOA/DFB laser diode based all-optical flip-flop. Used abbreviations: TL: tunable laser diode, 3dB: 3dB splitter/combiner, EDFA: Erbium doped fiber amplifier, att: variable optical attenuator, OBPF: tunable optical band-pass filter. 125

5.20 Laser output power as a function of signal input power into the SOA for a SOA drive current of 103.5mA and a laser diode drive current of 101.4mA. The wavelength of the input signal is 1555nm. 126

5.21 Pulse train of 150ps long pulses with a period of 1.6ns. The axis scales are 2ns/div for the horizontal and 500 μ W/div for the vertical axis. 127

5.22 Dynamic flip-flop operation for 150ps set and reset pulses and a CW input power of 6.4dBm. The axis scales are 1ns/div for the horizontal and 1mW/div for the vertical axis. 127

5.23	Set and reset switch times for 150ps set and reset pulses and a CW input power of 6.4dBm. The axis scales are 100ps/div for the horizontal and 600 μ W/div for the vertical axis.	128
5.24	Dynamic flip-flop operation in the laser output power for different set and reset pulse lengths and a CW input power of 6.4dBm. The axis scales are 1ns/div for the horizontal and 1mW/div for the vertical axis. Top left: 200ps long pulses. Top right: 300ps long pulses. Bottom: 400ps long pulses.	129
5.25	Minimal required set (right hand side) and reset (left hand side) pulse energy to obtain switching as a function of the pulse length for different CW input powers chosen inside the bistable domain shown in Figure 5.20.	130
5.26	Switch on and switch off times for the laser output power corresponding with the set and reset pulse energies from Figure 5.25. The switch time is defined as the 10%-90% transition between the states.	131
5.27	Contrast ratio between the two states in the laser output power corresponding with the set and reset pulse energies from Figure 5.25.	131
5.28	Static laser and signal output power as a function of the signal input power for different input signal wavelengths. Left: laser output power. Right: Signal output power. . .	132
5.29	Set and reset pulse train used to obtain all-optical flip-flop operation. The pulse trains consist of 100ps long pulses and are periodical with a period of 6.4ns. The pulse trains are shifted relatively over 3.2ns.	133
5.30	All-optical flip-flop operation in the laser and signal output power for different input signal wavelengths. From top to bottom the wavelength of the input signal is 1547, 1553 and 1557nm. The laser output power is shown on the left and the signal output power is shown on the right each time. The corresponding set and reset pulse energy of the 100ps long pulses used is shown in Table 5.3. The CW input power is 3.9dBm for each input signal wavelength.	134

5.31 Minimal required set and reset pulse energy as a function of the pulse length for different CW input powers chosen inside the bistable domain. The results are shown for different wavelengths of the input signals (CW input power and pulses). From top to bottom the wavelength of the input signals is given as 1447, 1553 and 1557nm. The left graph each time shows the minimal required set pulse energy and the right hand side graph shows the minimal required reset pulse energy. 136

5.32 All-optical flip-flop operation in the laser output power for different combinations of set and reset pulse energies. The input signals wavelength is 1547nm and the CW input power is 3.9dBm. The pulses are 400ps long. Top left: 1.12pJ set pulse energy and 1.23pJ reset pulse energy. Top right: 1.14pJ set pulse energy and 5.64pJ reset pulse energy. Bottom left: 6.23pJ set pulse energy and 5.64pJ reset pulse energy. Bottom right: 10.39pJ set pulse energy and 5.64pJ reset pulse energy. 139

5.33 All-optical flip-flop operation in the signal output power for different combinations of set and reset pulse energies. The input signals wavelength is 1547nm and the CW input power is 3.9dBm. The pulses are 400ps long. Top left: 1.12pJ set pulse energy and 1.23pJ reset pulse energy. Top right: 1.14pJ set pulse energy and 5.64pJ reset pulse energy. Bottom left: 10.69pJ set pulse energy and 1.44pJ reset pulse energy. Bottom right: 10.69pJ set pulse energy and 5.64pJ reset pulse energy. 140

5.34 Static bistable response of the laser output power as a function of the input power. The drive currents of the laser diode and the SOA are 105.8mA and 83mA respectively. The input signal wavelength was 1550nm. 142

5.35 All-optical flip-flop operation in the laser output power for a CW input power of 4.5dBm and a set and reset pulse energy of 1pJ and 1.3pJ respectively. The pulses are 50ps long. The axis scales are 500ps/div for the horizontal and 1mW/div for the vertical axis. 142

5.36 Zoom in around the set and reset operation shown in Figure 5.35. The axis scales are 100ps/div for the horizontal and 1mW/div for the vertical axis. 143

- 5.37 All-optical flip-flop operation in the laser output power for a CW input power of 4.5dBm and a set and reset pulse energy of 0.8pJ and 0.9pJ respectively. The pulses are 150ps long. The axis scales are 500ps/div for the horizontal and 1mW/div for the vertical axis. 143
- 5.38 Experimental setup used for the all-optical flip-flop operation of the SOA and DFB laser diode feedback scheme where two laser diodes are driven at the same time. . . . 144
- 5.39 Static bistable domain in both driven laser output powers as a function of the input power. 145
- 5.40 Simultaneous all-optical flip-flop operation at the wavelengths of the two laser diodes used. The pulse length is 100ps and the CW input power is 0.5dBm. The set and reset pulse energy is 340fJ and 240fJ respectively. 146
- 6.1 Experimental setup used for the 2R-regeneration and wavelength conversion measurements. TL: tunable laser. VOA: variable optical attenuator. MOD: 10Gbit/s modulator. DUT: device under test. Opt Rec: Optical receiver. 150
- 6.2 Static signal output versus input power transfer function of the SOA and DFB laser diode feedback scheme. The drive currents of the laser diode and SOA are 65mA and 45mA respectively. 151
- 6.3 Measured eye diagrams of a 10Gbit/s NRZ signal. The output signal considered is the output signal at the right hand side facet of the laser diode. The left graph shows the input signal with an ER of 3.4dB. The right graph shows the output graph 10.3dB. The division along the x-axis is 50ps/div. The division along the y-axis is 200 μ W and 500 μ W for the left and right graph respectively. The zero power level is depicted by the ground symbol. . . . 152
- 6.4 Measurement of the BER as a function of the signal power incident on the pre-amplified receiver. Both the back to back signal and the output signal after passage through the device are considered. 153
- 6.5 Extinction ratio of the output signal as a function of the extinction ratio of the input signal. 153

6.6	Static signal output versus input power transfer function of the SOA and DFB laser diode feedback scheme. The output signal considered is the output signal at the left hand side facet of the SOA. The drive currents of the laser diode and SOA are 65mA and 45mA respectively.	154
6.7	Measured eye diagrams of a 10Gbit/s NRZ signal. The output signal considered is the output signal at the left hand side facet of the SOA. The left graph shows the input signal with an ER of 3.9dB. The right graph shows the output graph 9.1dB. The division along the x-axis is 20ps/div. The division along the y-axis is 1mW/div. The zero power level is depicted by the ground symbol.	155
6.8	Static laser output versus input power transfer function of the SOA and DFB laser diode feedback scheme. The drive currents of the laser diode and SOA are 100mA and 125mA respectively.	156
6.9	Measured eye diagrams of a 2.5Gbit/s NRZ signal. The output signal considered is the laser output signal at the right hand side facet of the DFB laser diode. The left graph shows the input signal with an ER of 6.9dB. The right graph shows the output graph 18.5dB. The division along the x-axis is 50ps/div. The division along the y-axis is 1mW/div. The zero power level is depicted by the ground symbol.	156
6.10	Measurement of the BER as a function of the signal power incident on the pre-amplified receiver. Both the back to back signal and the wavelength converted laser output signal are considered.	157

Tables

2.1	Explanation of the parameters in the equations used to describe the traveling wave SOA.	16
3.1	Explanation of the parameters in the equations used to describe a semiconductor laser diode.	50
4.1	Device properties of the scheme used in the simulations.	87
4.2	Default parameters of the software package used for the numerical simulations.	87
5.1	Device properties of different all-optical flip-flops presented in literature.	111
5.2	Set and reset pulse energy corresponding with the all-optical flip-flop operation shown in Figure 5.24.	128
5.3	Set and reset pulse energy corresponding with the all-optical flip-flop operation shown in Figure 5.30.	135

Bibliography

- [1] "Internet world stats: Usage and population statistics.."
- [2] R. H. Zakon, "Hobbes' internet timeline v8.2,"
- [3] T. Maiman, "Stimulated optical radiation in ruby," *Nature*, vol. 187, pp. 493–494., 1960.
- [4] F. P. Kapron, D. B. Keck, and R. D. Maurer, "Radtion losses in glass optical waveguides," *Appl. Phys. Lett.*, vol. 17, pp. 423–425, 1970.
- [5] L. Leng, S. Stulz, B. Zhu, L. E. Nelson, B. Edvold, L. Gruner-Nielsen, S. Radic, J. Centanni, and A. Gnauck, "1.6-Tb/s (160 x 10.7 Gb/s) transmission over 4000 km of nonzero dispersion fiber at 25-GHz channel spacing," *IEEE Photon. Technol. Lett.*, vol. 15, no. 8, pp. 1153–1155, 2003.
- [6] T. N. Nielsen, A. J. Stentz, K. Rottwitt, D. S. Vengsarkar, Z. J. Chen, P. B. Hansen, J. H. Park, K. S. Feder, S. Cabot, S. Stulz, D. W. Peckham, L. Hsu, C. K. Kan, A. F. Judy, S. Y. Park, L. E. Nelson, and L. Gruner-Nielsen, "3.28-Tb/s transmission over 3x100 km of nonzero-dispersion fiber using dual C- and L-band distributed Raman amplification," *IEEE Photon. Technol. Lett.*, vol. 12, no. 8, pp. 1079–1081, 2000.
- [7] H. Suzuki, J. Kani, H. Masuda, N. Takachio, K. Iwatsuki, Y. Tada, and M. Sumida, "1-Tb/s (100 x 10 Gb/s) super-dense WDM transmission with 25-GHz channel spacing in the zero-dispersion region employing distributed raman amplification technology," *IEEE Photon. Technol. Lett.*, vol. 12, no. 7, pp. 903–905, 2000.
- [8] M. Morisaki, H. Sugahara, T. Ito, and T. Ono, "2.56-Tb/s (64 x 42.7 Gb/s) WDM transmission over 6000 km using all-raman am-

- plified inverse double-hybrid spans," *IEEE Photon. Technol. Lett.*, vol. 15, no. 11, pp. 1615–1617, 2003.
- [9] I. Tafur Monroy, E. Van Breusegem, T. Koonen, J. Jennen, C. Peucheret, and E. Zouganeli, "Optical label switched networks: Laboratory trial and network emulator in the IST-STOLAS project," *IEEE Communications Magazine*, vol. 44, pp. 43–51, 2006.
- [10] F. Ramos, E. Kehayas, J. M. Martinez, R. Clavero, J. Marti, L. Stampoulidis, D. Tsiokos, H. Avramopoulos, J. Zhang, P. V. Holm-Nielsen, N. Chi, P. Jeppesen, N. Yan, I. T. Monroy, A. M. J. Koonen, M. T. Hill, Y. Liu, H. J. S. Dorren, R. Van Caenegem, D. Colle, M. Pickavet, and B. Riposati, "IST-LASAGNE: Towards all-optical label swapping employing optical logic gates and optical flip-flops," *J. Lightwave Technol.*, vol. 23, no. 10, pp. 2993–3011, 2005.
- [11] S. Kamei, A. Ishii, M. Itoh, T. Shibata, Y. Inoue, and T. Kitagawa, "64x64-channel uniform-loss and cyclic-frequency arrayed-waveguide grating router module," *IEE Electron. Lett.*, vol. 39, no. 1, pp. 83–84, 2003.
- [12] K. Kato, A. Okada, Y. Sakai, K. Noguchi, T. Sakamoto, S. Suzuki, A. Takahara, S. Kamei, A. Kaneko, and M. Matsuoka, "32 x 32 full-mesh (1024 path) wavelength-routing WDM network based on uniformloss cyclic-frequency arrayed-waveguide grating," *IEE Electron. Lett.*, vol. 36, no. 15, pp. 1294–1296, 2000.
- [13] R. N. Nogueira, J. R. F. da Rocha, and J. L. Pinto, "Tunable polarization optical delay line based on a linear chirped fiber Bragg grating," *Microwave and Optical Technology Letters*, vol. 48, no. 11, pp. 2357–2359, 2006.
- [14] F. Ohman, K. Yvind, and J. Mork, "Voltage-controlled slow light in an integrated semiconductor structure with net gain," *Opt Express*, vol. 14, no. 21, pp. 9955–9962, 2006.
- [15] C. Tian, Z. W. Zhang, M. Ibsen, P. Petropoulos, and D. J. Richardson, "A reconfigurable optical header recognition system for optical packet routing applications," *IEEE Photon. Technol. Lett.*, vol. 18, no. 21-24, pp. 2395–2397, 2006.

- [16] K. H. Park and T. Mizumoto, "The packet-recognition of header for all-optical self-routing," *Ieice Transactions on Communications*, vol. E83b, no. 7, pp. 1577–1579, 2000.
- [17] T. Fjelde, D. Wolfson, A. Kloch, B. Dagens, A. Coquelin, I. Guillemot, F. Gaborit, F. Poingt, and M. Renaud, "Demonstration of 20Gbit/s all-optical logic XOR in integrated SOA-based interferometric wavelength converter," *IEE Electron. Lett.*, vol. 36, no. 22, pp. 1863–1864, 2000.
- [18] A. Srivatsa, H. D. Waardt, M. T. Hill, G. D. Khoe, and H. J. S. Dorren, "All-optical serial header processing based on two-pulse correlation," *IEE Electron. Lett.*, vol. 37, no. 4, pp. 234–235, 2001.
- [19] H. S. Chung, R. Inohara, K. Nishimura, and M. Usami, "All-optical multi-wavelength conversion of 10 Gbit/s NRZ/RZ signals based on SOA-MZI for WDM multicasting," *IEE Electron. Lett.*, vol. 41, no. 7, pp. 432–433, 2005.
- [20] M. Matsuura, N. Kishi, and T. Miki, "All-optical wavelength conversion with large wavelength hopping by utilizing multistage cascaded SOA-based wavelength converters," *IEEE Photon. Technol. Lett.*, vol. 18, no. 5-8, pp. 926–928, 2006.
- [21] E. Kehayas, K. Vyrsoinos, L. Stampoulidis, K. Christodoulopoulos, K. Vlachos, and H. Avramopoulos, "ARTEMIS: 40-Gb/s all-optical self-routing node and network architecture employing asynchronous bit and packet-level optical signal processing," *J. Lightwave Technol.*, vol. 24, no. 8, pp. 2967–2977, 2006.
- [22] E. Kehayas, J. Seoane, Y. Liu, J. M. Martinez, J. Herrera, P. V. Holm-Nielsen, S. Zhang, R. McDougall, G. Maxwell, F. Ramos, J. Marti, H. J. S. Dorren, P. Jeppesen, and H. Avramopoulos, "All-optical network subsystems using integrated SOA-based optical gates and flip-flops for label-swapped networks," *IEEE Photon. Technol. Lett.*, vol. 18, no. 13-16, pp. 1750–1752, 2006.
- [23] A. Ackaert, P. Demeester, P. Lagasse, C. Politi, M. O'Mahony, T. Berg, B. Tromborg, J. Saniter, E. Patzak, S. Rao, P. Vogel, C. Minot, and D. Erasme, "European IST-programme roadmap for optical communications generated by the OPTIMIST thematic network," *Annales Des Telecommunications-Annals of Telecommunications*, vol. 58, no. 11-12, pp. 1550–1585, 2003.

- [24] Z. J. Huang, A. Gray, I. Khrushchev, and I. Bennion, "10-Gb/s transmission over 100 Mm of standard fiber using 2R regeneration in an optical loop mirror," *IEEE Photon. Technol. Lett.*, vol. 16, no. 11, pp. 2526–2528, 2004.
- [25] D. A. O. Davies, A. D. Ellis, and G. Sherlock, "Regenerative 20 Gbit/s wavelength conversion and demultiplexing using a semiconductor-laser amplifier nonlinear loop mirror," *IEE Electron. Lett.*, vol. 31, no. 12, pp. 1000–1001, 1995.
- [26] S. Boscolo, S. K. Turitsyn, and K. J. Blow, "All-optical passive 2R regeneration for $N \times 40$ gbit/s WDM transmission using NOLM and novel filtering technique," *Optics Communications*, vol. 217, no. 1-6, pp. 227–232, 2003.
- [27] M. Pantouvaki, M. J. Fice, R. Feced, E. P. Burr, R. Gwilliam, A. B. Krysa, J. S. Roberts, and A. J. Seeds, "10-Gb/s all-optical 2R regeneration using an MQW Fabry-Perot saturable absorber and a nonlinear fiber," *IEEE Photon. Technol. Lett.*, vol. 16, no. 2, pp. 617–619, 2004.
- [28] J. De Merlier, G. Morthier, P. Van Daele, I. Moerman, and R. Baets, "All-optical 2R regeneration based on integrated asymmetric mach-zehnder interferometer incorporating MMI-SOA," *IEE Electron. Lett.*, vol. 38, no. 5, pp. 238–239, 2002.
- [29] M. S. Zhao, G. Morthier, and R. Baets, "Demonstration of extinction ratio improvement from 2 to 9 db and intensity noise reduction with the MZI-GCSOA all-optical 2R regenerator," *IEEE Photon. Technol. Lett.*, vol. 14, no. 7, pp. 992–994, 2002.
- [30] O. Leclerc, B. Lavigne, E. Balmefrezol, P. Brindel, L. Pierre, D. Rouvillain, and F. Segueineau, "Optical regeneration at 40 Gb/s and beyond," *J. Lightwave Technol.*, vol. 21, no. 11, pp. 2779–2790, 2003.
- [31] D. Wolfson, P. Hansen, A. Kloch, T. Fjelde, C. Janz, A. Coquelin, I. Guillemot, F. Garorit, F. Poingt, and M. Renaud, "All-optical 2R regeneration at 40Gbit/s in a SOA-based Mach-Zehnder interferometer," in *OFC-IOOC 1999*, p. PD36 suppl, 1999.
- [32] R. J. Manning, I. D. Phillips, A. D. Ellis, A. E. Kelly, A. J. Poustie, and K. J. Blow, "10Gbit/s all-optical regenerative memory using

- single SOA-based logic gate," *IEE Electron. Lett.*, vol. 35, no. 2, pp. 158–159, 1999.
- [33] J. De Merlier, G. Morthier, S. Verstuyft, T. Van Caenegem, I. Moerman, P. Van Daele, and R. Baets, "Experimental demonstration of all-optical regeneration using an MMI-SOA," *IEEE Photon. Technol. Lett.*, vol. 14, no. 5, pp. 660–662, 2002.
- [34] J. Leuthold, L. Moller, J. Jaques, S. Cabot, L. Zhang, P. Bernasconi, M. Cappuzzo, L. Gomez, E. Laskowski, E. Chen, A. Wong-Foy, and A. Griffin, "160 Gbit/s SOA all-optical wavelength converter and assessment of its regenerative properties," *IEE Electron. Lett.*, vol. 40, no. 9, pp. 554–555, 2004.
- [35] V. Lal, M. L. Masanovic, J. A. Summers, G. Fish, and D. J. Blumenthal, "Monolithic wavelength converters for high-speed packet-switched optical networks," *IEEE J. Select. Topics Quantum Electron.*, vol. 13, no. 1, pp. 49–57, 2007.
- [36] H. Ju, S. Zhang, D. Lenstra, H. de Waardt, E. Tangdiongga, G. D. Khoe, and H. J. S. Dorren, "SOA-based all-optical switch with subpicosecond full recovery," *Opt Express*, vol. 13, no. 3, pp. 942–947, 2005.
- [37] K. E. Zoiros, T. Houbavlis, and M. Kalyvas, "Ultra-high speed all-optical shift registers and their applications in OTDM networks," *Optical and Quantum Electronics*, vol. 36, no. 11, pp. 1005–1053, 2004.
- [38] G. Talli and M. Adams, "Gain dynamics of semiconductor optical amplifiers and three-wavelength devices," *IEEE J. Quantum Electron.*, vol. 39, no. 10, pp. 1305–1313, 2003.
- [39] A. Reale, A. Di Carlo, and P. Lugli, "Gain dynamics in traveling-wave semiconductor optical amplifiers," *IEEE Journal on Selected Topics in Quantum Electronics*, vol. 7, no. 2, pp. 293–299, 2001.
- [40] D. Cassioli, S. Scotti, and A. Mecozzi, "A time-domain computer simulator of the nonlinear response of semiconductor optical amplifiers," *IEEE J. Quantum Electron.*, vol. 36, no. 9, pp. 1072–1080, 2000.

- [41] A. Lowery, "Amplified spontaneous emission in semiconductor laser amplifiers; validity of the transmission-line laser model," *IEE Proceedings*, vol. 137, Pt. J, no. 4, pp. 241–247, 1990.
- [42] A. Bogoni, L. Poti, A. Bizzi, and A. Reale, "Novel extended SOAs model for applications in very high-speed systems and its experimental validation," *IEEE Photon. Technol. Lett.*, vol. 14, no. 7, pp. 905–907, 2002.
- [43] M. Connelly, "Wideband semiconductor optical amplifier steady-state numerical model," *IEEE J. Quantum Electron.*, vol. 37, no. 3, pp. 439–447, 2001.
- [44] T. Durhuus, B. Mikkelsen, and K. E. Stubkjaer, "Detailed dynamic model for semiconductor optical amplifiers and their crosstalk and intermodulation distortion," *J. Lightwave Technol.*, vol. 10, no. 8, pp. 1056–1065, 1992.
- [45] J. Pleumeekers, M.-A. Dupertuis, T. Hessler, P. Selbmann, S. Haacke, and B. Deveaud, "Longitudinal spatial hole burning and associated nonlinear gain in gain-clamped semiconductor optical amplifiers," *IEEE J. Quantum Electron.*, vol. 34, no. 5, pp. 879–886, 1998.
- [46] G. P. Agrawal and N. A. Olsson, "Self-phase modulation and spectral broadening of optical pulses in semiconductor-laser amplifiers," *IEEE J. Quantum Electron.*, vol. 25, no. 11, pp. 2297–2306, 1989.
- [47] G. P. Agrawal and N. Dutta, *Long-wavelength semiconductor lasers*. Van Nostrand Reinhold Company Inc., 1986.
- [48] S. Verspurten, G. Morthier, and R. Baets, "Experimental and numerical small-signal analysis of two types of gain-clamped semiconductor optical amplifiers," *IEEE J. Quantum Electron.*, vol. 42, no. 3-4, pp. 302–312, 2006.
- [49] T. Durhuus, B. Mikkelsen, C. Joergensen, S. L. Danielsen, and K. E. Stubkjaer, "All-optical wavelength conversion by semiconductor optical amplifiers," *J. Lightwave Technol.*, vol. 14, no. 6, pp. 942–954, 1996.

- [50] M. L. Nielsen, D. J. Blumenthal, and J. Mork, "A transfer function approach to the small-signal response of saturated semiconductor optical amplifiers," *J. Lightwave Technol.*, vol. 18, no. 12, pp. 2151–2157, 2000.
- [51] J. Mork, A. Mecozzi, and G. Eisenstein, "The modulation response of a semiconductor laser amplifier," *IEEE J. Select. Topics Quantum Electron.*, vol. 5, no. 3, pp. 851–860, 1999.
- [52] F. Ginovart and J. C. Simon, "Gain dynamics studies of a semiconductor optical amplifier," *Journal of Optics A-Pure and Applied Optics*, vol. 4, no. 3, pp. 283–287, 2002.
- [53] F. Ginovart and J. C. Simon, "Semiconductor optical amplifier length effects on gain dynamics," *Journal of Physics D-Applied Physics*, vol. 36, no. 13, pp. 1473–1476, 2003.
- [54] L. Occhi, *Semiconductor optical amplifiers made of ridge waveguide bulk InGaAsP / InP: Experimental characterisation and numerical modelling of Gain, Phase and Noise*. Phd., Eidgenössische Technische Hochschule Zrich, 2002.
- [55] R. Hall, G. Fenner, J. Kingsley, T. Soltys, and R. Carlson, "Coherent light emission from GaAs junctions," *Physical Review Letters*, vol. 9, pp. 366–368, 1962.
- [56] G. Morthier and P. Vankwikelberge, *Handbook of distributed feedback laser diodes*. Artech House Publishers, 1997.
- [57] R. Kaiser and B. Huttel, "Monolithic 40-GHz mode-locked MQW DBR lasers for high-speed optical communication systems," *IEEE J. Select. Topics Quantum Electron.*, vol. 13, no. 1, pp. 125–135, 2007.
- [58] S. H. Oh, K. S. Kim, C. W. Lee, H. Ko, S. Park, M. H. Park, J. M. Lee, S. Kim, and Y. Chung, "Design and fabrication of butt-coupled sampled grating DBR lasers using planar buried heterostructures," *Journal of the Korean Physical Society*, vol. 50, no. 1, pp. 64–71, 2007.
- [59] R. Todt, T. Jacke, R. Meyer, R. Laroy, G. Morthier, and M. C. Amann, "Wide wavelength tuning of sampled grating tunable twin-guide laser diodes," *IEE Electron. Lett.*, vol. 40, no. 23, pp. 1491–1493, 2004.

- [60] P. Vankwikelberge, G. Morthier, and R. Baets, "CLADISS - a longitudinal multimode model for the analysis of the static, dynamic, and stochastic-behavior of diode-lasers with distributed feedback," *IEEE J. Quantum Electron.*, vol. 26, no. 10, pp. 1728–1741, 1990.
- [61] G. Morthier, "An accurate rate-equation description for DFB lasers and some interesting solutions," *IEEE J. Quantum Electron.*, vol. 33, no. 2, pp. 231–237, 1997.
- [62] G. Morthier and B. Moeyersoon, "Improvement of the direct modulation behavior of semiconductor lasers by using a holding beam," *IEEE Photon. Technol. Lett.*, vol. 16, no. 7, pp. 1616–1618, 2004.
- [63] K. Yashiki, K. Sato, T. Morimoto, S. Sudo, K. Naniwae, S. Ae, K. Shiba, N. Suzuki, T. Sasaki, and K. Kudo, "Wavelength-selectable light sources fabricated using advanced microarray-selective epitaxy," *IEEE Photon. Technol. Lett.*, vol. 16, no. 7, pp. 1619–1621, 2004.
- [64] A. Champagne, J. Camel, R. Maciejko, K. J. Kasunic, D. M. Adams, and L. Tromborg, "Linewidth broadening in a distributed feedback laser integrated with a semiconductor optical amplifier," *IEEE J. Quantum Electron.*, vol. 38, no. 11, pp. 1493–1502, 2002.
- [65] A. Champagne, M. Lestrade, J. Camel, R. Maciejko, and B. Tromborg, "Degradation of side-mode suppression ratio in a DFB laser integrated with a semiconductor optical amplifier," *IEEE J. Quantum Electron.*, vol. 40, no. 7, pp. 871–877, 2004.
- [66] B. Moeyersoon, G. Morthier, and M. S. Zhao, "Degradation of the mode suppression in single-mode laser diodes due to integrated optical amplifiers," *IEEE J. Quantum Electron.*, vol. 40, no. 3, pp. 241–244, 2004.
- [67] G. Morthier and B. Moeyersoon, "Intensity noise and linewidth of laser diodes with integrated semiconductor optical amplifier," *IEEE Photon. Technol. Lett.*, vol. 14, no. 12, pp. 1644–1646, 2002.
- [68] L. B. Soldano and E. C. M. Pennings, "Optical multimode interference devices based on self-imaging - principles and applications," *J. Lightwave Technol.*, vol. 13, no. 4, pp. 615–627, 1995.

- [69] D. H. P. Maat, Y. C. Zhu, F. H. Groen, H. van Brug, H. J. Frankena, and X. J. M. Leijtens, "Polarization-independent dilated InP-based space switch with low crosstalk," *IEEE Photon. Technol. Lett.*, vol. 12, no. 3, pp. 284–286, 2000.
- [70] W. D'Oosterlinck, G. Morthier, R. Baets, and T. Erneux, "Optical bistability in a traveling-wave SOA connected to a DFB laser diode: Theory and experiment," *IEEE J. Quantum Electron.*, vol. 42, no. 7-8, pp. 739–746, 2006.
- [71] B. Maes, M. Soljacic, J. D. Joannopoulos, P. Bienstman, R. Baets, S. P. Gorza, and M. Haelterman, "Switching through symmetry breaking in coupled nonlinear micro-cavities," *Opt Express*, vol. 14, no. 22, pp. 10678–10683, 2006.
- [72] V. V. P. Inc, "VPI transmission and componentmaker."
- [73] K. Huybrechts, W. D'Oosterlinck, G. Morthier, and R. Baets, "Optical flip-flop operation using an AR-coated distributed feedback laser diode," in *CLEO 2007*, (Baltimore, USA), p. JWA36, 2007.
- [74] R. Van Caenegem, J. A. Martinez, D. Colle, M. Pickavet, P. Demeester, F. Ramos, and J. Marti, "From IP over WDM to all-optical packet switching: Economical view," *J. Lightwave Technol.*, vol. 24, no. 4, pp. 1638–1645, 2006.
- [75] E. Bahaa and A. Saleh, *Fundamentals of Photonics*. John Wiley and Sons, Inc., 1991.
- [76] J. Wakerly, *Digital design; principles and practices (2nd ed.)*. 1994.
- [77] K. L. Hall and K. A. Rauschenbach, "100-Gbit/s bitwise logic," *Opt Lett.*, vol. 23, no. 16, pp. 1271–1273, 1998.
- [78] N. S. Patel, K. L. Hall, and K. A. Rauschenbach, "40-Gbit/s cascaded all-optical logic with an ultrafast nonlinear interferometer," *Opt Lett.*, vol. 21, no. 18, pp. 1466–1468, 1996.
- [79] M. Takenaka, K. Takeda, Y. Kanema, and Y. Nakano, "All-optical switching of 40 Gb/s packets by MMI-BLD optical label memory," *Opt Express*, vol. 14, no. 22, pp. 10785–10789, 2006.
- [80] J. Herrera, E. Tangdiongga, Y. Liu, M. T. Hill, R. McDougall, A. J. Poustie, and G. Maxwell, "160 Gb/s all-optical packet switching

- employing in-band wavelength labelling and a hybrid-integrated optical flip-flop," in *Proc. ECOC 2006*, pp. 9–10.
- [81] E. Kehayas, J. Seoane, Y. Liu, J. M. Martinez, J. Herrera, P. V. Holm-Nielsen, S. Zhang, R. McDougall, G. Maxwell, F. Ramos, J. Marti, H. J. S. Dorren, P. Jeppesen, and H. Avramopoulos, "All-optical network subsystems using integrated SOA-based optical gates and flip-flops for label-swapped networks," *IEEE Photon. Technol. Lett.*, vol. 18, no. 13-16, pp. 1750–1752, 2006.
- [82] J. Seoane, E. Kehayas, H. Avramopoulos, and P. Jeppesen, "40 Gbit/s NRZ packet-length insensitive header extraction for optical label switching networks," in *LEOS annual 2006*, pp. 555–556, 2006.
- [83] H. J. S. Dorren, E. Tangdiongga, Y. Liu, M. T. Hill, J. van Zantvoort, G. D. Khoe, J. den Besten, E. Smallbrugge, T. de Vries, Y. Oei, X. J. M. Leijtens, and M. K. Smit, "High bit-rate all-optical packet switching," in *Leos annual 2006*, pp. 553–554, 2006.
- [84] M. Takenaka, M. Raburn, and Y. Nakano, "All-optical flip-flop multimode interference bistable laser diode," *IEEE Photon. Technol. Lett.*, vol. 17, no. 5, pp. 968–970, 2005.
- [85] M. Takenaka and Y. Nakano, "Multimode interference bistable laser diode," *IEEE Photon. Technol. Lett.*, vol. 15, no. 8, pp. 1035–1037, 2003.
- [86] M. Takenaka, K. Takeda, and Y. Nakano, "All-optical packet switching and label buffering by MMI-BLD optical flip-flop," *IEEE Electronics Express*, vol. 3, no. 15, pp. 368–372, 2006.
- [87] K. Takeda, M. Takenaka, M. Raburn, X. Song, J. Barton, and Y. Nakano, "Single mode and dynamic all-optical flip-flop operation of multimode interference bistable laser diodes with distributed Bragg reflectors," in *Proc. ECOC 2006*, p. Th 1.4.4, 2006.
- [88] M. Takenaka and Y. Nakano, "Realization of all-optical flip-flop using directionally coupled bistable laser diode," *IEEE Photon. Technol. Lett.*, vol. 16, no. 1, pp. 45–47, 2004.
- [89] M. T. Hill, H. de Waardt, G. D. Khoe, and H. J. S. Dorren, "All-optical flip-flop based on coupled laser diodes," *IEEE J. Quantum Electron.*, vol. 37, no. 3, pp. 405–413, 2001.

- [90] E. Tangdiongga, X. Yang, Z. Li, Y. Liu, D. Lenstra, G. D. Khoe, and H. J. S. Dorren, "Optical flip-flop based on two-coupled mode-locked ring laser," *IEEE Photon. Technol. Lett.*, vol. 17, no. 1, pp. 208–210, 2005.
- [91] M. T. Hill, H. J. S. Dorren, T. de Vries, X. J. M. Leijtens, J. den Besten, E. Smallbrugge, Y. Oei, H. Binsma, G. D. Khoe, and M. K. Smit, "A fast low-power optical memory based on coupled micro-ring lasers," *Nature*, vol. 432, pp. 206–209, 2004.
- [92] M. Sorel, G. Giuliani, A. Scir, R. Miglierina, S. Donati, and P. Laybourn, "Operating regimes of GaAs-AlGaAs semiconductor ring lasers: experiment and model," *IEEE J. Quantum Electron.*, vol. 39, no. 10, pp. 1187–1195, 2003.
- [93] J. Van Campenhout, P. Rojo Romeo, P. Regreny, C. Seassal, D. Van Thourhout, S. Verstuyft, L. Di Cioccio, J.-M. Fedeli, C. Lagahe, and R. Baets, "Electrically pumped InP-based microdisk lasers integrated with a nanophotonic silicon-on-insulator waveguide circuit," *Opt Express*, vol. 15, no. 11, pp. 6744–6749, 2007.
- [94] M. T. Hill, H. J. S. Dorren, X. J. M. Leijtens, J. den Besten, T. de Vries, J. van Zantvoort, E. Smallbrugge, and Y. Oei, "Coupled Mach-Zehnde interferometer memory element," *Opt Lett.*, vol. 30, no. 13, pp. 1710–1712, 2005.
- [95] M. T. Hill, H. de Waardt, and H. J. S. Dorren, "Fast alloptical flip-flop using coupled Mach-Zehnder interferometers," in *CLEO 2001*, p. 188, 2001.
- [96] Y. Liu, R. McDougall, J. Seoane, E. Kehayas, M. T. Hill, G. Maxwell, S. Zhang, R. Harmon, F. Huijskens, L. Rivers, P. V. Holm-Nielsen, J. M. Martinez, J. Herrera, F. Ramos, J. Marti, H. Avramopoulos, P. Jeppesen, A. M. J. Koonen, A. J. Poustie, and H. J. S. Dorren, "Characterization of hybrid integrated all-optical flip-flop memory," in *LEOS 2006*, pp. 943–944, 2006.
- [97] R. McDougall, Y. Liu, G. Maxwell, M. T. Hill, R. Harmon, S. Zhang, L. Rivers, F. Huijskens, A. J. Poustie, and H. J. S. Dorren, "Hybrid integrated all-optical flip-flop memory for optical packet networks," in *Proc. ECOC 2006*, p. Th 1.4.5, 2006.

- [98] R. Clavero, F. Ramos, J. M. Martinez, and J. Marti, "All-optical flip-flop based on a single SOA-MZI," *IEEE Photon. Technol. Lett.*, vol. 17, no. 4, 2005.
- [99] R. Clavero, F. Ramos, and J. Marti, "All-optical self-routing latching switch based in active Mach-Zehnder interferometer," *IEEE Photon. Technol. Lett.*, vol. 28, no. 23, pp. 2475–2477, 2006.
- [100] T. Mori, Y. Yamayoshi, and H. Kawaguchi, "Low-switching-energy and high-repetition-rate-frequency all-optical flip-flop operations of a polarization bistable vertical-cavity surface-emitting laser," *Appl. Phys. Lett.*, vol. 88, pp. 101–102, 2006.
- [101] Y. Kim, J. Kim, S. Lee, D. Ha Woo, S. Kim, and T. Yoon, "Broadband all-optical flip-flop based on optical bistability in an integrated SOA/DFB-SOA," *IEEE Photon. Technol. Lett.*, vol. 16, no. 2, pp. 398–400, 2004.
- [102] D. Maywar, G. P. Agrawal, and Y. Nakano, "Robust optical control of an optical-amplifier-based flip-flop," *Opt Express*, vol. 6, no. 3, pp. 75–80, 2000.
- [103] W. D'Oosterlinck, J. Buron, F. Ohman, G. Morthier, and R. Baets, "All-optical flip-flop based on an SOA/DFB-laser diode optical feedback scheme," *IEEE Photon. Technol. Lett.*, vol. 19, no. 5-8, pp. 489–491, 2007.
- [104] W. D'Oosterlinck, F. Ohman, J. Buron, S. Sales, A. P. Pardo, A. Ortigosa-Blanch, G. Puerto, G. Morthier, and R. Baets, "All-optical flip-flop operation using a SOA and DFB laser diode optical feedback combination," *Opt Express*, vol. 15, no. 10, pp. 6190–6199, 2007.
- [105] W. D'Oosterlinck, G. Morthier, and R. Baets, "Sub-ps and simultaneous multiple wavelength switching of an all-optical flip-flop based on a DFB-LD with integrated SOA," in *Proc. ECOC 2007*.